POLYMER-SUPPORTED CATALYSTS FOR OXYGEN REDUCTION AND METHANOL OXIDATION

JINGNING SHAN

INFORMATION TO USERS

This manuscript has been reproduced from the microfilm master. UMI films the text directly from the original or copy submitted. Thus, some thesis and dissertation copies are in typewriter face, while others may be from any type of computer printer.

The quality of this reproduction is dependent upon the quality of the copy submitted. Broken or indistinct print, colored or poor quality illustrations and photographs, print bleedthrough, substandard margins, and improper alignment can adversely affect reproduction.

In the unlikely event that the author did not send UMI a complete manuscript and there are missing pages, these will be noted. Also, if unauthorized copyright material had to be removed, a note will indicate the deletion.

Oversize materials (e.g., maps, drawings, charts) are reproduced by sectioning the original, beginning at the upper left-hand corner and continuing from left to right in equal sections with small overlaps.

Photographs included in the original manuscript have been reproduced xerographically in this copy. Higher quality 6" x 9" black and white photographic prints are available for any photographs or illustrations appearing in this copy for an additional charge. Contact UMI directly to order.

Bell & Howell Information and Learning
300 North Zeeb Road, Ann Arbor, MI 48106-1346 USA
800-521-0600

Polymer-Supported Catalysts for Oxygen Reduction and Methanol Oxidation

by

Jingning Shan

A thesis submitted to the school of Graduate Studies in partial fulfillment of the requirements for the degree of Master of Science

Department of Chemistry

Memorial university of Newfoundland

St. John's, Newfoundland, Canada

August 2000

Abstract

This thesis is focused on the synthesis and characterization of poly(3,4-ethylenedioxythiophene)/poly(styrene-4-sulfonate) (PEDOT/PSS)-supported catalysts for the anodic oxidation of methanol as well as for cathodic oxygen reduction in low-temperature polymer electrolyte membrane fuel cells (PEFMCs).

Chapter 2 focuses on the electrochemical and electrocatalytic properties of PEDOT/PSS supported Pt catalysts for cathodic oxygen reduction. Performances for oxygen reduction obtained in gas diffusion electrodes that are similar to those used in current PEMFC technology were inferior to those for commercial carbon supported Pt catalysts. Thus, the catalysts were immobilized on glassy carbon electrodes and were studied by cyclic voltammetry and rotating disc voltammetry. The results show that PEDOT/PSS supported Pt catalysts exhibit similar oxygen reduction activities to commercial carbon supported catalysts when results are normalized for active Pt area. Exchange current densities and mechanisms appear to be the same. The inferior performance seen for the PEDOT/PSS supported Pt catalysts in gas diffusion electrodes, and reproduced at rotating disc electrodes have been shown to be due to low Pt utilization, and to slightly higher Pt particle sizes. The poor utilization appears to be due to electronic isolation of some Pt particles, and to blocking or poisoning of the Pt surface.

Chapters 3 and 4 focus on the preparation and characterization of PEDOT/PSS supported binary Pt-Ru, ternary Pt-Ru-OS and quaternary Pt-Ru-Os-Ir catalysts for anodic methanol oxidation. The

compositions of the metal alloys can be controlled through the molar ratio of metal salts in the reaction mixture and by the reaction time. Energy-dispersive X-ray analysis and X-ray diffraction were applied to determine the metal compositions and particle sizes. The electrocatalytic properties of these catalysts were investigated by several electrochemical techniques, including cyclic voltammetry (including reduced CO_2 oxidation), transient and steady state polarization experiments and chronoamperometry. Although PEDOT/PSS supported binary catalysts have exhibited good electrocatalytic activities for methanol oxidation, their performances are inferior to commercial binary catalysts. PEDOT/PSS supported ternary and quaternary catalysts exhibited, as expected, superior performances to PEDOT/PSS supported binary catalysts, but are still inferior to those for commercial binary catalysts.

Acknowledgements

My most sincere gratitude goes to my supervisor Dr. P. G. Pickup for his guidance throughout the course of the degree programme. I have greatly benefited from and been influenced by his research attitude, critical judgement and invaluable advice.

I would like to thank my supervisory committee, Dr. L. K. Thompson and Dr. F. R. Smith for reading this thesis and for their advice, and the staff working in the Chemistry Department of Memorial University of NFLD for their enthusiastic help.

Thanks are also given to our group members Dr. Mark Lefebvre, Brian J. Maclean, Bradley Easton, Dr. Colin Cameron, John Halfyard, Eduardo Cammisa, Kris Kean and Brent Myron. They are full of intelligence and fun.

Financial support in the form of a Graduate Fellowship from the School of Graduate Studies, Teaching Assistantships from the Chemistry Department, and supplements from an NSERC grant are gratefully acknowledged.

List of Abbreviations and Symbols Used

Symbol	Meaning	Units
α	symmetry factor	
ν	kinematic viscosity	$cm^2\ sec^{-1}$
σ	electronic conductivity	$S\ cm^{-1}$
AFC	alkaline fuel cell	
C^*_0	concentration of dissolved O_2 in the solution	$mol\ cm^{-3}$
CA	chronoamperometry	
CP/PA	conducting polymer/polyanion	
CV	cyclic voltammetry or cyclic voltammogram (s)	
D_0	diffusion coefficient of oxygen	$cm^2\ s^{-1}$
DMFC	direct methanol fuel cell	
EDX	energy dispersive X-ray analysis	
E_{onset}	onset potential	
F	Faraday constant	
FTIR	Fourier transform infrared spectroscopy	
GDE	gas diffusion electrode	
I	current	A
M	reaction order	

MEA	membrane & electrode assembly
MCFC	molten carbonate fuel cell
n	reaction order (Section 2.1.1), number of electrons (Section 2.3.3.3)
NP	normal pulse polarography
ORR	oxygen reduction reaction
PANI	polyaniline
PEDOT/PSS	poly(3,4-ethylenedioxythiophene) / poly(styrene-4-sulfonate)
PEMFC	polymer electrolyte membrane fuel cell
PPY	polypyrrole
PTFE	polytetrafluoroethylene
PW	pulse width
PY	pyrrole
Q1	a specific PEDOT/PSS composite
RDE	rotating disc electrode
rpm	revolutions per minute
RSD	relative standard deviation
SOFC	solid oxide fuel cell
SPE	solid polymer electrolyte
SSCE	saturated sodium chloride calomel electrode
RT	room temperature
TEM	transmission electron microscopy
YSZ	yttria stabilized zirconia

Table of Contents

List of Tables

List of Figures

Chapter 1

General Review of Polymer Electrolyte Membrane Fuel Cells (PEMFCs)

1.1 General history of fuel cells

Since the first oil crisis of 1973, the world energy perspective has changed. The outbreak of the Gulf War in 1991 as well as the recent steep increase in the price of oil has attracted many nations to reduce their dependency on oil by exploiting other primary energy sources. On the other hand, over the last few years, discussions on the green house effect have led to general acceptance of the theory that carbon dioxide emissions cause global warming. This increasing environmental awareness has led to strict emission legislation in, for example, Japan and California. Studies have also concluded that the earth's fossil fuel resources should be better maintained in order to secure a sustainable future. These concerns have led to the enactment of major laws (eg. The clean Air Act Amendment of 1990 in USA) to impose strict regulation on pollution sources and generate an increasing interest in the development of fuel cells (eg. The Energy Policy Act of 1992).

A fuel cell is defined as an electrochemical device that can continuously convert the chemical energy of a fuel and oxidant to electrical energy without chemical combustion [1]. In principle, a fuel cell operates like a battery, but unlike a battery a fuel cell does not run down or require recharging. A hydrogen fuel cell running on hydrogen derived from a renewable source will produce clean non-polluting energy in the form of electricity, and

produce only heat and water as byproducts. The hydrogen fuel cell is bound to be one of the alternative power sources of the future. The commercialization of fuel cells for use in homes, offices, hospitals [2,3], shopping complexes, automobiles [4] and space missions has shown a promising vision of the beginning of the hydrogen economy.

It was William Grove who first demonstrated the hydrogen-air fuel cell in 1839 [5] and the late Francis T. Bacon produced a successful device in the first major fuel cell development project in 1932 [6]. Bacon's work culminated in the use of hydrogen-air cells in the Apollo Space program in 1960 [7] and resulted in a diversification into five main classifications of fuel cells.

Generally, according to their electrolyte materials, the five types of fuel cell are the Alkaline Fuel Cell (AFC) working below 100 ^{0}C with 30 wt % KOH as the electrolyte; the Phosphoric Acid Fuel Cell (PAFC) working at approximately 200 ^{0}C with concentrated (~100 wt %) phosphoric acid as the electrolyte; the Molten Carbon Fuel Cell (MCFC) which most frequently uses a eutectic melt containing 38/62 mole % potassium and lithium carbonate and less frequently 48/52 mole % lithium and sodium carbonate; the Solid Oxide Fuel Cell (SOFC) which uses oxide conducting yttria stabilized zirconia (YSZ) as the electrolyte and the Polymer Electrolyte Membrane Fuel Cell (PEMFC) with a water-swollen perfluorinated sulfonic acid ionomer as the electrolyte, which is also called a solid polymer electrolyte (SPE). These fuel cells are all designed to work on hydrogen-rich reformates as the fuel and oxygen or air as the oxidant. AFCs have long been used by NASA on space missions operating as an auxiliary power supply [8,9]. The PAFC was developed in the mid-1970s and is the most commercially developed. It is already being used in diverse applications and shows very

promising results [10,11]. The development of MCFCs in the 1980s and SOFCs in the 1990s was due to their better overall efficiency together with the useful heat generated by their high temperature plants. MCFCs and SOFCs operate at higher temperature (>650 ^{0}C) and are aimed primarily at big, high-power applications including industrial and large-scale central electricity generating stations [12]. The PEMFC has attracted growing interest recently particularly for road transportation with use of methanol as the fuel being a key goal [13,14] as will be discussed in section **1.3**. Of all the fuel cell systems, only the AFC and PEMFC can achieve high power densities (> 1 W cm^{-2}) [15]. However, poor performance has been a key problem ever since Grove described the fuel cell [16] and it is still the major issue requiring improvement in present-day fuel cells.

As pollution-free energy sources, fuel cells are showing undoubted prospects for future power and transportation applications [17,18]. A more detailed review of the background of the development of fuel cells can be found in references [18-21].

1.2. General review of polymer electrolyte membrane fuel cells (PEMFCs)

The PEMFC is perhaps the most elegant of all fuel cell systems in design and mode of operation. Its electrolyte is an acid type polymer ion-exchange membrane and is, generally, a perfluorosulfonic acid membrane, of which Nafion made by DuPont is the best-known. The structure of Nafion is shown in **Fig. 1.1**.

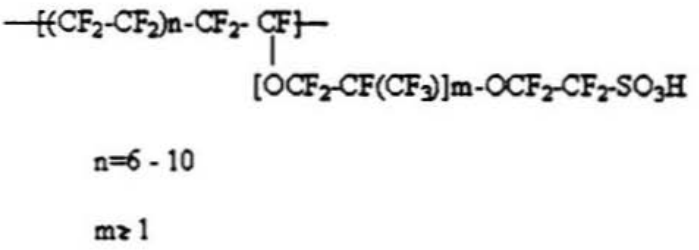

Fig. 1.1 The structure of Nafion [12].

These membranes are electrochemically stable at temperatures up to about 150°C but above this temperature (Nafion has a glass transition temperature of 130 ^{0}C), they will change to a gel state. Therefore, PEMFCs are operated under mild conditions (the temperature range is 50 ^{0}C – 90 ^{0}C, and the pressure is 1-6 atm). Nafion membranes have high oxygen solubility, high proton conductivity, high chemical stability, low density and high mechanical strength and are one of the most important parts of the PEMFC. A typical PEMFC consists of a composite of two porous electrocatalytically active electrodes on either side of a PEM (typically 50-175 μm thick), as shown schematically in **Fig. 1.2.** This core structure of the sandwiched cell is commonly called a membrane electrode assembly (MEA).

For a hydrogen/oxygen fuel cell, hydrogen is electrochemically oxidized at the anode and broken down into positive ions (protons) and negatively charged electrons as shown in **Eq. 1.1.** At the cathode, oxygen electrochemically combines with the hydrogen ions and electrons to produce water according to **Eq. 1.2.** Protons are attracted to the negatively charged sulfonic acid groups of the Nafion membrane and transported to the

cathode; electrons are transported through the external load from the anode to the cathode.

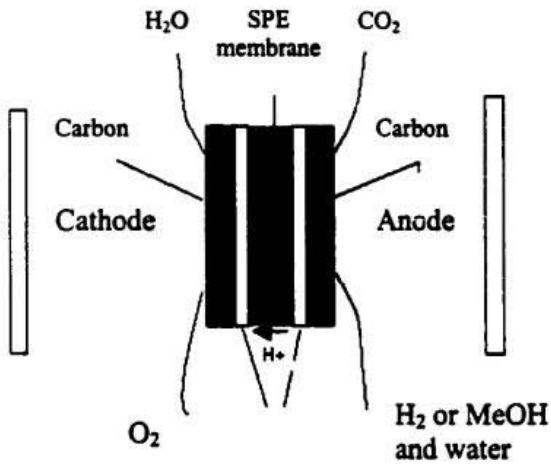

Fig. 1.2 Schematic diagram of a PEMFC.

$$H_2 \rightarrow 2H^+ + 2e^- \qquad (1.1)$$

$$O_2 + 4e^- + 4H^+ \rightarrow 2H_2O \quad (1.2)$$

The following advantages of PEMFCs have been summarized [22]:

- high power density and efficiency
- fast startup and shutdown
- absence of liquid electrolyte minimizes corrosion
- insensitive to differential pressures
- low sensitivity to CO_2

- no carbonate formation
- long life and potable liquid water product
- versatility of application

The early development and the current status of PEMFC technology can be found in references [12, 23-32]. Briefly, the development of reliable solid electrolyte membranes, the improvement of catalyst performance and the development of MEAs are the three most active research areas on PEMFCs.

1.3 General review of direct methanol fuel cells (DEMFCs)

The current advantage of the hydrogen/air cell is that hydrogen oxidation at the anode is very fast and consequently its performance and efficiency are better than for any other fuel. However, for reasons such as safety, ease of storage, transportation and refueling etc., a liquid fuel would be preferred. Thus, methanol has been widely studied as a fuel [33] and in many respects, the methanol-air fuel cell (DMFC) is a promising power source for electric vehicles.

Using methanol as the anodic reactant in an acid medium, the anodic reaction can be written as follows:

$$CH_3OH + H_2O \rightarrow CO_2 + 6H^+ + 6e^- \qquad (1.3)$$

An acidic environment is useful to reject CO_2 produced during the electro-oxidation of methanol. Sulfuric-acid solution has been most commonly used.

The history of the DMFC is shorter than that of hydrogen-air fuel cell. The pioneering work was started during the 1960s by Shell Research in England and in the 1970s by Exxon-Alsthom in France [13]. Shell's work on fuel cells began in the late 1950s; the initial goal was to discover whether the fuel cell could be a viable choice for road transportation. At that time, all existing fuel-cell gas diffusion electrodes suffered poor performance when operating on air and Shell realized that this was due to physical rather than chemical factors. To solve these problems, Shell made a very thin electrode that could be manufactured on a large-scale. The electrode consisted of a very uniform, microporous polyvinyl chloride substrate, on which was evaporated silver or gold. A layer of catalyst was then attached to this metallic layer [34]. A number of stacks were built to test whether a fuel cell could be operated at ambient pressure and temperature. The fuel, H_2, was generated from methanol-water and the whole system was tested under various conditions [35].

Shell's design was too complex and the electrode with Pt as the electrocatalyst was very easily poisoned by reaction products. For methanol, six electrons must be exchanged for complete oxidation and consequently the oxidation kinetics are inherently slow. A wide range of Pt alloys were examined by researchers at Shell who found that Pt-Ru was the most effective binary catalyst for CO tolerance in DMFCs. There has now been active research on Pt-Ru binary catalysts for more than 30 years and it still continues [36-40].

Shell's efforts were devoted to improving catalysts and investigating the mechanism of the methanol oxidation reaction. During the period of 1973-1981, Shell's research groups in the UK and Netherlands made considerable progress in the development of DMFCs. However, Shell disbanded its research teams in 1981 as a result of the lower

growth in oil consumption and unfounded fears of oil shortage [41]. The Exxon-Alsthom group in France mainly worked with alkaline and buffer electrolyte technology and ceased in the late 1970s.

In the mid-to-late 1980s, research on fuel cells was aroused again in the USA, Canada, Europe, and Japan when environmental protection became a serious global issue. The development of fuel cells for road vehicles without or with low emissions is pursued by many companies and car manufacturers. Ballard Power Systems and Daimler-Benz are the pioneers with their solid polymer electrolyte technology. In Europe, a program has been set up to study the DMFCs and at the same time the possibilities of utilizing indirect hydrogen-based fuel cells or gaseous methanol cells are also receiving much attention.

Recent DMFC work has strongly focused on cells with PEMs and the most likely type of DMFC to be commercialized in the near future seems to be polymer electrolyte membrane direct methanol fuel cell (PEMDMFC). To date, the DMFC is a strong competitor with hydrogen energy systems and it has become a real opportunity for commercialization in the near future.

1.4. Objectives of this thesis - the catalysts and methodology issues

The heart of a PEMFC (**Fig.1.2**) has the following structure when viewed from either the anode or the cathode side:

/ porous wet-proofed carbon backing / **catalyst layer** // Nafion membrane (PEM) // **catalyst layer** / porous wet-proofed carbon backing /

Studies on PEMFCs are focused on the PEM, the catalyst layer and fuels. For PEMDMFCs, methanol crossover from the anode to the cathode and catalytic inefficiency are the two main challenges in the current technology. This thesis is focused on the catalyst layers on either side of the Nafion membrane. Generally, the work is on catalyst performances for oxygen reduction at the cathode and methanol oxidation at the anode.

To date, the biggest impediment to the commercialization of PEM fuel cells is the poor performance of the state-of -the-art cell, which causes costs to be much higher than for internal-combustion engines and therefore unacceptable. Almost certainly, DMFCs will require Pt-based catalysts for both the anode and the cathode. Given the high cost of Pt, the amount of the metal must be minimized in order to match the cost of the metal of an equivalent heat engine.

One way to reduce cost is to decrease the amount of precious metal catalyst required. Thus, the application of carbon as a catalyst support has played a vital role and is considered to be the most important breakthrough for catalyst cost reduction in fuel cell development [42]. Carbon-supported Pt or Pt+Ru electrodes have greatly improved performance per gram of precious metal both for oxygen reduction and for methanol oxidation [43]. On the other hand, catalyst pre (or post-) treatment and the choice of a suitable support other than carbon could also play a vital role in cost reduction and performance enhancement [44].

In this thesis, a conducting polymer instead of carbon has been used as a catalyst support in oxygen reduction and methanol oxidation studies. The conducting polymer is used to enhance the proton conductivity of the catalyst layer. A detailed discussion of the

benefits and use of polymer-supported catalysts for oxygen reduction are included in **Chapter 2**.

In **Chapter 3**, the performance of polymer-supported binary (Pt-Ru) catalysts for methanol oxidation was investigated. Recently, a ternary catalyst (Pt-Ru-Os) [45] and a quaternary catalyst (Pt-Ru-Os-Ir) [46] have been found to show superior electro-catalytic activity to binary catalysts for methanol oxidation. Thus in **Chapter 4**, preliminary results for polymer-supported ternary and quaternary catalysts are presented.

Results for commercial Pt/C and Pt-Ru (1:1)/C catalysts are presented throughout the thesis, for comparisons with results for the new catalysts, and to illustrate method development.

References

1. G.T. Young, "*Fuel cells*," Rheinhold Publishing, New York, **Vol. 1**: *Symposium of Am. Chem. Soc.*, 1959; **Vol. 2**: Symposium of Am. Chem. Soc., 1961.
2. T. A. Pamberger, *J. Power Sources*, **71**, 45 (1998).
3. F. Panik, *J. Power Sources*, **71**, 36 (1998).
4. S. G. Chalk, J. Milliken, J. F. Miller, S.R. Venkateswaren, *J. Power Sources*, **71**, 26 (1998).
5. W. R. Grove, *Philos. Mag. Ser.*, **314**, 127 (1839).
6. A. J. Appleby, *J. Power Source*, **37**, ix-xi (1992).
7. Pratt & Whitney Aircraft, *Design and Development of H_2-O_2 Fuel Cell Power Plants for Apollo Command Module*, NASA/Houston, Final Report 6/16/1962.
8. K. K Ordesch, J. Gsellman, P. Kalal, J.C.T. Oliverira and K. H. Steininger, *Proceedings of the 33rd International Power Sources Symposium*, p.817, The Electrochemical Society, Inc. Pennington, NJ. 1998.

9. M. Warshay and P. R. Prokopius, *J. Power Sources*, **29**, 193 (1989).
10. International Fuel cells (IFC), "*The PC 25 200KW Fuel Cell Plant*", p.81, CEC-Italian Fuel Cell Workshop, Proceedings (P. Zegers, ed.) Taormina, Italy, 1987.
11. A. J. Appleby and F. R. Foulkes, *Fuel Cell Handbook*, Krieger Publishing Company, 1993.
12. L. J. M. J. Blomen and M. N. Mugerwa, *Fuel Cell Systems*, Plenum Press, New York and London, 1993.
13. S. Escribano and P. Aldebert, *Solid State ionics*, **77**, 318 (1995).
14. B. D. McNicol, D. A. J. Rand and K. R. Williams, *J. Power Sources*, **83**, 15 (1999)
15. S. Srinivasan, D. J. Manko, H. Koch, M. A. Enayetullah and A.J. Appleby, *J. Power Sources*, **29**, 367 (1990).
16. W. R. Grove, *Phil. Mag.*, **21**, 417 (1842).
17. K. B. Prataer, *J. Power Sources*, **51**, 129 (1994).
18. P. F. Howard and C. J. Greenhill, *Proc. 1993 Future Transportation Technical Conf.*, San Antonio, TX. USA, 9-12 Aug. 1993, SAE Special Publication No. 984, Warrandale, PA, USA, 1993, pp. 113 – 119.
19. Supramaniam Srinivasan, *Electrochemistry in Transition – From the 20^{h} to the 21st century*, Edited by O.J. Murphy, Supramamiam Srinivasan and Brian E. Conway (1992).
20. K. V. Kordesch and G. R. Simader, *Chemical Reviewers*, **95**, 191 (1995).
21. H. Wendt, T. Brenscheidt and A. Fischer, *Phil. Trans. R. Soc. Lond. A*, **354**, 1627 (1996).
22. K. Straber, *Ber. Bunsengs, Phys. Chem.*, **94**, 1005 (1990).
23. L. W. Niedrach and A. Steck, *Anal. Chem.*, **51**,862 (1979).
24. H. J. R. Magnet in C. Berger (Ed.), *Handbook of Fuel Cell Technology*, Prentice Hall, Englewood Cliffs, NJ, 1967, pp.425-491.
25. J. Appleby and R. R. Foulkes, *Fuel Cell Handbook*, Van Nostrand Reinhold, New York, 1989.
26. S. Srinivasan, D. J. Manko, H. Koch, M.A. Enayetullah and A. J. Appleby, *J. Power Sources*, **29**, 367 (1990).

27. S. Srinivasan, O. A. Velev, A. Parthasarathy, D. J. Manko and A. J. Appleby, *J. Power Sources*, **36**, 299 (1991).

28. H. P. Dhar, *J. Electroanal. Chem.*, **357**, 237 (1993).

29. S. Mukerjee and S. Srinivasan, *J. Electroanal. Chem.*, **357**, 201 (1993).

30. K. Kordesch and G. Simader, *Fuel cells and Their Applications*, VCH, 1996, p. 72.

31. J. P. Shoesmith, R. D. Collins, M. J. Oakley and D. K. Stevenson, *J. Power Sources*, **49**, 129 (1994).

32. S. Gottesfeld and T. A. Zawodzinski in: *Advances in Electrochemical Science and Engineering*, edited by R. C. Alkire, H. Gerischer, D. M. Kolb and C. W. Tobias, WILEY-VCH, **Vol. 5**, 1997, p.195.

33. R. Metkmeijer, P. Achard, *Int. J. Hydrogen Energy*, **19**, 535 (1994).

34. K. R. Williams, J. W. Pearson, W. J. Gressler, in: *D. H. Collins (Ed.), Batteries 2. Reasearch and Development in Non-Mechanical Electrocal Power Sources*, Pergamon, Oxford, 1965, p. 337.

35. J. W. Pearson, in: K. R. Willams (Ed.), *An Introduction to Fuel Cells*, Elsevier, 1966, p. 307.

36. J. O'M. Bockris and H. Wroblowa, *J. Electroanal. Chem.*, **7**, 428 (1964).

37. M. Watanabe and S. Motoo, *J. Electroanal. Chem.*, **60**, 267 (1975).

38. K. Franaszczuk and J. Sobkowski, *J. Electroanal., Chem.*, **327**,1235(1992)

39. R. Ianniello, V. M. Schimidt, U. Stimming, J. Stumper and A. Wallau, *Electrochim. Aata.*, **39**, 1863 (1994)

40. T. J. Schmidt, M. Noeske, H. A. Gasteiger, and R. J. Behm, *J. Electrochem. Soc.*, **145**, 925 (1998).

41. D. A. J. Rand, R. Woods, R. M. Dell, *Batteries for Electric Vehicles*, Research Studies Press, Taunton, England, 1998.

42. P. Stonehart, "*State-of-the-Art for Dispersed Platinum Electrocatalysts*", p. 96, Extended Abstarcts, 31st Meeting ISE, Venice, Italy 1980.

43. J. B. Goodenough, A. Hamnett, B. J. Kennedy, R. Manoharan and S. A. Week, *J. Electroanal. Chem.*, **240,** 133-145 (1988).

44. S. Wasmus, A. Küver, *J. Electroanal. Chem.*, **461,** 14-31 (1999).

45. K. L. Ley, R. Liu, C. Pu, Q. Fan, N. Leyarovska, C. Segre and E. S. Smotkin, *J. Electrom. Soc.*, **44**, 1543 (1997).

46. E. Reddington, A. Sapienza, B. Gurau, R. Viswanathan, S. Sarangapani, E. S. Smotkin and T. E. Mallouk, *Science*, **280,** 1735 (1998).

Chapter 2

Polymer-Supported Catalyst for Oxygen Reduction

2.1 Introduction

2.1.1 Catalysts for the oxygen reduction reaction (ORR) in PEMFCs.

Platinum supported on carbon is a commonly used electrocatalyst for the anodic oxidation of hydrogen as well as for cathodic oxygen reduction in low-temperature PEMFCs [1-3]. The kinetics and mechanisms of oxygen reduction have been extensively studied on dispersed Pt supported on different carbon materials [4-9]. The role of the carbon support is to provide electrical connection between the widely dispersed Pt catalyst (nano) particles and the porous current collector (carbon cloth or paper). Although carbon is a good electronic conductor, carbon-supported catalysts still suffer from high overpotentials for oxygen reduction in low-temperature fuel cells in acidic electrolytes. Enhancement of the kinetics of oxygen reduction has become the main impetus for the extensive studies to improve the performance of electrochemical systems.

Damjanovic has given a generalized rate expression for oxygen reduction with the rate-determining step as the first electron transfer and the equation is given by [10]

$$I = k\,[P_{O2}]^{n}\,[H^{+}]^{m}\,\exp(-\alpha FE/RT) \qquad 2.1$$

Where n and m are the reaction orders with respect to O_2 and H^+, α is the symmetry factor, k is a constant, and the other terms have their usual electrochemical significance. Damjanovic reported that n and α are both equal to 1, and that m is close to 1.5 for oxide-free platinum in acid electrolytes. From the equation above, it is very clear that the ORR on the Pt surface would be enhanced when the concentration of H^+ or O_2 is increased, especially for H^+ concentration because of 1.5 power index. Some experiments have shown that at a given potential, the reduction current varies nearly linearly with oxygen pressure [11] and that a much better performance is obtained when a proton conducting ionomer (Nafion) is added to the catalyst layer [12].

Although the addition of ionomer solution to the catalyst layer improves the performance of a fuel cell, it also increases the electronic resistance of the catalyst layer and restricts oxygen diffusion. Therefore, there has been much effort to find a way to improve the ionic conductivity of the catalyst layer without compromising its electronic conductivity. One method adopted is to modify the surface of the carbon support or carbon-supported catalyst by chemical oxidation with strong oxidizing agents, such as H_2SO_4 and HNO_3 [13]. These agents can add oxygen functional groups such as phenol, carbonyl, carboxyl, quinone and lactone that enhance the sensitivity and activity of carbon-supported catalysts to the carbon surface. Some results for carbon supported catalysts modified in this way will be presented in this chapter.

The other method applied is to chemically synthesize conducting polymer/polyanion (CP/PA) composites that are different from conventional carbon in that they conduct electrons as well as protons. Two kinds of composites, polypyrole /

polystyrenesulfonate (PPY/PSS) [14] and poly(3,4-ethylenedioxythiophene) / poly(styrene-4-sulfonate) (PEDOT/PSS) (**eq. 2.2**) [15], have been developed and shown to efficiently conduct both protons and electrons (**eq. 2.3**) [16,17]. Platinum is then deposited on these composites by the reduction of $H_2PtCl_6 \cdot H_2O$ or $Pt(NH_3)_4Cl_2$ with formaldehyde or hydrazine [**eq. 2.4**].

$$PY(\text{or EDOT}) + NaPSS + Fe(NO_3)_3 \rightarrow PPY(\text{or PEDOT})PSS \text{ particles} \qquad \textbf{2.2}$$

$$(\text{-PPY(or PEDOT)-})_n^{+}PSS^{-} + H^{+}(\text{solution}) + e^{-} \leftrightarrow (\text{-PPY(or PEDOT)-})_nHPSS \qquad \textbf{2.3}$$

$$PPY(\text{or PEDOT})/PSS + H_2PtCl_6(aq) + H_2CO \rightarrow Pt/PPY(\text{or PEDOT})/PSS \qquad \textbf{2.4}$$

PY = 

EDOT = 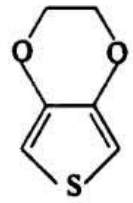

Besides not being a proton conductor, carbon is also impermeable to gases (oxygen, hydrogen and water vapor), which limits achievable performance. The polymer composites, however, remove these deficiencies. The next generation of conducting polymer-supported catalysts is shown in **Fig. 2.1.** In view of these important characteristics, polymer supported catalysts have definitely opened a new vision of catalysis issues in PEMFC technology.

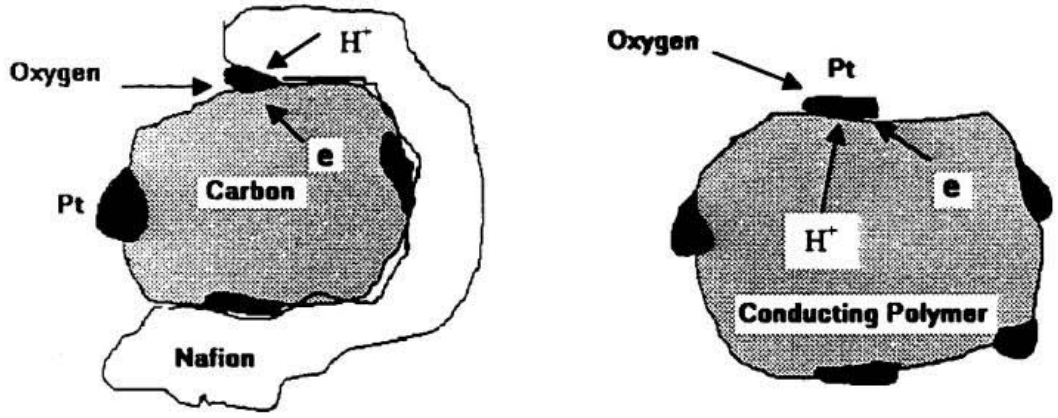

The state of the art

The next generation

Fig. 2.1 Conducting polymer supported catalysts

2.1.2 Objectives of the chapter

Although using conducting polymers as catalyst supports has been attracting research interest for more than 10 years, the reported work is mainly restricted to electrochemically synthesized polymer films and electrochemically deposited Pt particles [18-21]. The disadvantages of these methods are that the resulting catalyst layers have unsatisfactory porosity, and the Pt particles are usually deposited near the surface of the polymer layer. These deficiencies limit the performance for ORR. The only reports on the chemical deposition of metal particles on conducting polymer particles come from our group [14-17].

Pickup *et al* has reported chemically prepared polymer composites such as PPY/PSS that have a good Pt distribution, polymer porosity and superior ionic conductivity than electrochemically prepared films growing on an electrode surface [20,21]. However, a major problem with chemically prepared catalysts is that the electronic conductivity of the polymer is often lost during the deposition of Pt particles. In previous work, the electronic conductivity of the polymer (PPY or Polyaniline (PANI)) was seriously degraded by the deposition of the catalyst particles under both reducing (formaldehyde, hydrogen, or citrate) and oxidizing (H_2O_2) conditions [14]. As a result, the performances of these catalysts for oxygen reduction were poor compared to the performance of commercial carbon supported catalysts. PEDOT was found to be more stable than PPY under oxidizing condition [22] and at elevated temperatures [23], and PEDOT/PSS supported catalysts have been found to be the best polymer-supported catalyst developed to date. Thus a series of studies have been conducted on the electrochemical and electrocatalytic properties of these PEDOT/PSS composites and catalysts in gas diffusion electrodes (GDE) similar to those used in current PEMFC technology [16,17]. This has demonstrated the potential of the new catalysts in real applications, but has also revealed surprising limitations. Performances for oxygen reduction in particular were lower than would be expected based on the measured Pt loadings and conductivities.

The aims of the work in this chapter were first to test the electrocatalytic properties of polymer supported catalysts developed by our group [16,17] with GDEs in half and full cells, and secondly, to investigate the activities of these catalysts under more carefully controlled conditions. Thus, the catalysts have been immobilized on glassy carbon

electrodes following a procedure developed by Gojkovic *et al* [24], and studied by cyclic voltammetry and rotating disc voltammetry.

Two similar methods have recently been reported for immobilizing carbon supported fuel cell catalysts on rotating disk electrodes. Schmidt *et al* [25] coated the electrode with an aqueous suspension of the catalyst, and then coated the dried catalyst layer with a thin Nafion film, while Gojkovic *et al* [24] used a one step procedure in which the catalyst was applied to the electrode as a suspension in a Nafion solution. Both groups characterized their electrodes by cyclic voltammetry and reported similar charge to Pt mass relationships for the hydrogen adsorption/desorption region. Schmidt *et al* [25] estimated that virtually all of the Pt in the coating was electrochemically active in these experiments. Both types of electrode proved to be durable in rotating disc voltammetry and provided high quality results in studies of hydrogen oxidation [25] and oxygen reduction [24]. This type of methodology was applied in this thesis to investigate Pt utilization and oxygen reduction kinetics for PEDOT/PSS supported Pt catalysts. For comparison purposes, a commercial 20% Pt on carbon black catalyst and chemically deposited Pt on carbon black catalyst were also used.

2.2 Experimental

2.2.1 Synthesis of PEDOT/PSS

The chemical synthesis of the PEDOT/PSS composite (designated as Q1 [14]) used in this work was carried out at room temperature in deionized water. The EDOT monomer

(Bayer), NaPSS [Aldrich, avg. MW ≈ 70,000] and Fe $(NO_3)_3 \cdot 9H_2O$ (BDH) were used as received. The EDOT (30 mmol) and NaPSS (6 mmol of repeat units) were added in deionized water (1.6 L) and the mixture was stirred at 60-80 °C for 30 min to obtain the homogenous solution. An excess of solid $Fe(NO_3)_3 \cdot 9H_2O$ oxidant (75 mmol) was then added and the reaction mixture was stirred for about 2 hours at room temperature, and filtered. The collected polymer was washed first with 0.1 M nitric acid to remove Fe^{3+}, and then with a large amount of water. The resulting composite was stored in 5% aqueous CH_3OH to prevent oxidative degradation by air [17] and used without drying.

2.2.2 Electrocatalyst preparation

Q1-supported catalysts were made as follows. A suspension of Q1 in 20 ml of aqueous H_2PtCl_6 (Aldrich; concentration based on desired Pt loading) was prepared in a round bottom flask by ultrasonication for 30 min, and then this suspension was stirred at ca. 80-100 °C for 30 min to allow equilibration. A ca. 30 molar excess of aqueous formaldehyde (36.5%) was added followed by heating at reflux for ca. 40 min. The catalyzed polymer was collected by filtration, washed thoroughly with water and then stored in 5% aqueous CH_3OH. A portion of each batch of catalyzed polymer was collected and dried under vacuum to calculate its mass percentage in the wet samples. Total catalyst loadings were estimated by a gravimetric analysis in which the dried catalyst was burned at 900°C in a muffle furnace. Elemental Pt was assumed to be the only remaining product.

Carbon supported catalysts were made similarly, but without ultrasonication. Two methods for adding the formaldehyde have been tried. One method (Method 1) was as

described above, while the other method (Method 2) involved mixing H_2PtCl_6, carbon powder and 50 mL of 18 % formaldehyde at one time followed by heating at reflux for 40 min.

2.2.3 Experiments in gas diffusion electrodes (GDEs)

Dry catalyzed Q1, weighed to the desired metal loading, was mixed with 20% PTFE (polytetrafluoroethylene solution, DuPont) as a binder, blended in an ultrasonic bath for 5 min, then spread uniformly onto a 4 cm^2 area of carbon fiber paper (CFP; Toray TGPH090). A Nafion 117 membrane was then hot-bonded to the electrode under an applied load of 180 kg cm^{-2} for 90 s at ca. 125 °C. 1 cm^2 disks were cut from these membrane electrode assemblies (MEA) and tested in a homemade plexiglass holder. Electrochemical experiments (cyclic voltammetry and polarization) carried out in half-cells and full cells are shown schematically in **Fig. 2.2**.

In the half-cell used, a platinum wire and a saturated sodium chloride calomel (SSCE) electrode are used as counter and reference electrodes, respectively (**Fig. 2.2(a)**), and the cell can be described as:

N_2 (O_2) | C paper, Pt/Q1 (or Pt/C)| Nafion | 1M H_2SO_4 (aq), SSCE | Pt wire (Counter)

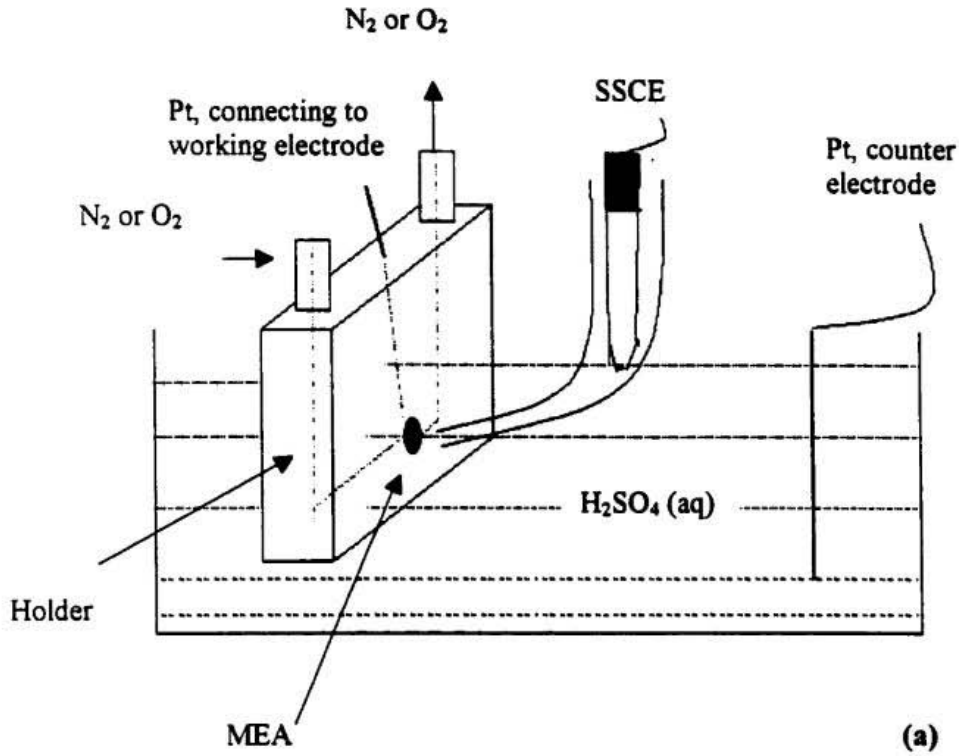

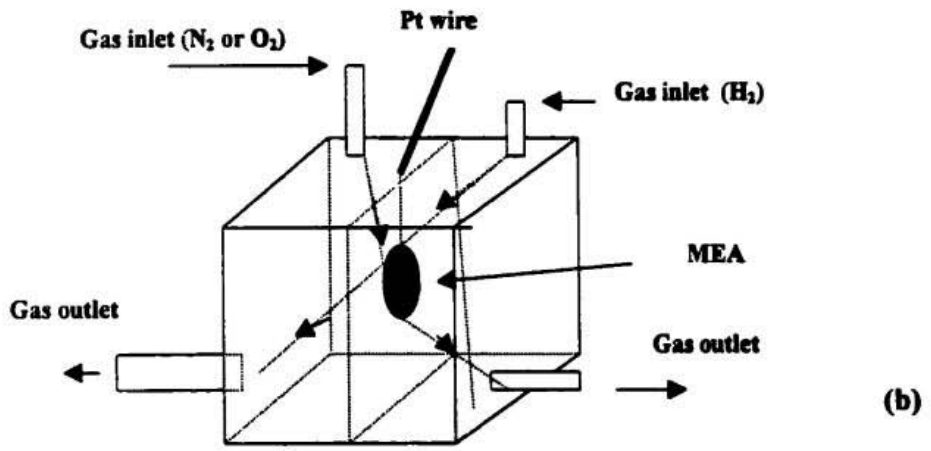

Fig. 2.2 Schematic of the half-cell (a) and the full cell (b).

In the full cell, the MEA is fixed in a holder without aqueous electrolyte and the Pt counter electrode is replaced by an gas diffusion anode exposed to H_2 (**Fig. 2.2(b)**). The MEA structure is just like that in **Fig. 1.2** and can be described as:

N_2 (O_2) | C paper, Pt/Q1 (or Pt/C) | Nafion | anode | H_2

In the full cell, no electrolyte solution and electrodes with 4 mg Pt black/ cm^2 (supplied by Ballard Power Systems) were used as anodes.

2.2.4 Pt particle size

Powder X-ray diffraction was applied to determine particle size, which was carried out on a Rigaku Ru 200 diffractometer using CuKα (0.15406 nm) radiation. Average Pt particle sizes were estimated from the spectral line broading with commercial software (Jade 1994, Materials Inc.) which uses the Scherrer equation and includes an instrument calibration parameter [17].

2.2.5 Immobilization of catalysts on carbon disc electrodes

The wet Q1-supported catalyst was weighed into a small vial to the desired metal loading, and 0.5 mL of 5 mass % Nafion solution in a mixture of lower aliphatic alcohols (Solution Technology Inc.) was added. The mixture was ultra-sonicated in a bath for one hour to make a suspension. A 0.5 – 2.5 μL amount of this suspension was placed on a

0.071 cm^2 glassy carbon disc electrode using a micro-syringe and left to dry at room temperature. After each experiment, the electrode was polished with alumina powder and a new catalyst coating was applied.

2.2.6 Electrochemistry of modified carbon disc electrodes

A three-compartment glass cell was used with a glassy carbon disc (RDE) working electrode, a Pt wire counter electrode, and a saturated sodium chloride calomel (SSCE) reference electrode (See **Fig. 2.3**). All potentials are quoted with respect to the SSCE reference electrode (0.236 V vs. NHE). Measurements were made at room temperature (22±2°C) using a E&G PARC Potentiostat/galvanostat. The electrolyte was 0.5 M H_2SO_4.

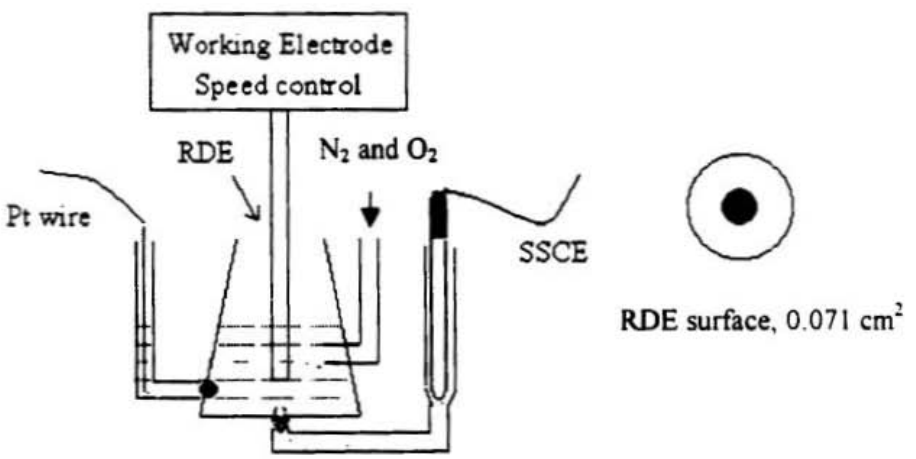

Fig. 2.3 Schematic of the RDE cell.

2.2.7 Reproducibility

Because of the large number of catalysts studied, it was impractical to repeat many experiments. Reproducibility was checked for yields and conductivity measurements (**Table 2.1**), particle sizes (**Table 2.3**) and some electrochemical experiments. Relative standard deviations (RSD) were ca. 10 % for yields, 100% for conductivities and 10% for particle sizes. Some figures in the thesis (see **Fig. 2.15** and **Fig. 2.30** for example) provide an indication of the reproducibility of the electrochemical experiments.

The high RSD for conductivities is due to such factors as variations in the catalyst preparation conditions, drying temperature and length, and storage method. However, conductivities for all catalysts are high enough (the lowest value is 0.03 S cm^{-1}) to not significantly influence the reported electrochemical experiments.

2.3 Results and discussion

2.3.1 Electronic conductivity of dried Q1 and Q1-supported catalysts

A series of Q1-supported catalysts with different Pt loadings were made for this work. Before measuring the conductivity of dried Q1 and Q1-supported catalysts, the wet catalysts were dried in a vacuum oven overnight at room temperature. Yields and dry conductivities of the catalysts are listed in **Table 2.1**.

The electronic conductivities of the catalysts were measured with a four-point probe assembly described elsewhere [16]. From **Table 2.1**, it can be seen that the yield of reduced Pt was generally very high and that the conductivities of the Q1-supported catalysts are high enough to support the currents involved in the electrochemical studies in this thesis.

Degradation of the electronic conductivities of conducting polymers in air has generally been ascribed to overoxidation by O_2 [27]. In order to test the stability of our polymers, Q1 and Polyaniline (PANI, prepared by the same method as for Q1) were heated at 100-120°C under nitrogen for two hours. At the same time, carbon black was heated in an oven in air at 125°C for two days. Initial and final electronic conductivities (at room temperature) are presented in **Table 2. 2**

It can be seen that although Q1 retained only 6.7% of its conductivity, its conductivity is still high enough for electrochemical studies. PANI, however, retained

Catalyst (%Pt/Q1)	Yield* (wt.%)	Dry conductivity (S/cm)
15%	66	0.14
21%	88	0.08
22%	101	0.26
30%	83	0.18
36%	96	0.19
40%	86	0.03
43%	90	0.88
45%	86	0.20
29%(Pt/C)	93	2.9
Carbon black	-	2.6
Q1	-	2.0

* Assuming no loss of carbon and Q1.

Yield = (metal loading obtained/Target metal loading)× 100%

- not measured

Table 2.1 Yields and conductivities of dry catalysts.

only 0.05 % conductivity. Carbon remains clearly the best substrate in terms of thermal stability. Initially, we prepared PANI and PANI/PSS supported catalysts, but their poor performances and loss of conductivities were not promising support materials. Therefore, Q1 and Q1-supported catalysts became the focus of the work in this thesis.

Sample	Initial conductivity ($S\ cm^{-1}$)	Final conductivity (S/cm^{-1})
PEDOT/PSS (Q1)	0.93	0.071
PANI	0.33	0.00018
C black	2.6	1.2

Table 2.2 Effect of thermal aging (2 hr at 100 – 120 ^{0}C) on conductivity of support materials.

2.3.2 Performance of Pt/Q1 in gas diffusion electrodes (GDE)

2.3.2.1 Polarization curves for oxygen reduction

Polarization experiments were conducted by stepping to each potential for 2 s. The potential was returned to the initial open circuit potential for 10 s between points. This procedure, although not strictly steady state, avoids complications due to flooding of the catalyst layer by water generated by the reduction of oxygen. **Fig. 2.4** shows polarization curves for a Pt/Q1 and a commercial Pt/C catalyst at GDEs in a half-cell. The Pt/Q1 electrode achieved a comparable performance to that with the commercial carbon supported catalyst, but a higher Pt loading was required. Polarization curves for catalysts obtained in a full cell are shown in **Fig. 2.5**. Although the Pt loading on Q1 is much higher than that of the commercial catalyst, the performance is still inferior. At low

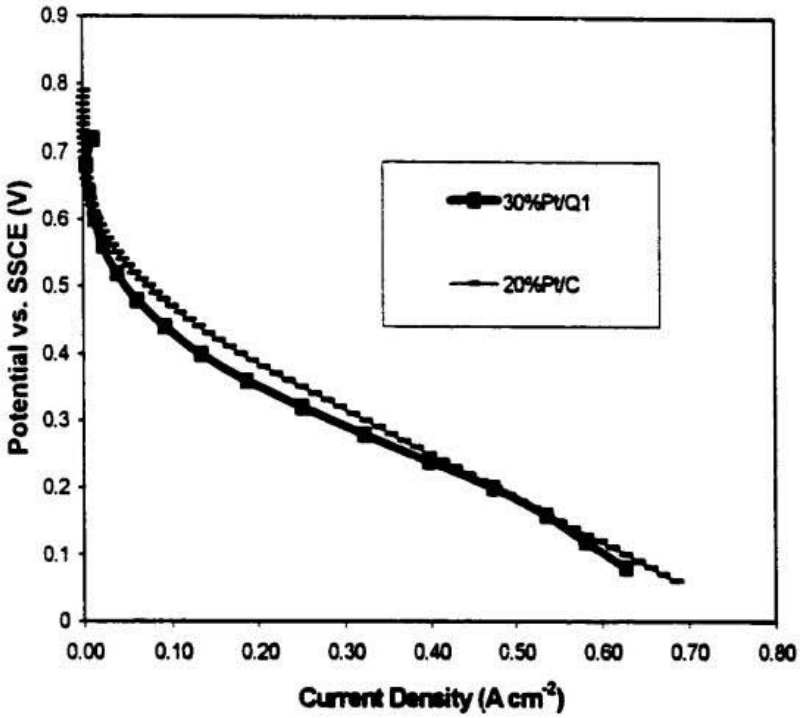

Fig. 2.4 Polarization curves for oxygen reduction in gas diffusion electrodes in a half-cell. Pt loadings were 0.75 mg cm^{-2} for 30% Pt/Q1 and 0.31 mg cm^{-2} for 20% Pt/C [15].

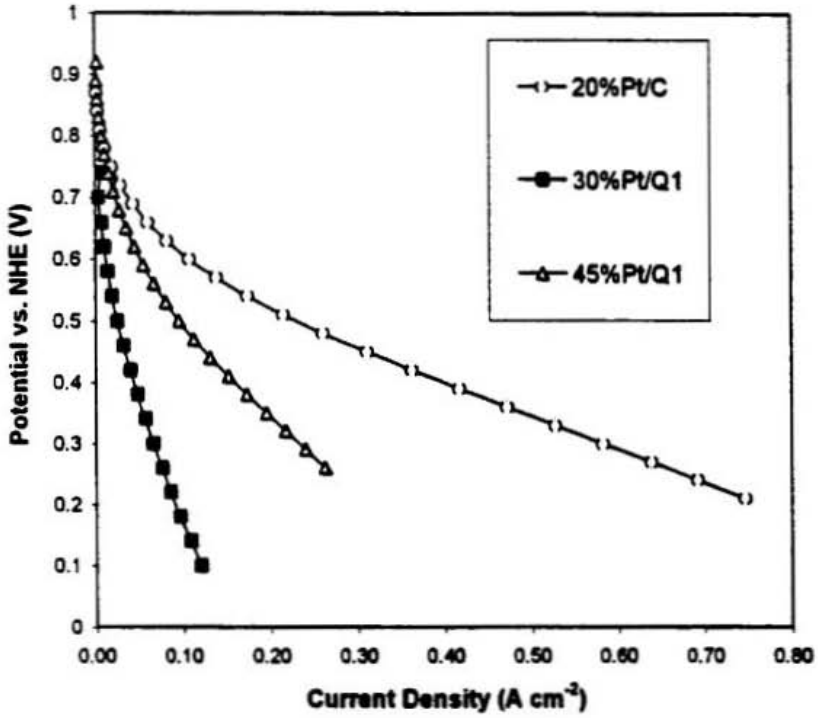

Fig. 2.5 Polarization curves for oxygen reduction in gas diffusion electrodes in a full-cell. Pt loadings were 0.5 mg cm^{-2} for 20% Pt/C , 0.75 mg cm^{-2} for 30% Pt/Q1 and 1.1 mg cm^{-2} for 45% Pt/Q1

current densities, overpotentials for oxygen reduction are similar for 45% Pt/Q1 and the 20%Pt/C commercial catalyst, but at higher currents, the potentials for the Q1-supported catalyst are much lower than for the commercial catalyst. Explanations for these differences were sought from voltammetric and RDE studies.

2.3.2.2 Cyclic voltammetry (CV) in half and full cells

Fig. 2.6 and **Fig. 2.7** show cyclic voltammograms of GDEs containing the 45%Pt/Q1 catalyst in half and full cells respectively. Waves for hydrogen adsorption/desorption, which were absent for Pt/PPY/PSS catalysts [16], are seen clearly in the -250 mV – +100 mV vs SSCE region. These peaks demonstrate that Pt/Q1 catalysts have superior electronic conductivity to Pt/PPY/PSS catalysts. There are sharp peaks between 0.6 and 0.8 V that are due to the redox of iron ions that can not be fully removed when washing Q1 [28].

CVs in full cells for Pt/Q1 catalysts with different Pt mass percentages (22%, 45%) and the 20%Pt/C commercial catalyst are compared in **Fig. 2.8.** Compared with the commercial catalyst, the Q1-supported catalysts exhibit much higher charging currents. On the other hand, in the case of 22% Pt/Q1, the Pt loading is the same as that of the commercial catalyst, but the peaks due to the hydrogen adsorption/desorption are much smaller than that of the commercial catalyst, which indicates a low utilization of Pt. The reason is not likely due to the electronic conductivity of Pt/Q1 catalyst that was quite high (0.26 S/cm).

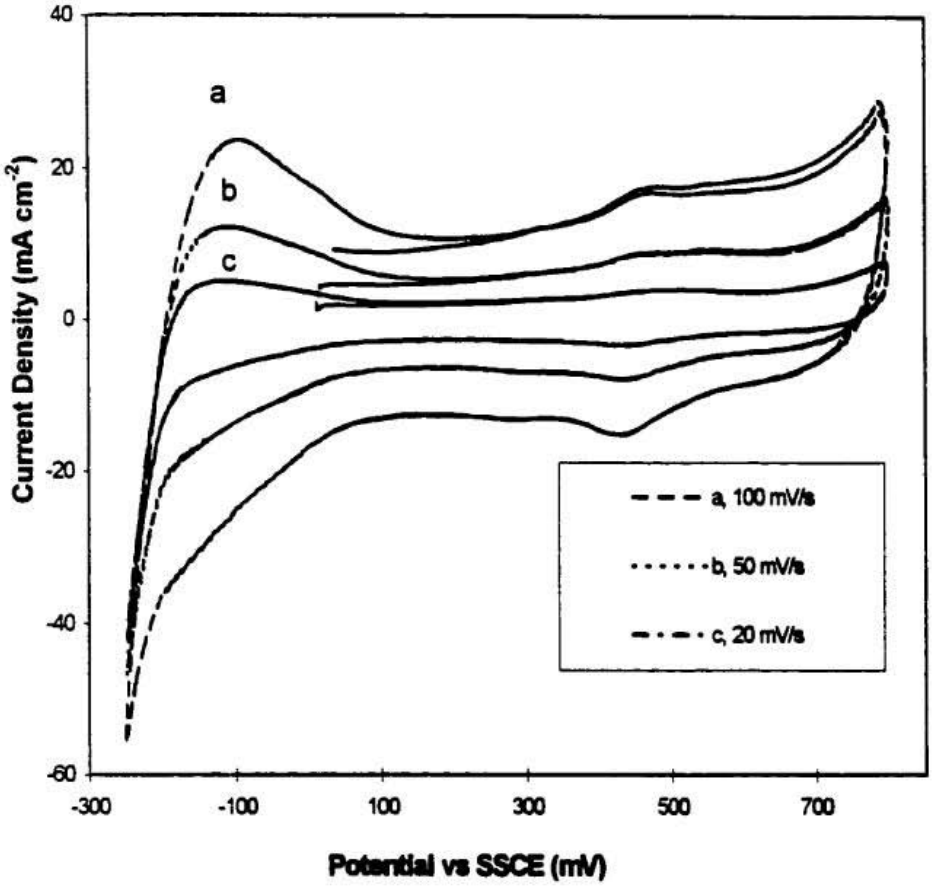

Fig. 2.6 Cyclic voltammograms(s) at different scan rates for 45% Pt/Q1 catalyst with 1.1 mg Pt cm^{-2} in a half-cell.

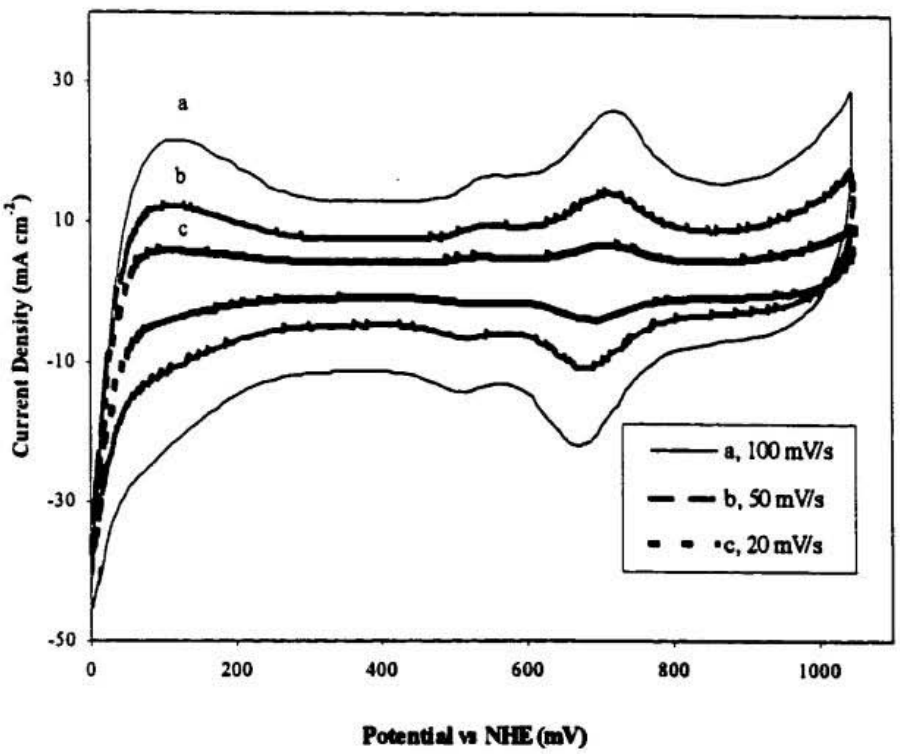

Fig. 2.7 Cyclic voltammogram(s) at different scan rates for 45% Pt/Q1 with 1.1 mg Pt cm^{-2} in a full-cell.

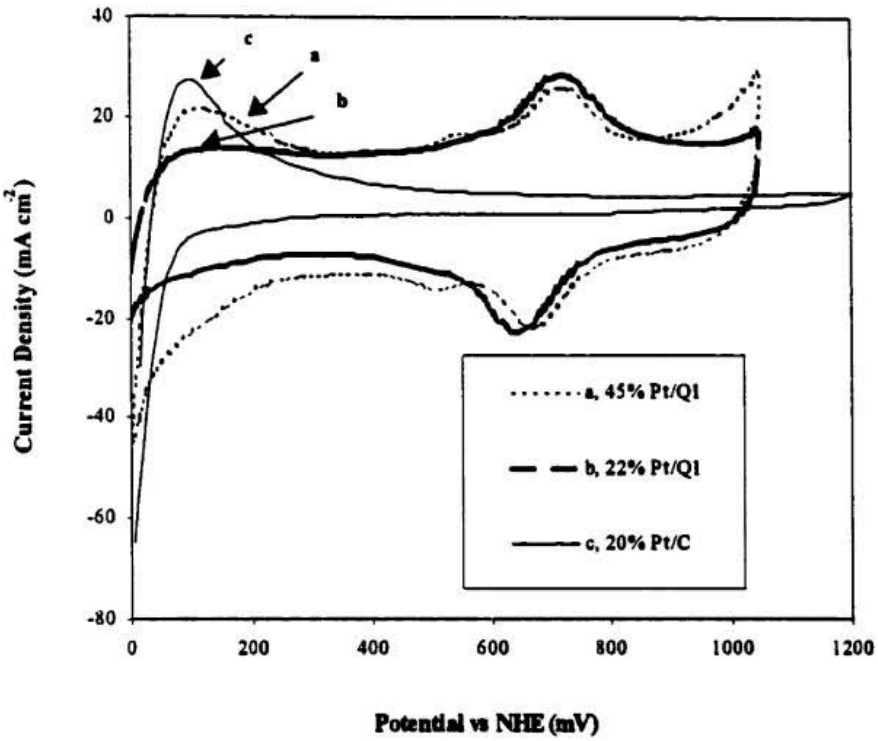

Fig. 2.8 Cyclic voltammogram(s) at 100 mV/s for 45% Pt/Q1 with 1.1 mg Pt cm^{-2} , 22% Pt/Q1 with 0.5 mg Pt cm^{-2} and 20% Pt/C with 0.5 mg Pt cm^{-2} in a full-cell.

The CV technique has commonly been used to ascertain the electrochemically active areas of Pt electrodes [9, 29-30]. By integrating the current in the hydrogen adsorption or desorption region of the CV and subtracting the double-layer charging current, the coulombic charge is obtained. Then, the Pt active area can be calculated by assuming a coulombic charge of 210 $\mu C\ cm^{-2}$ [31].

It was a concern that this method may not be accurate for MEAs in the half and full cell experiments, because the thickness of the catalyst layer (5-50μm) could lead to unacceptable mass-transport resistances and/or incomplete wetting of the electrode structure. To avoid these concerns and find the reasons for the low utilization of Pt/Q1, as well as its inferior performance in half and full cells, CV and RDE voltammetry was applied as described in the following section.

2.3.3 Characterization of Pt/Q1 catalysts on carbon disc electrodes.

2.3.3.1 Cyclic voltammetry (CV)

Before testing Pt/Q1 catalysts, a commercial 20% Pt/C catalyst was tested to find optimal conditions for running CV experiments (all CVs were run until reproducible curves were observed if not specified otherwise). **Fig. 2.9** shows representative CVs in deaerated 0.5 M H_2SO_4 for a commercial Pt/C catalyst dispersed in Nafion. A key difference between CVs obtained in half-cells and in this case is that two peaks are resolved in the hydrogen adsorption/desorption region as is seen in CVs of pure Pt electrodes. From the figure, it can also be seen that the currents in the hydrogen

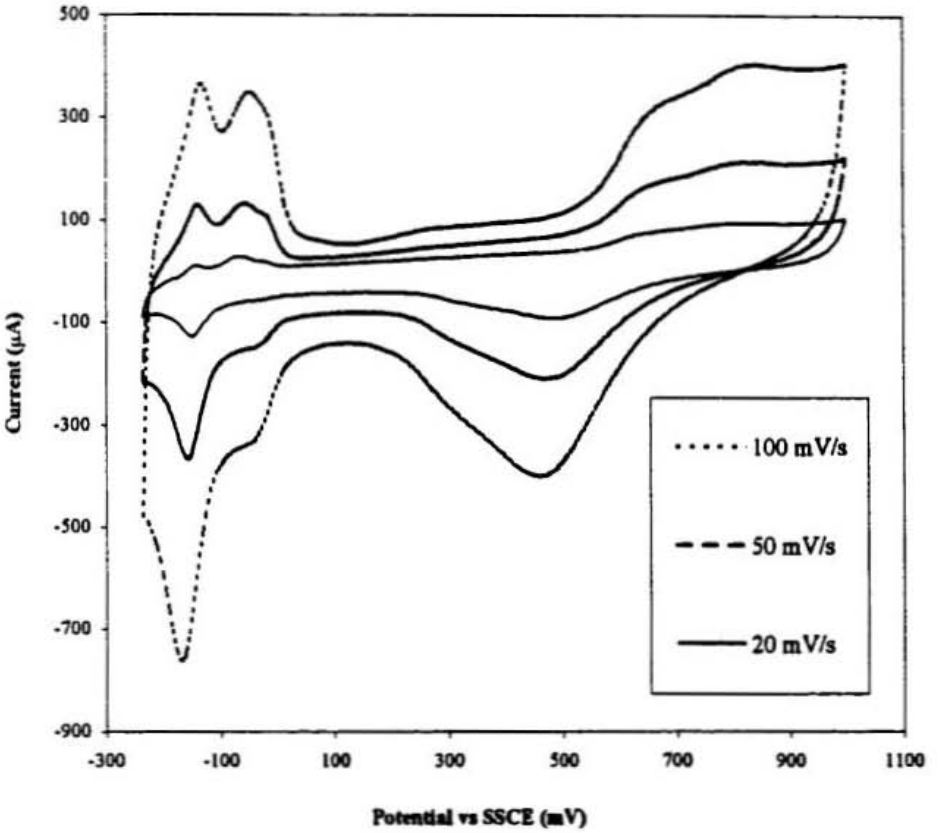

Fig. 2.9 CVs at different scan rates for a commercial 20% Pt/C coated electrode with 60 μg Pt cm^{-2} in N_2 saturated 0.5 M H_2SO_4.

adsorption/desorption region increase with scan rate. The currents at selected potentials in the adsorption region as a function of scan rate are shown in **Fig. 2.10**. These plots indicate that currents have linear relationship with scan rate.

In order to test the influence of Nafion in which the catalyst was immobilized on CVs, two volumes of Nafion solution (0.5 mL and 1 mL) were used to suspend the same mass of the commercial Pt/C catalyst. Then aliquots with the same Pt loading (1 μL of the first suspension and 2 μL of the second suspension) were applied to the electrode and CVs shown in **Fig. 2.11** were obtained. It can been seen, from the decreased areas for hydrogen adsorption/desorption and Pt oxide formation/reduction peaks at higher potentials, that doubling the amount of Nafion decreases the electroactivity of the catalyst. The reason for this is probably that too much Nafion decreases the electronic contact between catalyst particles. Schmidt has concluded that a Nafion film thickness of less than 0.5 μm at a RDE will minimize diffusion effects and avoid cumbersome mathematical modeling to calculate Pt utilization [25]. In our experiments, the thicknesses of the Nafion plus catalyst layers can be estimated to be ca. 0.4 μm and 0.8 μm, respectively for Nafion loading of 1.1 mg cm^{-2} and 2.2 mg cm^{-2}. Thus, Nafion loadings of 1.1 mg cm^{-2} were routinely used in our further work.

Fig. 2.12 shows representative CVs, in deaerated 0.5 M H_2SO_4, for 45% Pt/Q1. The CV at 100 mV/s is compared with that for the commercial 20%Pt/C catalyst in **Fig. 2.13**. For both catalysts, current waves for adsorption/desorption of hydrogen atoms on the Pt within the catalyst layer can clearly be seen in the region below +0.1 V, and Pt oxide formation/reduction waves can be seen at higher potentials. Despite the lower Pt loading used, the areas in the hydrogen adsorption/desorption region for the commercial catalyst

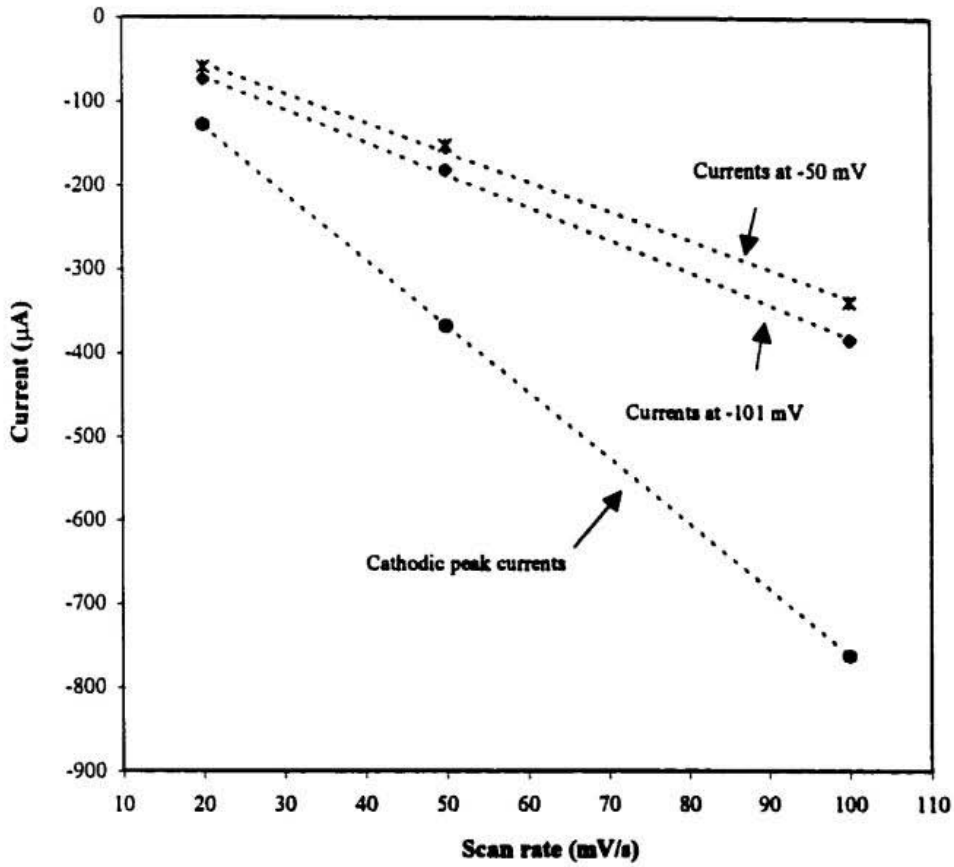

Fig.2.10 Selected currents from Fig. 2.9 as a function of scan rate.

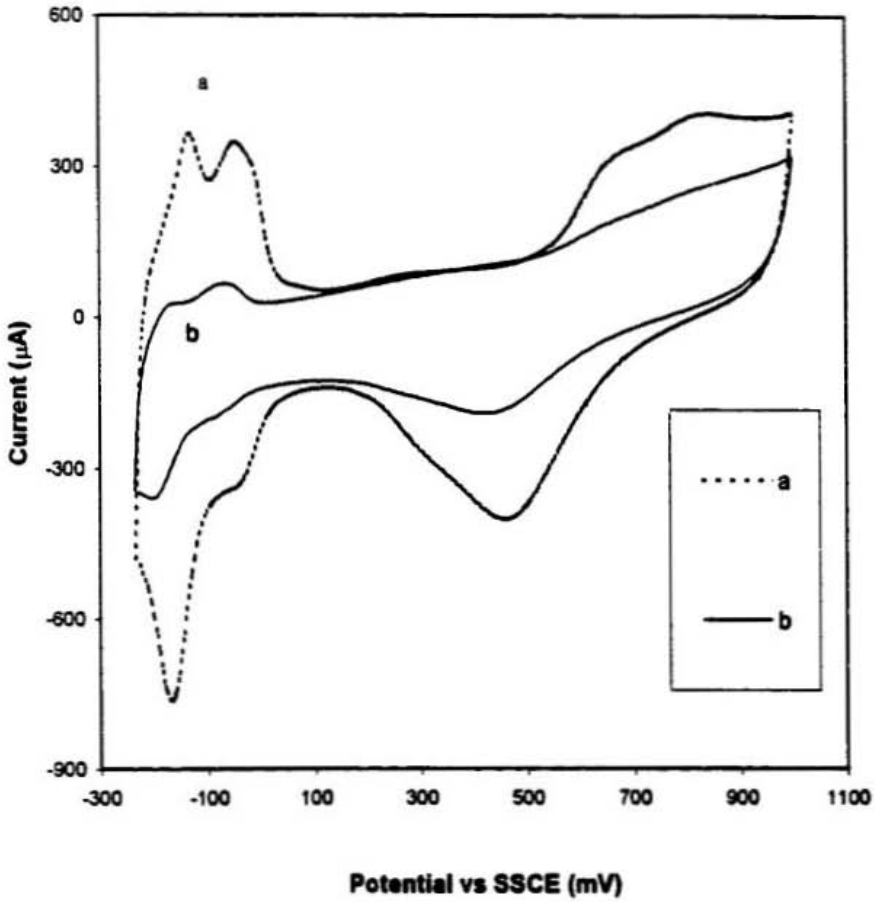

Fig. 2.11 CVs at 100 mV/s in N_2 saturated 0.5 M H_2SO_4 for 20% Pt/C coated electrodes with 60 μg Pt cm^{-2} and Nafion loadings of a, 1.1 mg cm^{-2}; b, 2.2 mg cm^{-2}.

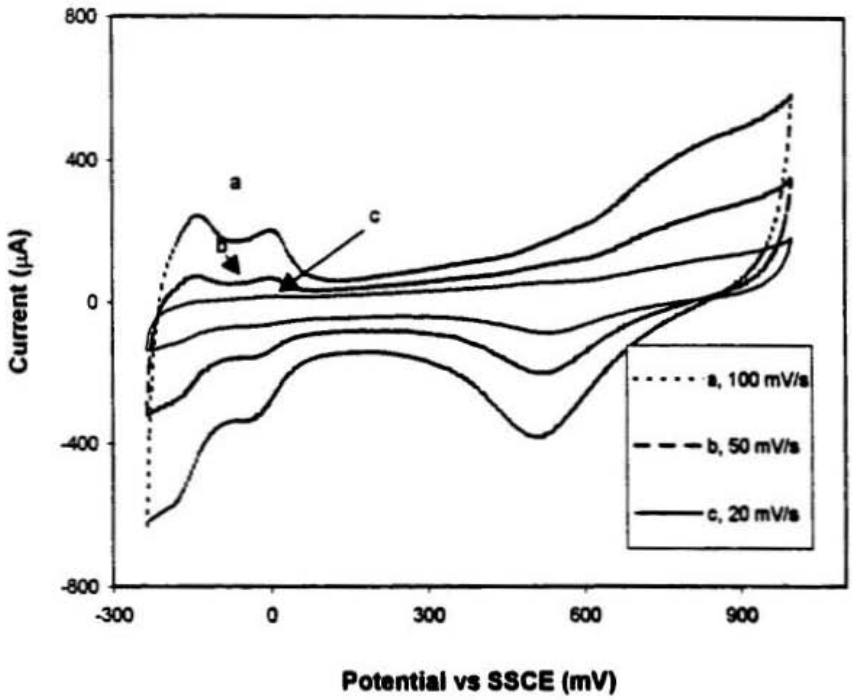

Fig. 2.12 CVs at different scan rates for a 45% Pt/Q1 coated electrode with 0.14 mg Pt cm^{-2} in N_2 saturated 0.5 M H_2SO_4.

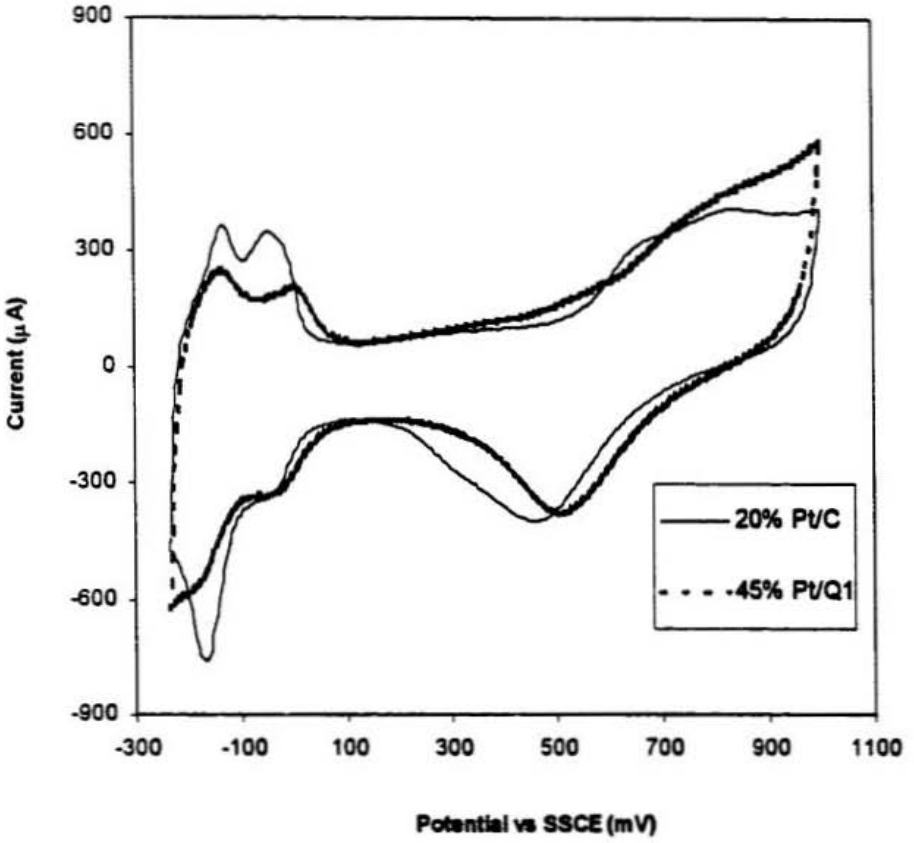

Fig. 2.13 CVs at 100 mV/s in N_2 saturated 0.5 M H_2SO_4 for 45% Pt/Q1 with 0.14 mg Pt cm^{-2} and 20% Pt/C with 60 μg Pt cm^{-2} coated electrodes.

are still larger than those for the 45% Pt/Q1 catalyst. The electrochemistry of the polymer support is masked by the dominance of the Pt surface electrochemistry.

The areas under the hydrogen adsorption/desorption regions were found to be related to both the amount of catalyst applied to the electrode (**Figs. 2.14 - 2.16**) and the catalyst loading on the support (**Fig. 2.17**). H-adsorption charges were calculated by integrating over the 0.01 V to – 0.231 V potential range and subtracting the double-layer charge (see inset of **Fig. 2.14**). A linear relationship was found between the H-adsorption charge and the volume of catalyst suspension applied to the electrode, up to ca. 2μL (**Fig. 2.15**). At higher loadings the catalyst tended to spread onto the insulating mantle and the catalyst layer also became too thick, resulting in lower charges than expected. This can be seen more clearly in **Fig. 2.16** where the CV curve for 2.0 μL of suspension shows smaller hydrogen desorption/adsorption areas than that for 1.5 μL.

The dependence on the catalyst loading on the support is more difficult to qualify. When Pt loadings below ca. 30% by mass are used, the cyclic voltammogram becomes dominated by the polymer support's electrochemistry and features due to the Pt are barely discernable (**Fig. 2.17**). However, for a fixed mass of Pt applied to the electrode (e.g. 60 $\mu g/cm^2$), the charge for H adsorption does not appear to be significantly dependent on its loading on the support (**Table 2. 3**).

2.3.3.2 Platinum utilization

Platinum utilization values were calculated as the ratio of the area of electroactive Pt, estimated from the charge under the H-adsorption waves in cyclic voltammetry, to the

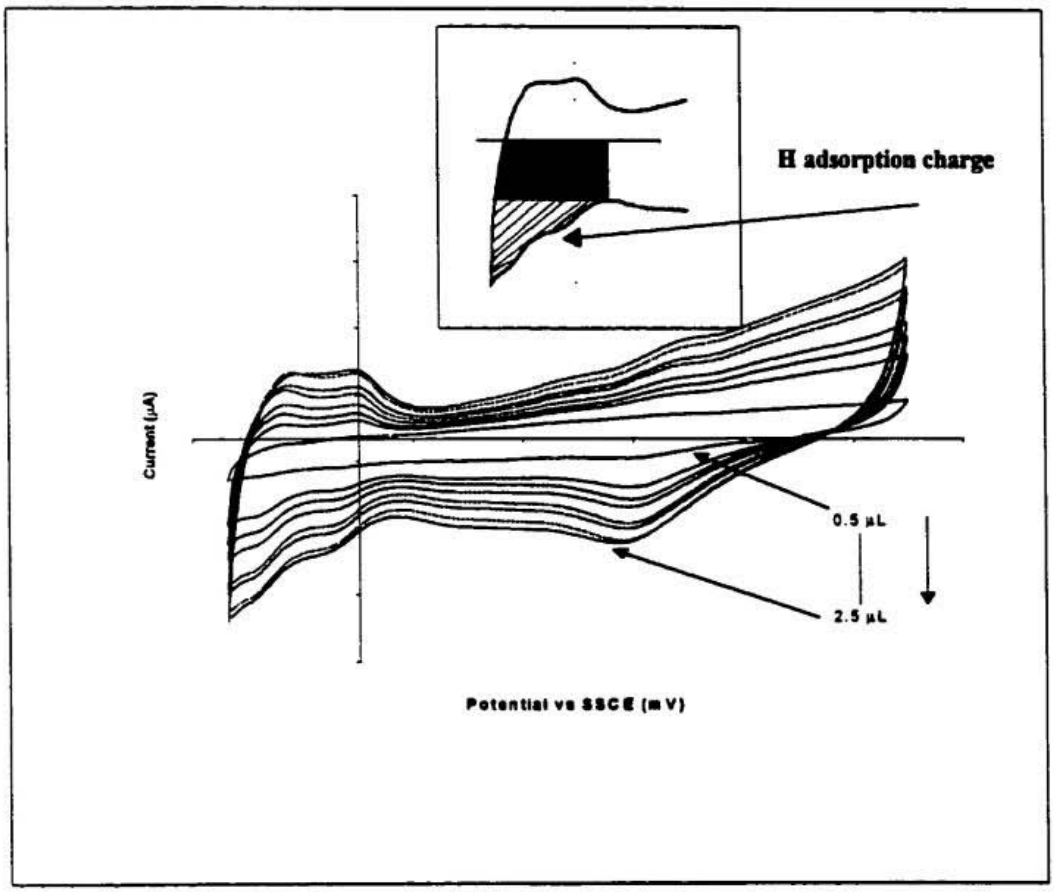

Fig. 2.14 CVs at 100 mV/s for 43% Pt/Q1 coated electrodes. Volumes of catalyst suspension used were 0.5 μL, 1.0 μL, 1.25 μL, 1.5 μL, 1.75 μL, 2.0 μL, 2.25 μL and 2.5 μL. Catalyst loading of suspension is 0.14 mg Pt μL^{-1}.

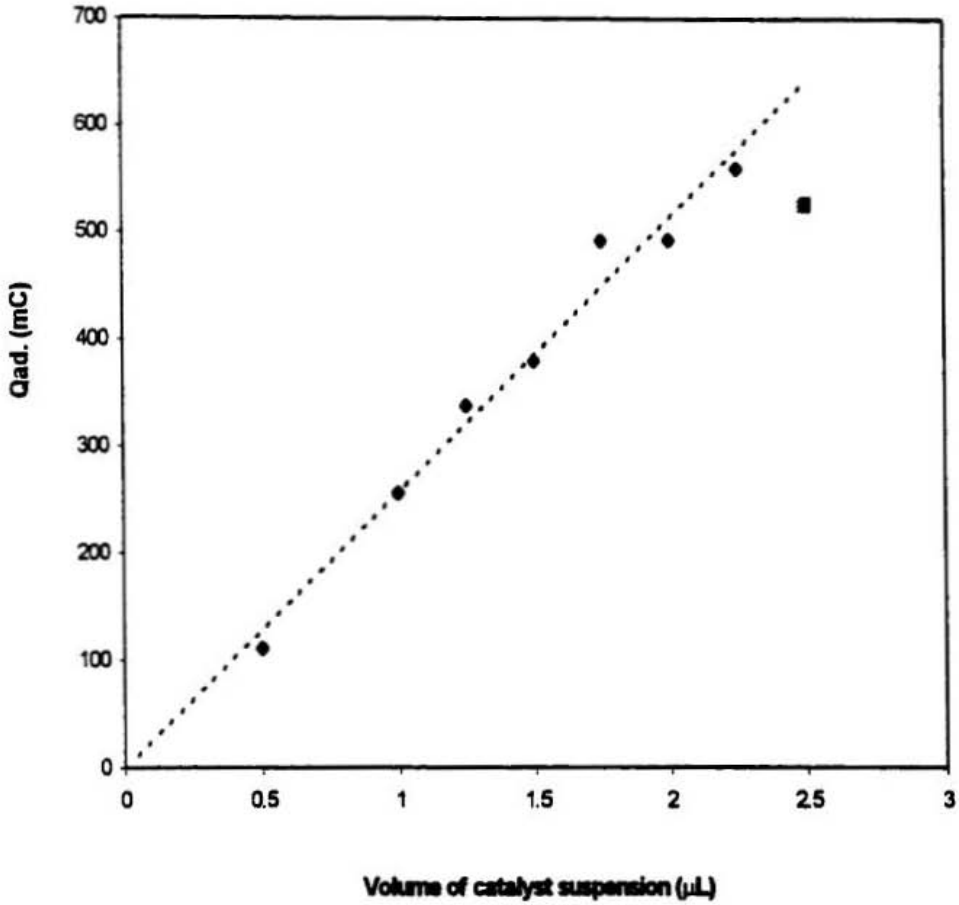

Fig. 2.15 Hydrogen adsorption coulombic charge, Qad., as a function of the volume of catalyst suspension (0.10 mg Pt μL^{-1}) applied to the electrode .

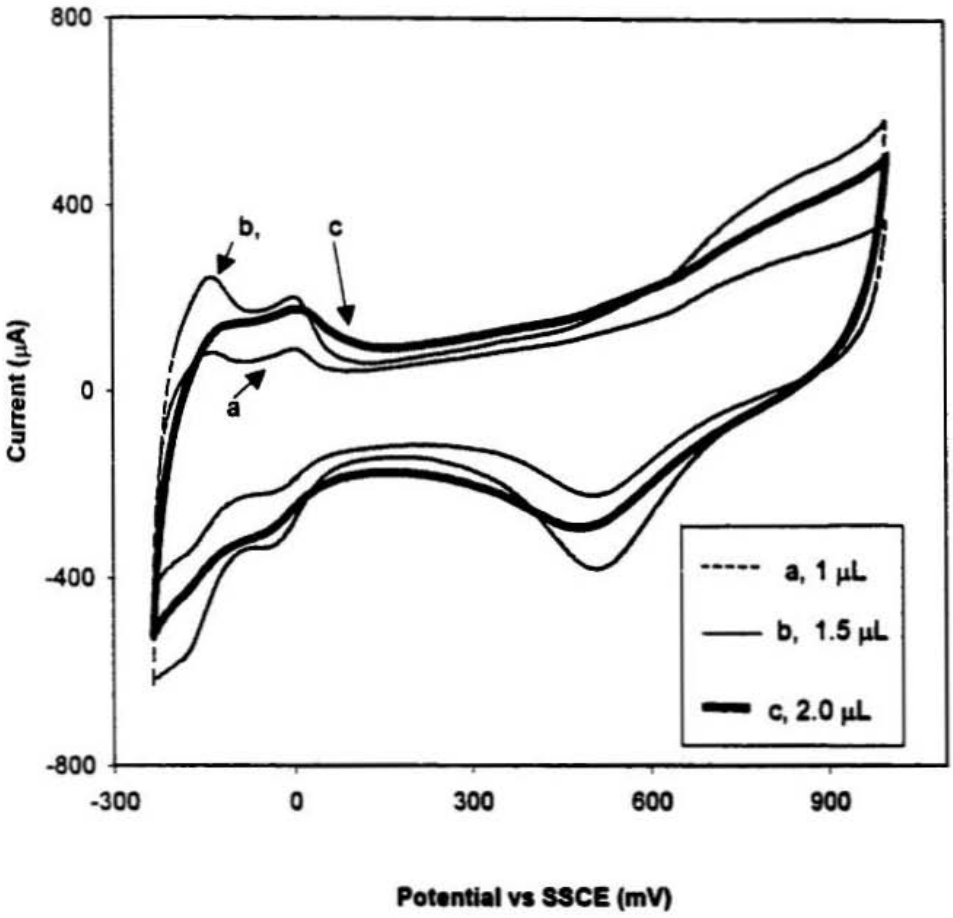

Fig. 2.16 CVs at 100 mV/s in N_2 saturated 0.5 M H_2SO_4 for 45% Pt/Q1 coated electrodes with increasing volumes of catalyst suspension (0.14 mg Pt μL^{-1}) being applied.

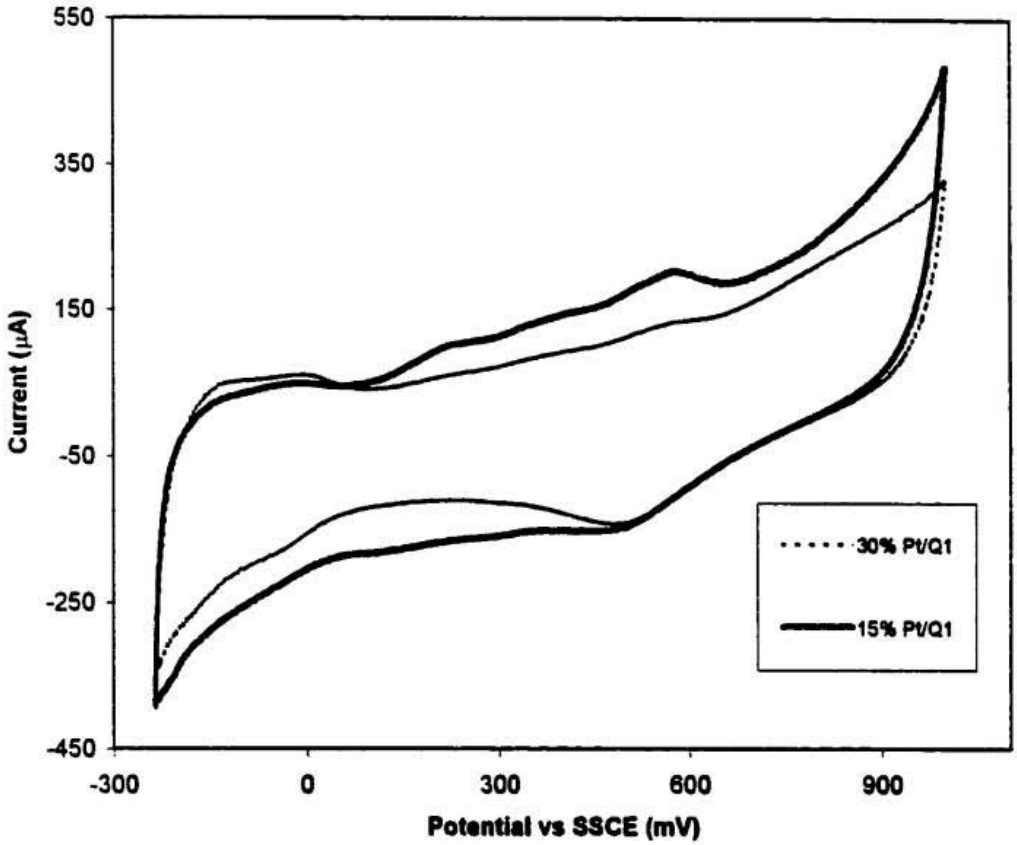

Fig. 2.17 CVs at 100 mV/s in N_2 saturated 0.5 M H_2SO_4 for 15% Pt/Q1 and 30% Pt/Q1 coated electrodes with Pt loadings of 60 μg cm^{-2} in a Nafion matrix.

total area of Pt estimated from the mean particle size (radius = r) on the assumption that the particles are spheres with surface area $4\pi r^2$. The results (**Table 2.3**) show that the commercial carbon supported catalyst shows essentially complete electroactivity of the Pt,

Catalyst	15%Pt on Q1	30%Pt on Q1	36%Pt on Q1	43%Pt on Q1	45%Pt on Q1	20%Pt on C
Average Pt particle diameter (nm)	7.0	6.3	7.4	7.6	6.3	4.0
H Adsorption[a] (mC)	0.22	0.2	0.19	0.12	0.17	0.78
Active Pt area[b] (cm^2)	1.05	0.97	0.9	0.56	0.82	3.71
Pt utilization[c]	62%	51%	56%	36%	43%	125%

a. Cathodic charge between +0.104 and –0.231 with the current at +0.104 V subtracted as background.

b. Assuming 0.21 mC per cm^2 of Pt.

c. Based on the assumption that the Pt particles are spherical and of uniform radius.

Table 2.3. Hydrogen adsorption charges and platinum utilizations for Q1-supported catalysts and a commercial carbon catalyst. All Pt loading were 60 $\mu g/cm^2$.

while for polymer supported catalysts approximately 50% of the Pt is inactive. The fact that the estimated utilization is greater than 100% for the Pt/C catalyst can be attributed to contributions from background currents (including that for H_2 evolution) to the measured H-adsorption charge.

Schmidt et al [25] have used a more sophisticated method for estimating total area, based on the particle size distribution from transmission electron microscopy. Their sample of 20% Pt on XC-72 from Etek had an average Pt diameter of 3.7 nm and a calculated dispersion (surface atoms/total atoms) of 26%. This study method, based on the mean diameter only, gives a dispersion of 29% for 3.7 nm particles.

The Pt utilizations for the Q1-supported catalysts show no significant dependence on Pt loading on the support (**Table 2.3**), nor on loading on the electrode (inferred from the data in **Fig. 2.15**). The variations seen in **Table 2.3** are within experimental uncertainty, which is large because of difficulties in controlling the synthesis conditions, aging of the catalyst sample, and electrode preparation. The magnitude and potential dependence of background currents was quite variable (see **Fig. 2.17** for example), leading to considerable uncertainty in the H-adsorption charge.

The low utilizations for the polymer-supported catalysts appear to arise from two main causes: poor electronic contact of Pt particles with the polymer support and blocking of the Pt surface by the polymer. The former effect is implicated by the fact that adding carbon black (Vulcan XC-72) to the catalyst suspension used to prepare a Pt/Q1 electrode increases the magnitude of the H-adsorption waves (**Fig. 2.18** and **Fig. 2.19**), although it does not lead to full utilization of the Pt. **Fig. 2.18** illustrates an experiment in which two 2

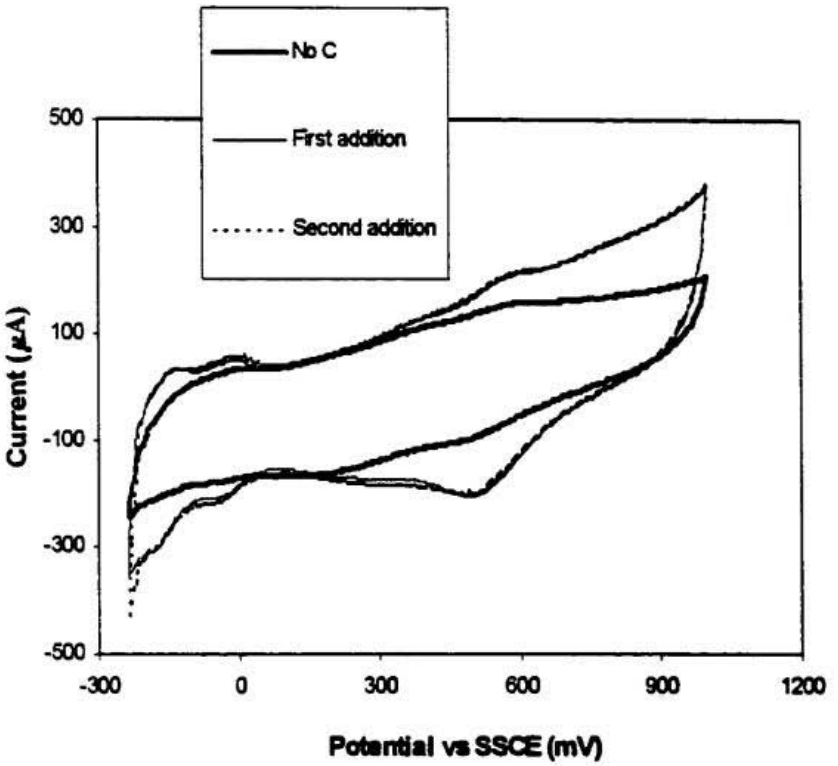

Fig. 2.18 CVs at 100 mV/s in N_2 saturated 0.5 M H_2SO_4 for 43% Pt/Q1 coated electrodes without C and with C, 80 μg C cm^{-2} (first) and 0.16 mg C cm^{-2} (second). Loadings of Q1 and Pt (60 μg cm^{-2}) are the same in all cases.

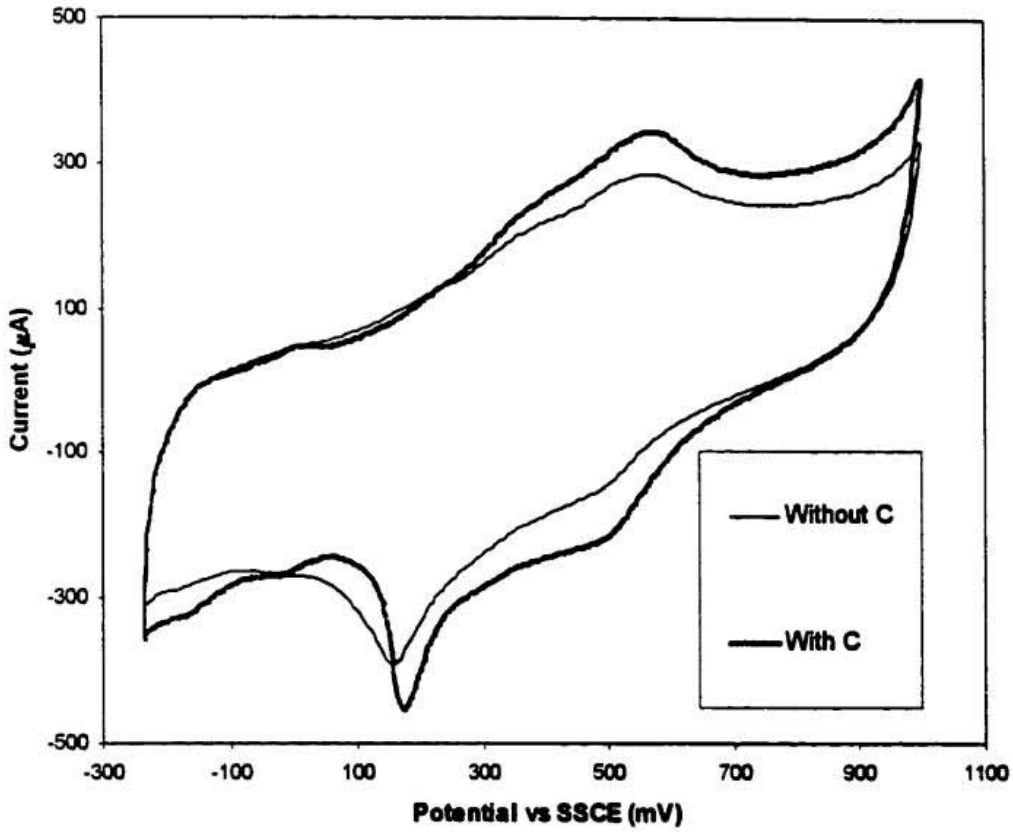

Fig. 2.19 CVs at 100 mV/s in N_2 saturated 0.5 M H_2SO_4 for 21% Pt/Q1 coated electrodes without C and with C (80 $\mu g/cm^2$) in supports. Q1 and Pt loadings (60 $\mu g/cm^2$) are same for both electrodes.

mg portions of carbon black were added to the 0.5 mL suspension of 43% Pt/Q1 catalyst before application onto the carbon disc electrode and tested. The first addition of carbon increased the utilization of Pt from 36% to 74%. However, the hydrogen adsorption/desorption areas change little with addition of the second portion of carbon black, indicating that a limit was reached. In **Fig. 2.19**, the same amount of carbon black was also added to 21% Pt/Q1, producing better defined hydrogen adsorption peaks. These changes are not thought to be a result of poor electronic conductivity of the Q1 support, since conductivities of pressed pellets (dry) of the catalysts (0.03 to 0.9 S cm^{-1}, **Table 2.1**) are much higher than are needed to support the currents observed in cyclic voltammetry. Thus, we conclude that some Pt particles must be electronically isolated from the polymer support either by physical separation or by poorly conducting segments of the support.

The blocking or poisoning of Pt sites by the Q1 support was demonstrated by two experiments. In the first experiment uncatalysed Q1 was added to the suspension used to prepare a Pt/C electrode, and resulted in suppression of the H-adsorption/desorption waves by ca. 50% (**Fig. 2.20**). The second experiment involved coating of a Pt disc with the supernatant of a Q1 suspension in Nafion solution, which did not result in suppression of its H-adsorption/desorption waves (**Fig. 2.21**). This indicates that the blocking appears to be by the polymer itself, rather than a soluble impurity.

Another two factors investigated in this work for Pt/Q1 catalysts were the amount of Nafion used and whether drying the catalyst before its addition to the Nafion solution influenced H-adsorption/adsorption. As for the commercial catalyst, increasing the amount of Nafion in a polymer-supported catalyst layer for a fixed mass of catalyst suppressed the H-adsorption/desorption waves (**Fig. 2.22**). When Pt/Q1 catalysts were stored in the dry

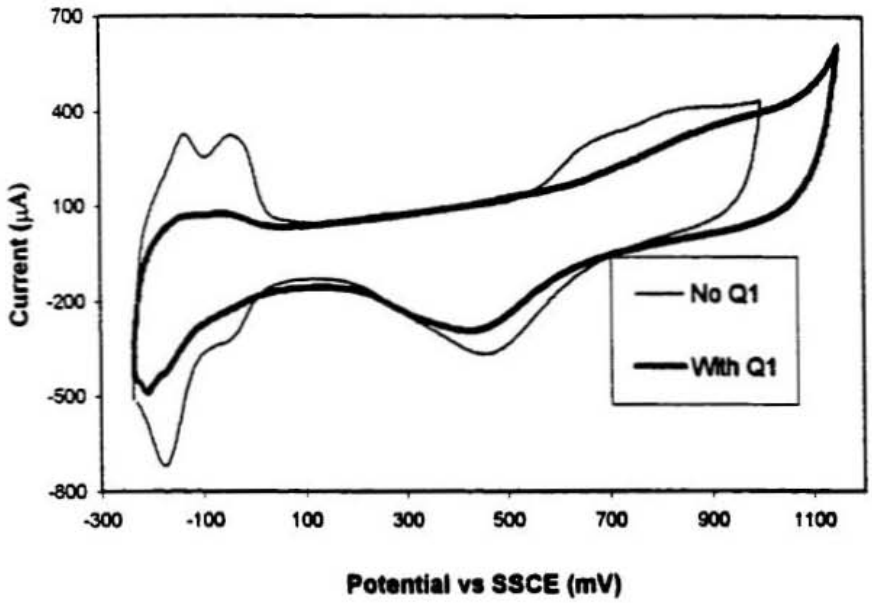

Fig. 2.20 CVs at 100 mV/s in N_2 saturated 0.5 M H_2SO_4 for 20% Pt/C (60 μg Pt/cm^2) coated electrodes without Q1 and with Q1 (0.42 mg Q1 cm^{-2}).

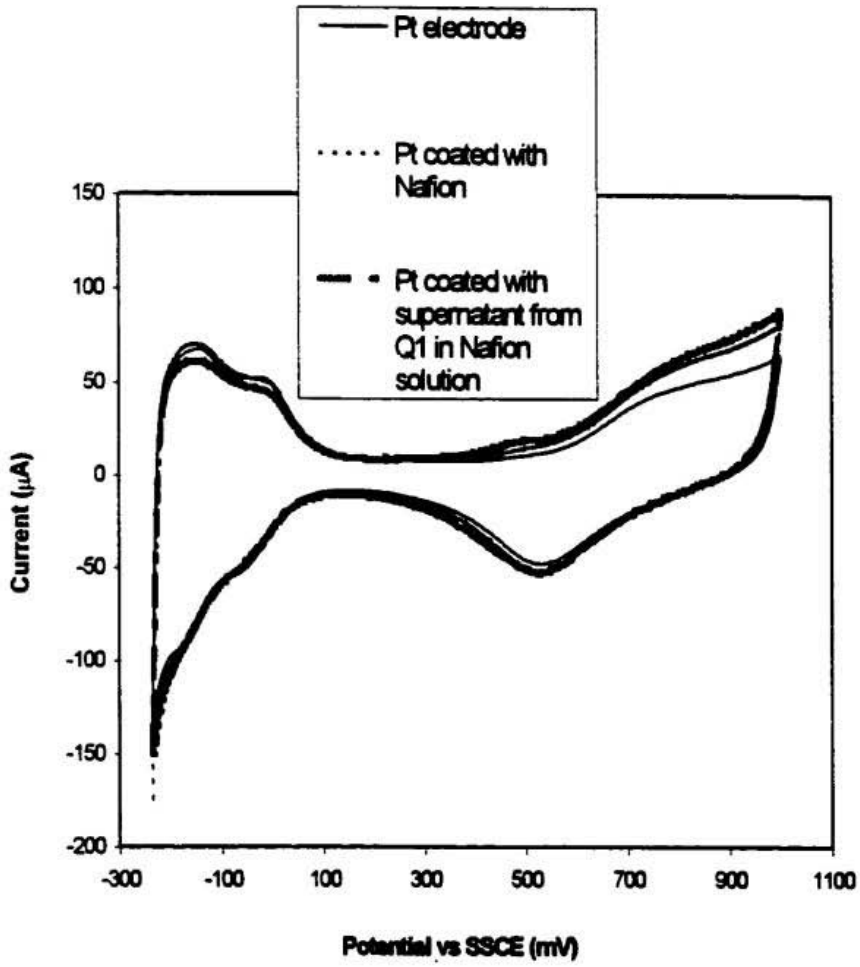

Fig. 2.21 CVs at 100 mV/s in N_2 saturated 0.5 M H_2SO_4 for a clean Pt disc electrode, and Pt electrodes coated with Nafion and the supernatant from a suspension of Q1 in Nafion solution.

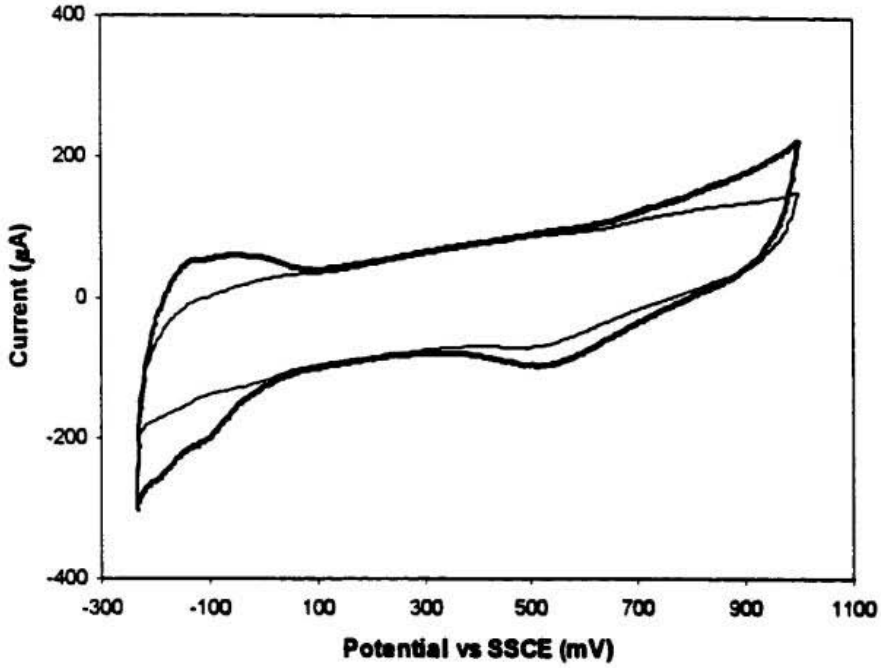

Fig. 2.22 CVs at 100 mV/s in N_2 saturated 0.5 M H_2SO_4 for electrodes coated with 45% Pt/Q1 (100 μg Pt cm^{-2}) in different Nafion loadings. Light curves, 2.2 mg Nafion cm^{-2}; bold curves, 1.2 mg Nafion cm^{-2}.

state before use, the utilization of Pt was also reduced (**Fig. 2.23**). Thus, it can be concluded that poor electronic contact of Pt particles with the polymer support is in part responsible for the low Pt utilization and low performance in GDEs.

2.3.3.3 Oxygen polarization curves.

Polarization curves for O_2 reduction were recorded by linear-sweep voltammetry at a sweep rate of 10 mV/s over a range of rotation rates (250-1500 rpm). Voltammograms were recorded in both N_2 and O_2 saturated 0.5 M H_2SO_4 solutions. The curves obtained under N_2 were subtracted from those obtained in the O_2 saturated solution as a background correction [24]. Voltammograms in N_2 saturated and O_2 saturated solution for 20% Pt/C and 45% Pt/Q1, both recorded in the cathodic sweep direction, are presented in **Fig. 2.24** and **Fig. 2.25**. When the curve in N_2 saturated solution is subtracted from the curve in O_2 saturated solution, the actual polarization curve for O_2 reduction is obtained (heavy lines in Figures). Typical corrected polarization curves for the above two catalysts at different rotation rates recorded in both cathodic and anodic sweep directions are shown in **Fig. 2.26** and **Fig. 2.27.** The hysteresis of the polarization curves for cathodic and anodic directions shows that the oxygen reduction reaction is faster on reduced than on oxidized electrode surface, which is characteristic of Pt [32]. Typical corrected polarization curves for the commercial carbon supported catalyst and several Q1-supported catalysts are shown in **Fig. 2.28**.

Levich plots of limiting currents I_{lim} vs. $\omega^{1/2}$ (ω = angular rotation rate) were slightly curved, presumably due to a slight mass transport limitation in the Nafion matrix, but

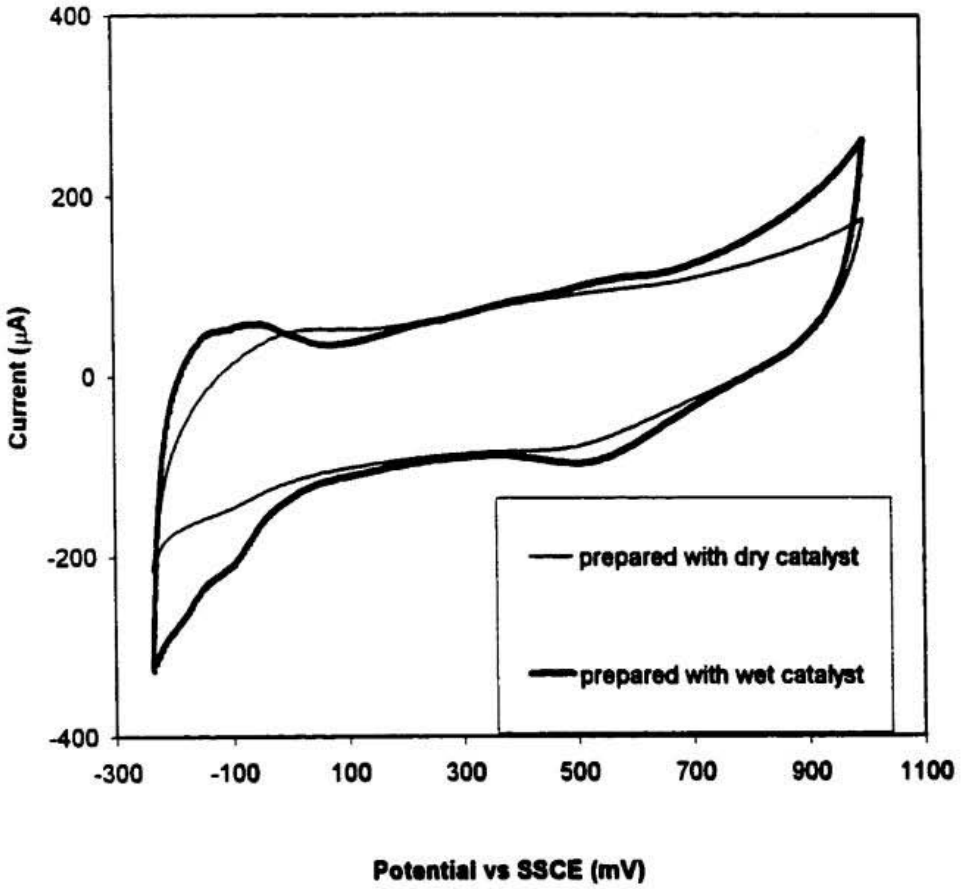

Fig. 2.23 CVs at 100 mV/s for electrodes coated with dry and wet 30% Pt/Q1 catalyst (100 μg Pt cm^{-2}) for both in N_2 saturated 0.5 M H_2SO_4.

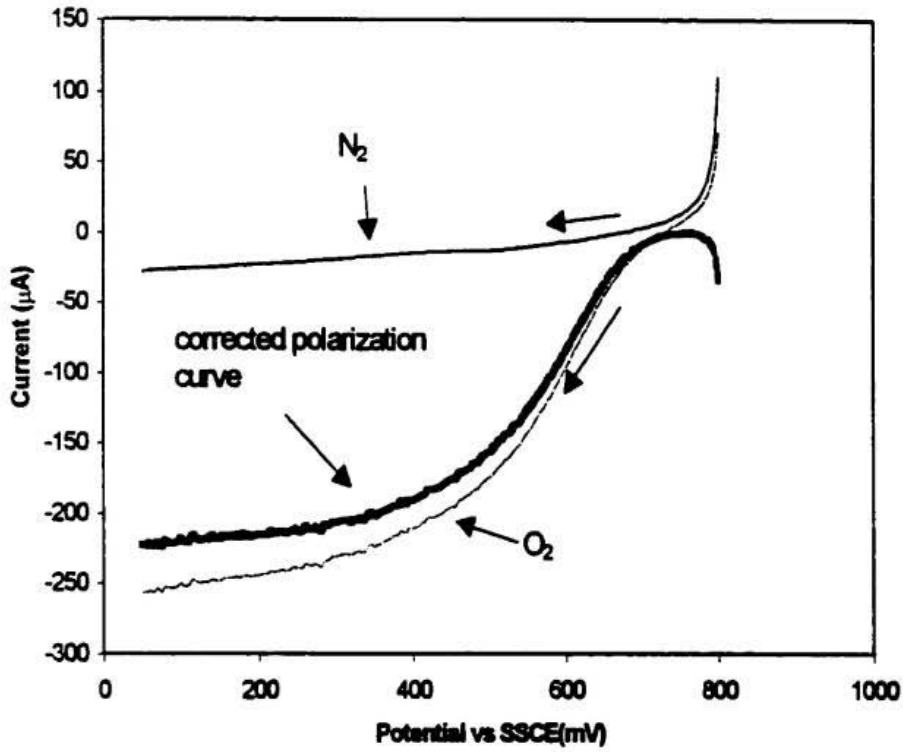

Fig. 2.24 Voltammograms (cathodic scan at 10 mV/s , rotation rate 1000 rpm of a 45% Pt/C1 coated electrode with 138 μg Pt cm^{-2} in N_2- and O_2- saturated 0.5 M H_2SO_4 and corrected polarization curve for O_2 reduction.

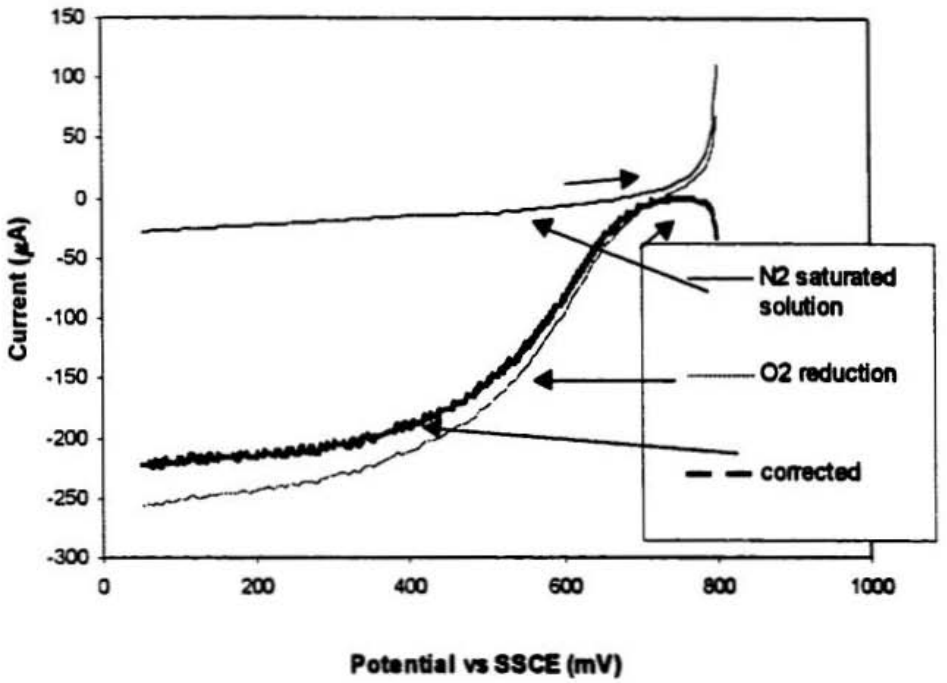

Fig. 2.25 Voltammograms (cathodic scan at 10 mV/s , rotation rate 1000 rpm) of a 20% Pt/C coated electrode with 40 μg Pt cm^{-2} in N_2- and O_2- saturated 0.5 M H_2SO_4 and corrected polarization curve for O_2 reduction.

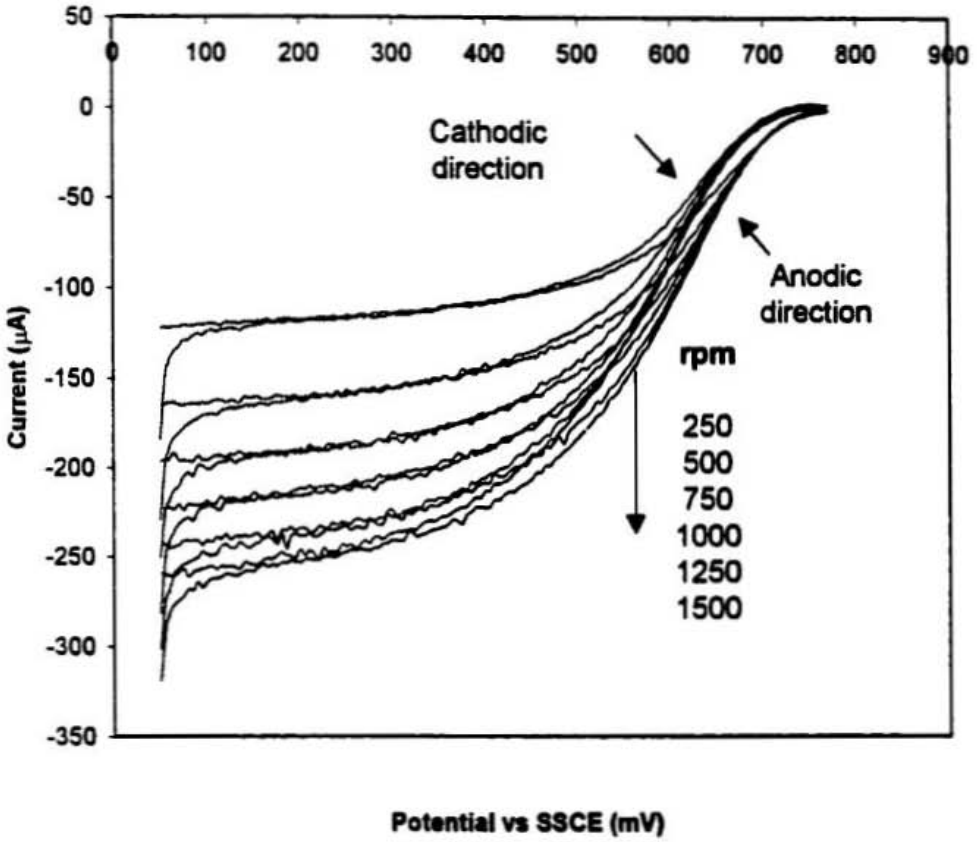

Fig. 2.26 Background corrected polarization curves for O_2 reduction at a 45% Pt/Q1 coated electrode with 138 μg Pt cm^{-2} at different rotation rates in cathodic and anodic sweep directions in 0.5 M H_2SO_4.

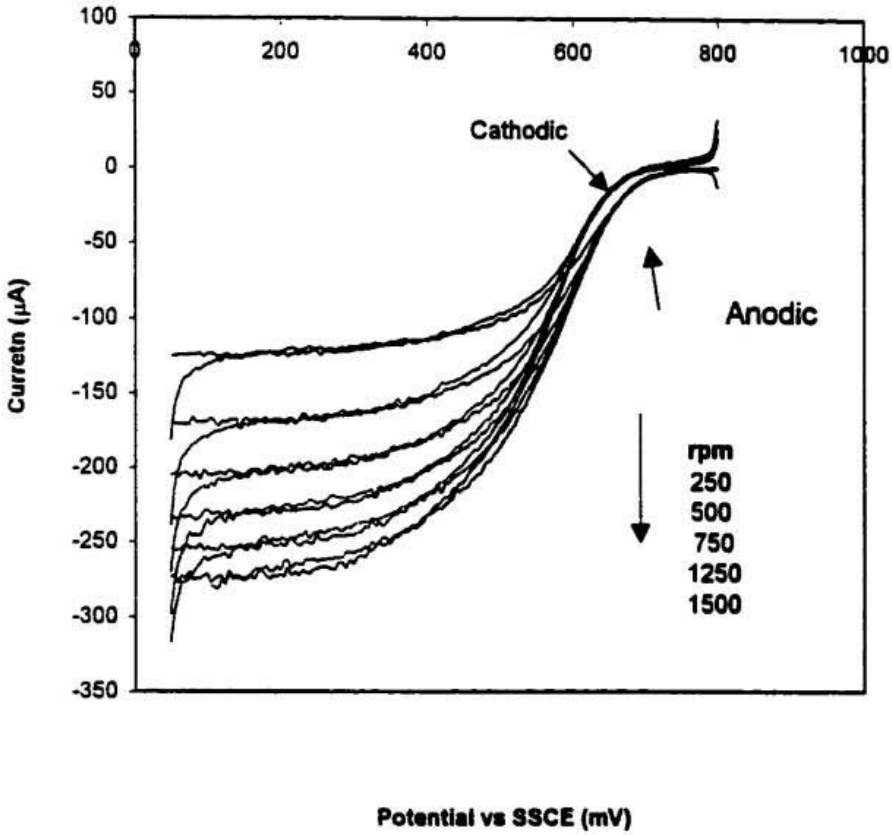

Fig. 2.27 Background corrected polarization curves for O_2 reduction at a 20% Pt/C coated electrode with 40 μg Pt cm^{-2} at different rotation rates in cathodic and anodic sweep directions in 0.5 M H_2SO_4.

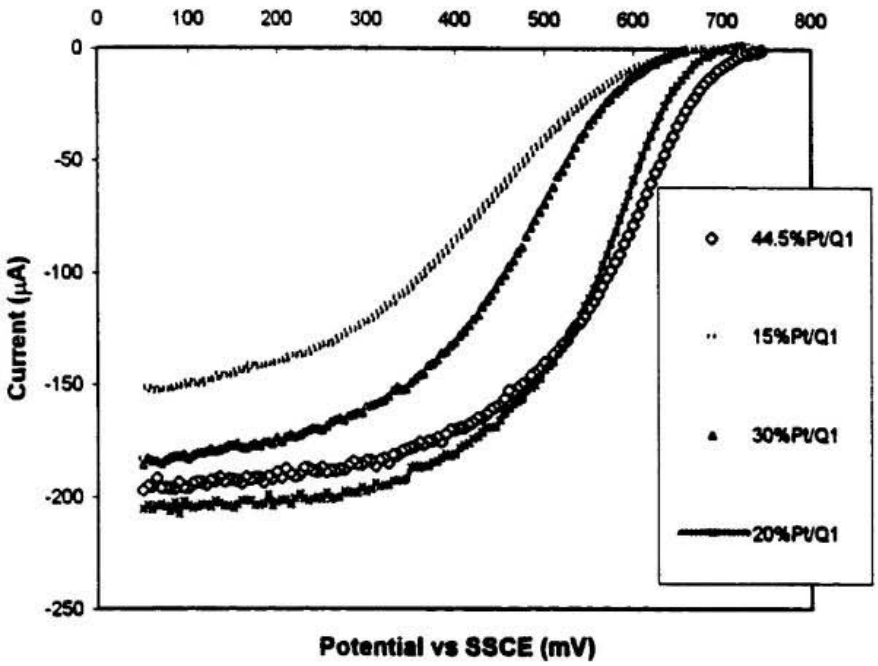

Fig. 2.28 Background corrected O_2 polarization plots (cathodic scans at 750 rpm) for glassy carbon disc electrodes coated with 45% Pt/Q1, 138 μg Pt cm^{-2}, 15% Pt/Q1, 30 μg Pt cm^{-2}, 30% Pt/Q1, 73 μg Ptcm^{-2}, and 20% Pt/C, 40 μg Pt cm^{-2} in a Nafion matrix.

inverse Levich plots of I^{-1} vs. $\omega^{-1/2}$ were linear and parallel for potentials from ca. 0.6 V to the limiting current region (eg. **Fig. 2.29**). The parallel lines in **Fig. 2.29** indicate that the number of electrons transferred does not change significantly with potential over the range studied and that the limiting currents in **Fig. 2.27** and **Fig. 2.28** should obey the Levich equation

$$I_{lim} = 0.620nFAD_0^{2/3}\omega^{1/2}\nu^{-1/6}C^*_o \qquad \textbf{2.6}$$

Where n is the number of electrons transferred per O_2 molecule, F is Faraday's constant, A the electrode surface area, C^*_o is the concentration of dissolved O_2 in the solution, D_0 is the diffusion coefficient of dissolved O_2 in the solution, and ν is the kinematic viscosity of the solution. According to **Eq. 1.2**, the value of n should be close to 4. According to the literature, C^*_o is ca. 1.2 mol m^{-3} [33], D_0 is 1.9 10^{-9} m^2 s^{-1} [33] and ν is close to 0.01 cm^2 sec^{-1} [34]. Then from the slopes of our inverse Levich plots, n is ca. 3.7 for 45% Pt/Q1 and ca. 3.4 for 20%Pt/C, demonstrating the validity of the RDE methods applied in study.

In theory, Tafel plots should be constructed from the kinetic currents given by the intercepts of inverse Levich plots. However, errors in the data from inexact background subtraction, aging of the electrode, and variations in conditions, can be magnified in this way, resulting in inaccuracy. Therefore a procedure was followed [24] in which the polarization curves in **Fig. 2.26** and **Fig. 2. 27** are corrected for mass transport effects by using **eq. 2.7**, and then plotted in Tafel form.

$$I_{kin} = I_{Lim}I/(I_{Lim} - I) \qquad \textbf{2.7}$$

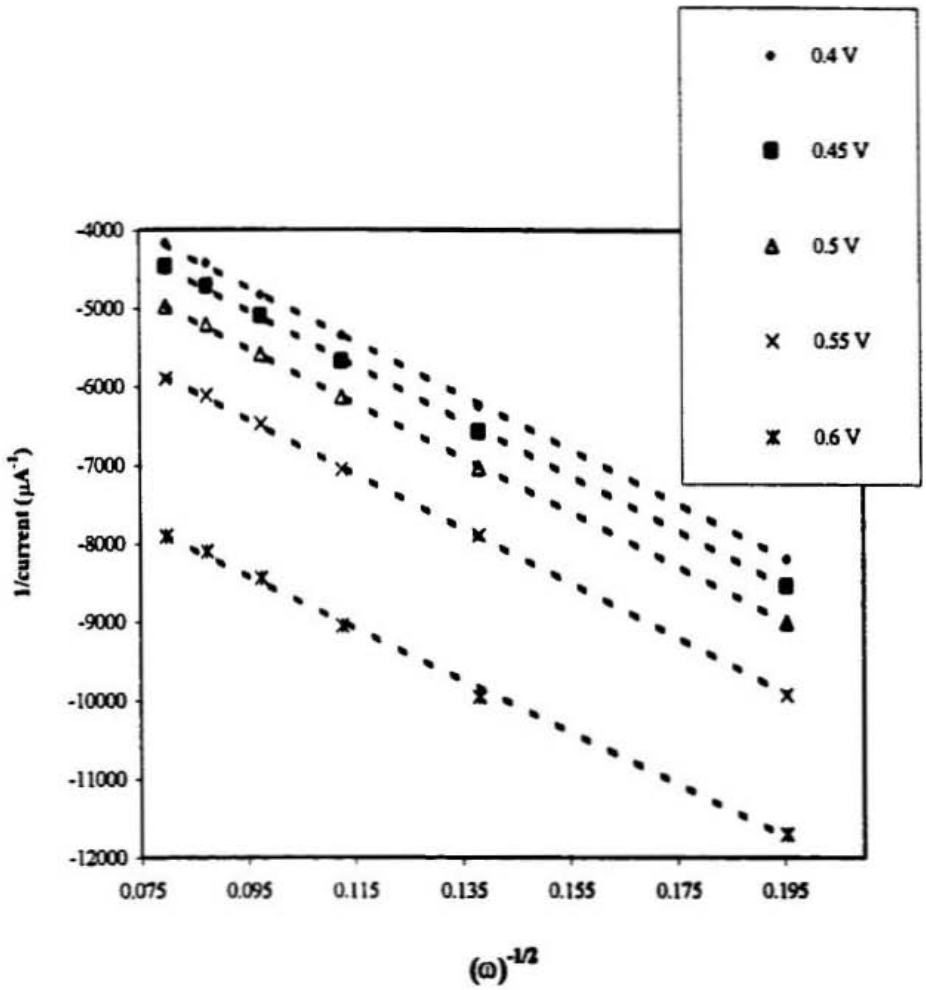

Fig. 2.29 Inverse Levich plots for O_2 reduction at 45% Pt/Q1 coated electrodes in anodic scan.

where I_{kin} is the kinetic current. **Fig. 2.30** shows Tafel plots ($\log(-I_{kin})$ vs. V)) [24] for oxygen reduction at a 44.5% Pt/Q1 coated electrode, obtained at various rotation rates, and for potential scans in both cathodic and anodic directions. At low currents, the Tafel plots obtained at different rotation rate overlap very well and are reasonably linear, but there is a clear dependence on the scan direction. At high currents, the plots do not exactly overlap but are reasonably linear and do not show any systematic differences. The scatter in this region can be attributed to errors arising from the mass transport correction (**eq. 2.7**) which will become larger as the current approaches the limiting current.

Slopes from the Tafel plots shown in **Fig. 2.30**, similar plots obtained with 20% Pt/C and other Pt/Q1 catalysts (see **Fig. 2.31**), and literature results for the Pt/C catalyst are shown in **Table 2.4**.

Catalyst	Tafel slope (mV decade^{-1})		
	low current cathodic scan	low current anodic scan	High current
45% Pt on Q1	-90	-110	-200
30% Pt on Q1	-66	-108	-159
15% Pt on Q1	-56	-130	-177
20% Pt on C	-80	-100	-200
20% Pt on C [24]	-60	-80	-180

Table 2.4. Tafel slopes for oxygen reduction at polymer and carbon supported catalysts.

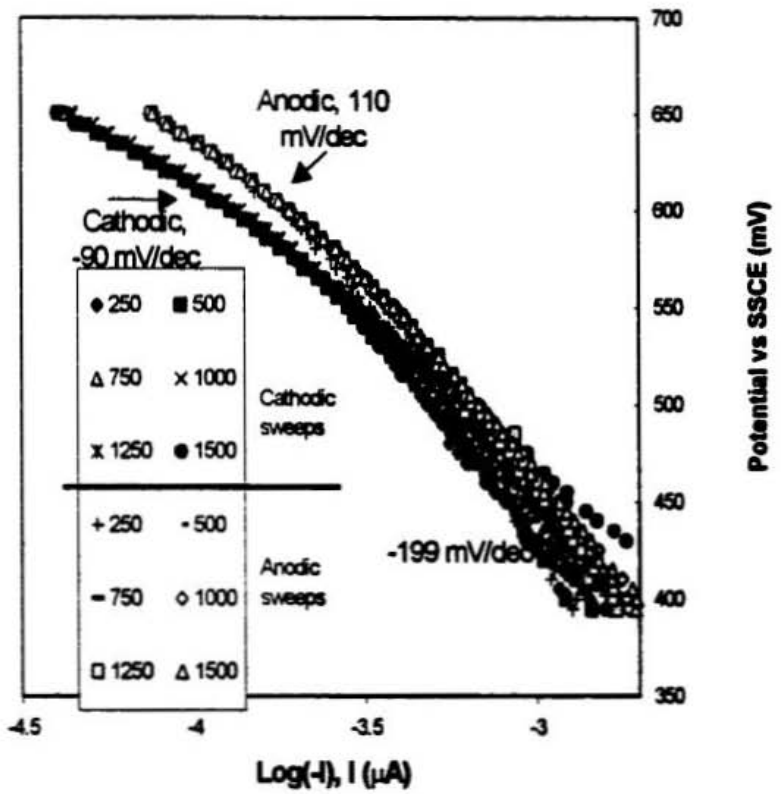

Fig. 2.30 Tafel plots for O_2 reduction (cathodic and anodic scans) at 45% Pt/Q1 coated electrodes in 0.5 M H_2SO_4 at different rotation rates (250 - 1500 rpm).

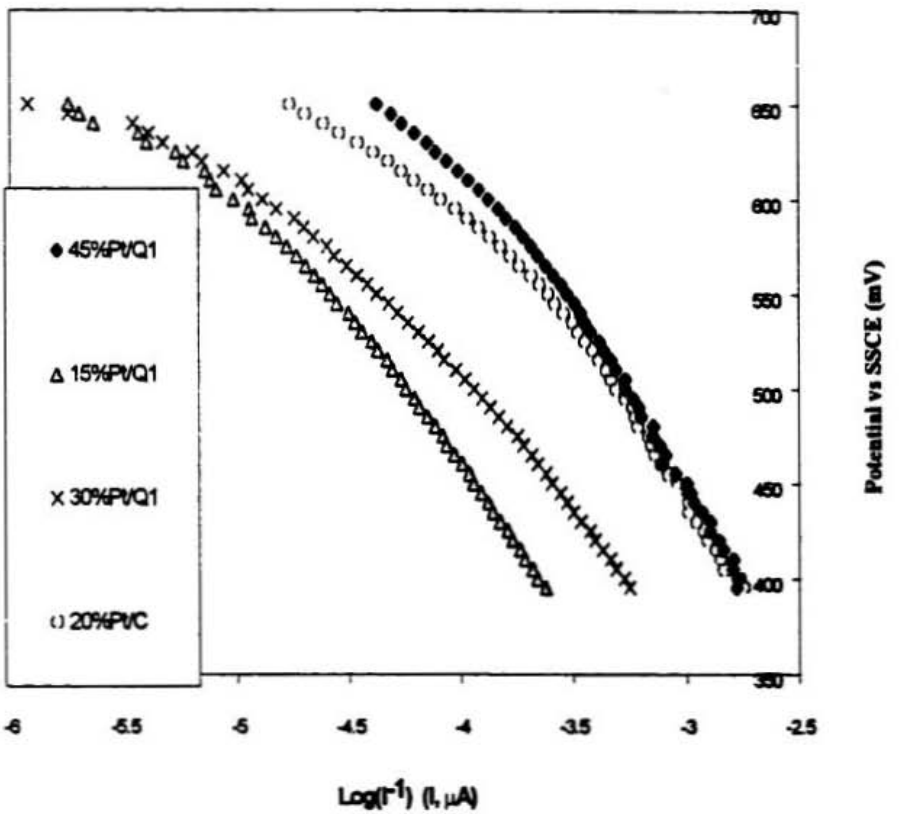

Fig. 2.31 Tafel plots (cathodic sweeps at 750 rpm) for glassy carbon electrodes coated with 15%, 30%, 45% Pt/Q1 and 20% Pt/C catalysts as in Fig. 2.28.

Tafel slopes for both the carbon and Q1 supported catalysts parallel those reported by Gojkovic et al in the Nafion matrix [24], although some are slightly higher. The high slopes at high currents for the 45% Pt/Q1 and Pt/C electrodes may be due to slightly lower mass transport rates in the Nafion matrix [24], while at low currents they are more likely due to errors arising from the background correction. Reliable data was not obtainable at such low overpotentials as Gojkovic et al, and so less data was available to define low current slopes. However, it can reasonably be concluded from the data in **Table 2.4** that the polymer-supported catalysts follow the same kinetics as the Pt/C catalysts. The similarity of the results is stressed by comparing Tafel plots obtained under the same condition as in **Fig. 2.31.** Within experimental error, the curves shown in **Fig. 2.31** can be regarded are approximately parallel. Their relative positions on the current axis can be attributed mainly to differences in active Pt areas, as shown by the data in **Table 2.5** for these and other electrodes.

Catalyst (and Pt loading($\mu g\ cm^{-2}$))	Active Pt area (cm^{-2})	Pt utilization	$-I_{kin,\ 600}$	$I_{kin,\ 600}$/active area ($mA\ cm^{-2}$)
45% Pt on Q1 (140)	1.5	35%	134	87
30% Pt on Q1 (73)	0.8	34%	13.1	30
15% Pt on Q1 (30)	0.3	37%	9.7	17
20% Pt on C (40)	2.7	135%	82	31

Table 2.5. Active Pt areas, oxygen polarization currents at 600 mV ($-I_{kin,600}$), and Pt utilizations for selected electrodes.

The current at 600 mV has been arbitrarily taken as a measure of the kinetic activity, in place of the exchange current that should strictly be used, since extrapolation to the equilibrium potential in which net current is zero would result in unacceptable uncertainty. Choice of a different reference potential within the range studied would not materially affect our conclusions.

The key parameter in **Table 2.5** is the ratio of the kinetic current ($-I_{kin,\ 600}$) to the active Pt area. The value for the carbon supported catalyst falls within the range of those for the polymer supported catalysts, indicating that the real current density (and exchange current density) is similar at both types of catalyst. However, a much higher Pt loading is needed for polymer supported catalysts to match the current delivered by a Pt/C electrode. This arises mainly from the poor Pt utilization of the polymer-supported catalysts (**Table 2.3**), and in part from their larger Pt particle sizes (lower Pt dispersion; see **Table 2.3**).

2.3.4 Pt/C catalysts prepared by chemical deposition

Some carbon-supported catalysts have been also prepared as outlined in Section 2.2. Cyclic voltammograms of these Pt/C catalysts had very small hydrogen adsorption/desorption peaks (**Fig. 2.32** and **Fig. 2.33**), indicating poor Pt utilization. However, heating catalysts prepared by Method 2 at reflux in concentrated nitric acid for ca. 40 min as described by Jia [13] produced more active materials (**Fig. 2.32**). Surprisingly, this treatment did not significantly increase the hydrogen adsorption/desorption charge for catalysts prepared by Method 1 (**Fig. 2.33**).

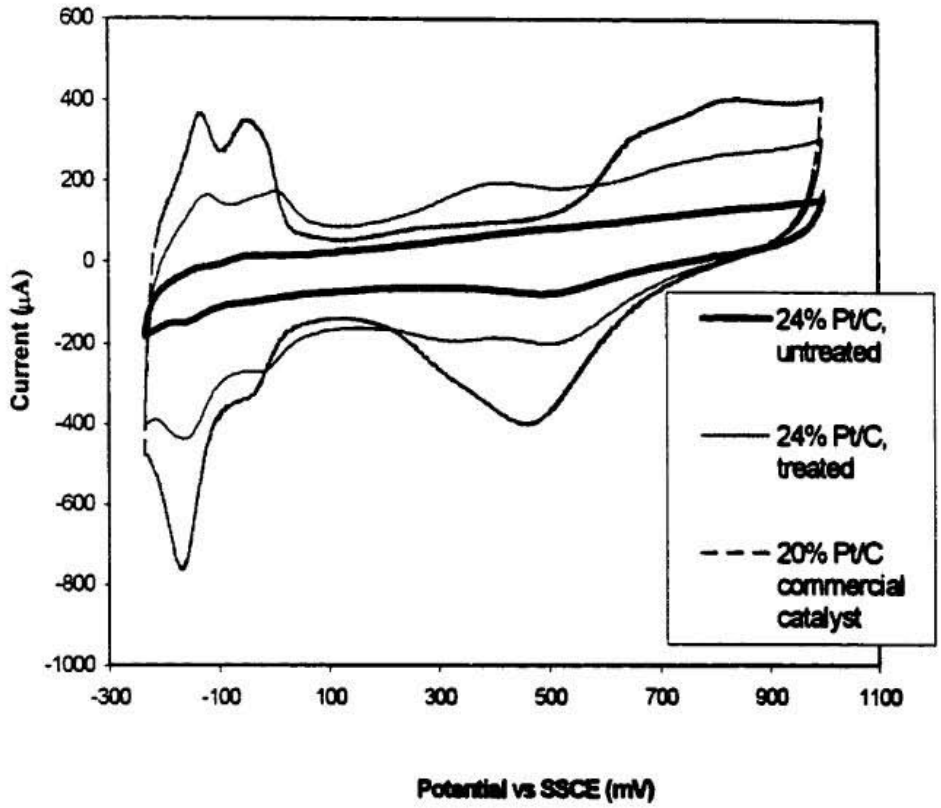

Fig. 2.32 CVs at 100 mV/s in N_2 saturated 0.5 M H_2SO_4 of glass carbon electrodes coated with commercial 20%Pt/C (40 μg cm^{-2}) catalyst and one of our Method 2, 24% Pt/C (60 μg cm^{-2}) catalysts before and after treatment with HNO_3.

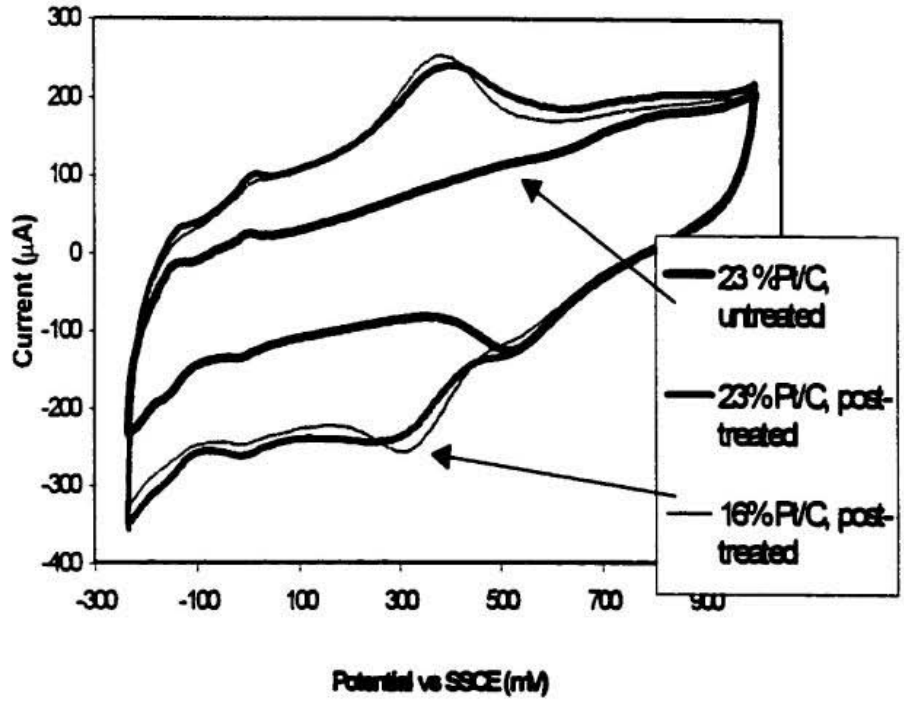

Fig. 2.33 CVs at 100 mV/s in N_2 saturated 0.5 M H_2SO_4 of glassy carbon electrodes coated with some catalysts prepared by Method 1 (60 μg Pt cm^{-2}) before and after treatment with HNO_3.

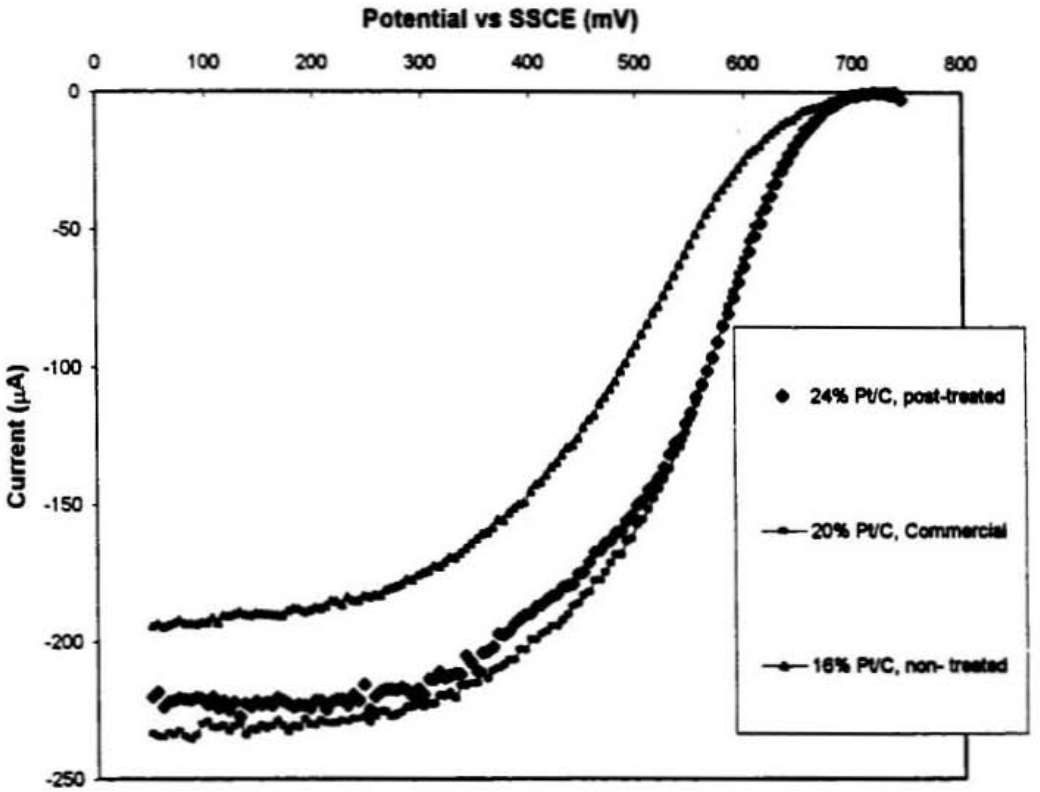

Fig. 2.34 Background corrected O_2 polarization curves (cathodic scans) for rotating (1000 rpm) carbon disc electrodes coated with un-treated and post-treated catalysts (both are 60 μg Pt cm^{-2}), and a commercial Pt/C catalyst (40 μg Pt cm^{-2}).

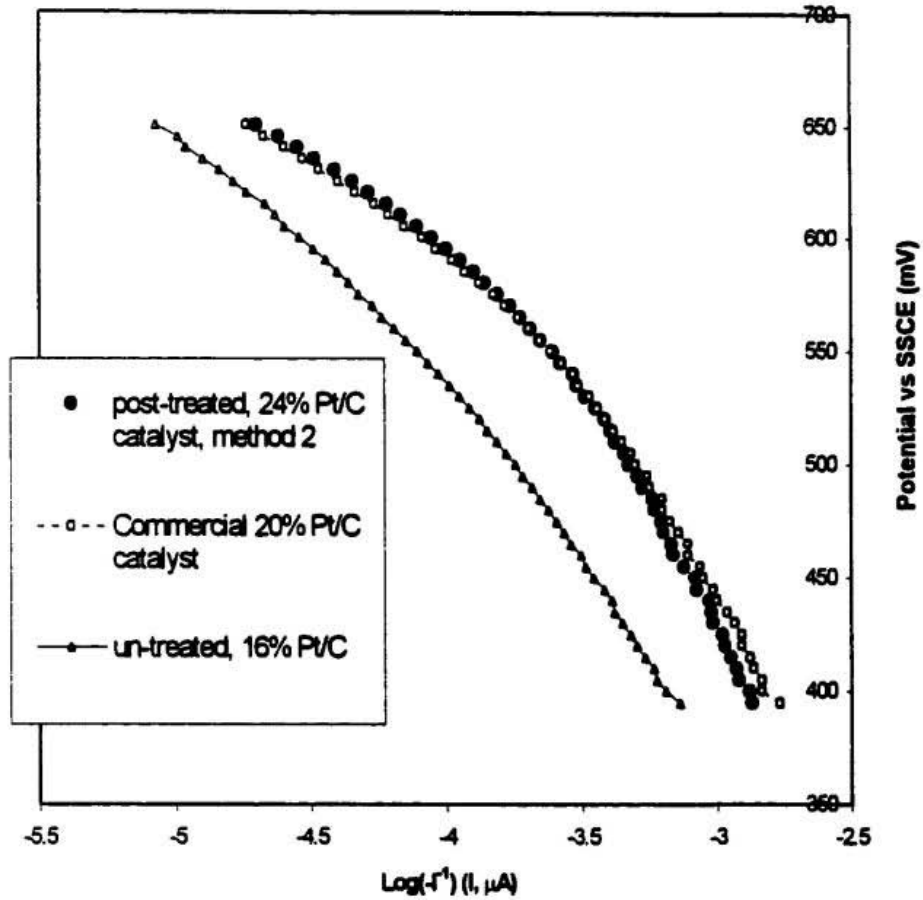

Fig. 2.35 Tafel plots for O_2 reduction (cathodic scans) at untreated 16% Pt/C (60 μg Pt cm^{-2}) and post-treated 24% Pt/C (60 μg Pt cm^{-2}) and a commercial 20% Pt/C (40 μg Pt cm^{-2}) coated electrodes in 0.5 M H_2SO_4 at 1000 rpm.

Fig. 2.34 shows oxygen polarization curves (cathodic sweep) for one of our carbon-supported catalysts, a nitric acid treated sample of the same catalyst and a commercial catalyst. **Fig. 2.35** shows the Tafel plots for these three data sets. Our nitric acid treated catalyst gives a similar performance to that of the commercial catalyst. Its improved performance over the original sample is believed to be due to a higher ionic conductivity in the catalyst layer since carboxylic acid groups or other acidic groups are produced on the surface of the carbon by the nitric acid treatment.

2.4 Conclusions

With gas diffusion electrodes in half-cells and full cells, and with rotating disk voltammetry techniques, poly (3,4-ethylenedioxythiophene)/poly(styrene-4-sulfonate) (Q1) supported Pt catalysts have been found to exhibit similar oxygen reduction activities to a commercial carbon supported catalyst when results are normalized for active Pt area. Exchange current densities per active area catalyst and and mechanisms appear to be the same.

The inferior performances compared with commercial catalyst seen for the polymer-supported catalysts in the work with gas diffusion electrodes were found when testing in half and full cells, and reproduced at rotating disc electrodes. The results have been shown to be due to the low Pt utilization (50-70% lower than for carbon supported Pt), and to slightly higher Pt particle sizes (ca. 7 nm vs. 4 nm, see **Table 2.3**). The poor utilization appears to be due to electronic isolation of some Pt particles, and to blocking or poisoning of the Pt surface. If these deficiencies can be removed, the superior performances

promised by the proton conductivity and water permeability of the polymer supported catalysts should be realized

The performance of self-made Pt/C catalyst can be improved greatly by post-treatment with concentrated nitric acid.

References

1. T. R. Ralph and G. A. Hards, *Chem. Ind.*, **337** (1998).
2. A. J. Appleby, *Sci. Amer.*, **281**,74 (1999).
3. E. J. Cairns, *Electrochim. Acta.*, **43**, 3629 (1998).
4. D. Hadzi and A. Novak, *Trans.Faraday Soc.*, **51**, 1641 (195).
5. W. Shummers and R. E. Offeman, *J. Am. Chem.Soc.*, **80**, 1339 (1958).
6. Y. Matsumura, S. Hagiwara and H. Takanhashi, *Carbon*, **14**, 163 (1976).
7. B. R. Puri and R. C. Bansal, *Carbon*, **1**, 457 (1964).
8. A. Esoinola, P. M. Miguel, M. R. Salles and A. R. Pinto, *Carbon*, **24**, 337 (1986).
9. P. R. de Sena, E. A. Ticianelli, and E. R. Gonzalez, *J. Electroanal. Chem.*, **357**, 225 (1993).
10. A. Damjanovic, *in Modern Aspects of Electrochemistry*, (J. O'M. Bockris and B. E. Conway, eds.), Vol. 5, p. 369. Plenum, New York, 1969.
11. H. R. Kunz and G. A. Gruver, *Electrochim. Acta.*, **23**, 219 (1978).
12. M. S. Wilson and S. Gotesfeld, *J. Appl. Electrochem.*, **22**, 1 (1992).
13. Nenyou Jia, M. S. Thesis. Memorial University, St. John's, NF, 1999.

14. Z. Qi and P. G. Pickup, *Chem. Commun.*, 15 (1998).

15. Z. Qi and P. G Pickup, *Chem. Commun.*, 2299 (1998).

16. Z. Qi and M. C. Lefebvre, and P. G. Pickup, *J. Electroanal. Chem.*, **459**, 9 (1998).

17. M. C. Lefebvre, Z. Qi, and P. G. Pickup, *J. Electrochem. Soc.*, **146**, 2054(1999).

18. C. S. C. Bose and K. Rajeshwar, *J. Electroanal. Chem.*, **333,** 235 (1992).

19. M. E. G. Lyons, *Analyst*, **119**, 805 (1994).

20. S. Holdcroft and B. L. Funt, *J. Electroanal. Chem.*, **240,** 89 (1988).

21. F. T. A Vork and B. Barendrecht, *Electrochim. Acta.*, **35,** 135 (1990).

22. H. Yamato, M. Ohwa and W. Wernet, *J. Electroanal. Chem.*, **397,** 163 (1995).

23. G. Heywang and F. Jones, *Adv. Mater.*, **4**, 116 (1992).

24. S. L. Gojkovic, S. K. Zecevic, and R. F. Savinell, *J. Electrochem. Soc.*, **145**, 3713 (1998).

25. T. J. Schmidt, H. A. Gasteiger, G. D. Stab, P. M. Urban, D. M. Kolb, and R. J. Behm, *J. Electrochem. Soc.*, **145**, 2354 (1998).

26. P. G. Pickup, C. L. Kean, M. C. Lefebvre, G. Li, Z. Qi, and J. Shan., *J. New Mat. Electreochem. Systems*, **3**, 21- 26 (2000).

27. A. A. Pud, *Synth. Metal*, **66**, 1(1994).

28. G. Li and P. G. Pickup, *J. Phys. Chem. B.*, **103**, 10143-10148 (1999).

29. M. Wakizoe, O. A. Velve and S. Srinivasan, *Electrochim. Acta.*, **40**, 335 (1995).

30. A. Parthararathy, S. Srinivasan and A. J. Appleby, *J. Electroanal. Chem.*, **339**, 101 (1992).

31. T. Biegler, D. A. J. Rand and R. Woods, *J. Electroanal. Chem.*, **29,** 269 (1971).

32. A. Damjanovic and G. Hudson, *J. Electrochem. Soc.*, **135**, 2269 (1988).

33. K. E. Gubbins and R. D. Walker, Jr., *J. Electrochem. Soc.*, **112,** 469 (1965).

34. A. J. Bard and L. R. Faulkner, *Electrochemical Methods, Fundamentals and applications*, 286 (1980).

Chapter 3

PEDOT/PSS Supported Binary (Pt-Ru) Catalysts for Methanol Oxidation

3.1 Introduction

3.1.1 Background of platinum based binary catalysts for methanol electro-oxidation

Pt-Based electrocatalysts have been widely studied for methanol oxidation since the Direct Methanol Fuel Cell (DMFC) was first proposed [1]. In fuel cells, platinum alone is not a sufficiently active methanol electrocatalyst since it is easily poisoned by intermediates, such as CO and HCHO, produced during methanol oxidation. The incorporation of a second metal into the catalyst has therefore been extensively studied to improve catalytic activity. Studies on Pt based bimetallic electrocatalysts, such as Pt-Sn [2-5], Pt-Rh [6], Pt-Ru [7-11], Pt-Re and Pt-Mo [12-14] have shown enhanced electrochemical activity compared with Pt alone, by lowering the overpotential for methanol oxidation and producing increased current density without increased Pt loadings. Among these binary catalysts, Pt-Ru has been found to be the most active and has become the most widely studied for improving the performance of the anodic reaction in DMFCs in the last ten years [11,15-27].

The mechanism of methanol oxidation on Pt is not thoroughly understood yet, and there are numerous possible routes from methanol to CO_2. The intermediates formed during methanol oxidation can vary with reaction conditions [28,29] and adsorption of intermediates usually occurs. The most generally accepted mechanism for methanol oxidation is written as [30]:

$$CH_3OH + 3Pt \rightarrow Pt_3\text{-}COH + 3H^+ + 3e^- \quad \textbf{3.1}$$

$$3Pt + 3H_2O \rightarrow 3Pt\text{-}OH + 3H^+ + 3e^- \quad \textbf{3.2}$$

$$Pt_3\text{-}COH + Pt\text{-}OH \rightarrow Pt_2\text{-}CO + H_2O + 2Pt \quad \textbf{3.3}$$

$$Pt_2\text{-}CO + Pt\text{-}OH \rightarrow Pt\text{-}COOH + 2Pt \quad \textbf{3.4}$$

$$Pt\text{-}COOH + Pt\text{-}OH \rightarrow CO_2 + H_2O + 2Pt \quad \textbf{3.5}$$

After the alloying modification of Pt with Ru, a negative shift in the methanol oxidation response of about 200 mV has been observed by most workers. The mechanism on the Pt-Ru binary catalyst is modified as presented by Freelink et al. [21] as

$$Ru + H_2O \rightarrow Ru\text{-}(H_2O)_{ads} \quad \textbf{3.6}$$

$$Ru\text{-}(H_2O)_{ads} \rightarrow Ru\text{-}(OH)_{ads} + H^+ + e^- \quad \textbf{3.7}$$

$$Pt\text{-}(CO)_{ads} + Ru\text{-}(OH)_{ads} \rightarrow Pt + Ru + CO_2 + H^+ + e^- \quad \textbf{3.8}$$

From the equations above, the function of Ru is to adsorb oxygen-containing species (eg. H_2O, OH), which will help to oxidize the carbonaceous intermediates produced from

methanol oxidation. The beneficial roles of Ru and other metals as promoters in Pt-based catalysts for methanol oxidation are summarized as follows [16].

1) Promoting the adsorption of water and/or oxygen, thus enabling the oxidation of the methanol residues that poison Pt.
2) Changing the electronic properties of the Pt surface.
3) Preventing adsorption of residues by blocking the Pt sites on the surface.

Although there are many different explanations under different experimental configurations, these binary systems are not completely understood even today [29]. It is generally accepted that Pt-Ru pair sites adsorb small molecules of oxygen-containing species, then carbonaceous species such as HCHO, HCOOH and CO are preferentially oxidized at Pt sites by surface diffusion from Ru [29].

The optimum surface composition of Ru will maximize the electrocatalytic activity. Saffarian et al. recently reported that 44/56 of Pt/Ru is the best composition based on a fractal technique [26]. Overall, a surface composition of 50 atom % Ru or close to it has been demonstrated to give the best performance for methanol oxidation [18-20].

3.1.2 Preparation of catalysts

The performance of a binary catalyst is not only dependent on the characteristics of the metals (Pt-Ru), but also on the catalyst preparation method, the choice of supporting material and pre- or post-treatment of the catalyst. Unsupported Pt-Ru alloy catalysts are

generally prepared by arc-melting or electro-codeposition methods. In the arc-melting method, the pure metals are mixed in the desired proportions and arc-melted under an argon atmosphere. After enough melt cycles, the alloys are fabricated into discs and machined to fit into the electrochemical cell. Their bulk composition can be assessed by X-ray fluorescence spectroscopy [17-20]. The electro-codeposition method is realized by direct electro-reduction of Pt and Ru salts solutions [21]. Carbon-supported Pt-Ru catalysts are generally prepared by chemical deposition methods in which most commonly $H_2PtCl_6 \cdot H_2O$ and $RuCl_3 \cdot XH_2O$ are reduced by various reductants under controlled stoichiometries and reaction conditions [15,16,31]. Recently, colloid systems were proposed as a promising method for catalyst preparation [23] in which ultra-fine metal particles of 1.7±0.5 nm could be obtained. Polymer-supported Pt-Ru catalysts prepared by an electro-deposition method [32] have been reported. The Pt and Ru particles were co-deposited into the polymer film during its electro-synthesis. As with depositing Pt alone, this method also met the problem such as unsatisfactory porosity of catalyst layer that has been discussed in Chapter 2 (Section 2.1.2).

Previously, chemically deposited polymer-supported catalysts have suffered from instability of the polymer at high temperatures (discussed in Section 2.3.1). A more stable conducting polymer (PEDOT/PSS (Q1)) has been developed by Pickup *et al.* Following the chemical deposition method, Q1-supported Pt-Ru catalysts were prepared and preliminary measurements of these catalysts tested in GDEs have been reported [33,34]. The work on polymer-supported binary catalysts in this chapter is based on this method.

3.1.3 Methodology.

The techniques, mainly the electrochemical, spectroscopic, X-ray and thermogravimetric methods, used for characterizing catalysts in fuel cell-related electrochemistry have been reviewed by Wasmus et al. [29]. Although many modern instrumental tools of analytical chemistry have been applied, there is still no consensus regarding the mechanism of the function of binary catalysts (and Pt alone) for methanol oxidation. Two of the reasons are that there is not a common basis for the comparison of different catalysts in fuel cell testing and there is less progress made in an on-line method to study the effects linked to electrochemistry under fuel cell conditions. If these two problems are resolved, a clear definition of the current state-of-the-art in anode catalysis should be revealed.

The techniques applied in this study include scanning electron microscopy (SEM) with an energy X-ray (EDX) analyser to observe the catalyst surface and obtain relative elemental concentrations; Transmission electron microscopy (TEM) to calculate the size of the particles; X-ray diffraction (XRD) to characterize the Pt surface structure and calculate the size of crystallites (generally Pt); Ac impedance to obtain kinetic and transport parameters; Fourier transform infrared spectroscopy (FTIR) to observe adsorbed species on modified catalysts. Although there are many methods in use, to test the performance of the catalysts being prepared, current (or current density) at an applied potential or current transients obtained during a potential step are still the most often applied technique in this work. Thus, the analysis of the experimental data obtained from

cyclic voltammetry (CV), chronoamperometry (CA) and pulse polarographic methods (Normal Pulse Polarography (NP)) are the main focus of this chapter.

3.1.4 Objective of this chapter

Our previous work on polymer (Q1)-supported catalysts for oxygen reduction has shown comparable activities to those obtained for commercial carbon-supported catalysts, while the preliminary work on testing polymer-supported binary catalysts for hydrogen and methanol oxidation were significantly inferior [34]. In the work described in this chapter, half-cell GDE and RDE configurations were applied to study the binary catalysts in more detail.

The first objective was to optimize the synthetic conditions to obtain catalysts with the required atomic compositions of Pt: Ru. Secondly, potentiostatic steady state and reduced CO_2 oxidation techniques were used in the GDE configuration to compare the activities of (Pt-Ru)/Q1 with those obtained for a commercial catalyst. Also, some work was done on commercial binary catalysts and Pt black anodes (4 mg Pt cm^{-2}) to characterize their performance in short and long potential steps under different conditions. Finally, the polymer-supported binary catalysts were investigated under more carefully controlled conditions using the RDE configuration. Methodologies such as CV (including O_2 polarization), transient polarization, and CA were used. Before testing catalysts, EDX was used to measure the relative amount of Pt and Ru, and XRD was used to observe Pt particle sizes and the lattice change of Pt crystallites after being alloyed with the second metal, Ru.

3.2 Experimental

Synthesis of PEDOT/PSS (Q1) polymer composites, XRD and the experimental configuration for the RDE experiments were the same as those described in Section 2.2. Q1-supported binary catalysts were prepared as follows.

A mixture of aqueous $H_2PtCl_6 \cdot H_2O$ and $RuCl_3 \cdot xH_2O$ (Aldrich; concentrations based on desired Pt and Ru loadings) was heated to 40°C-60°C and then neutralized with saturated Na_2CO_3 solution as indicated by pH paper. Then the mixture was boiled for 2 hr under a N_2 atmosphere. A suspension of Q1 in ca. 20 mL H_2O (ultra-sonicated for one hour) was then added and the new mixture was stirred at ca. 80-100°C for 30 minutes to allow equilibration. Finally, a ca. 30 or more molar excess of aqueous formaldehyde (36.5%) than Pt/Ru was added followed by heating at reflux for ca. 2hr. The catalyzed Q1 was collected by centrifugation, washed thoroughly with water and then stored in 5% methanol solution.

A portion of each batch of catalyzed Q1 was collected and dried under vacuum to calculate its mass percentage of Pt in the wet sample. Its electronic conductivity was then measured in this dry state. Total catalyst loadings were estimated by a gravimetric analysis in which the dried catalyst was ashed at 900°C in a muffle furnace. Elemental Pt and Ru were assumed to be the only remaining products. The trace amount of Fe remaining in the PEDOT/PSS following catalyst deposition was ignored because its level was not accurately known, and it would not make a significant difference to the results.

Scanning electron microscopy (SEM) and semi-quantitative analyses were obtained with a HITACHI S-570 scanning electron microscope with an energy dispersive

X-ray (EDX) analyser (Tracor Northern 5500). Relative elemental concentrations were calculated by fitting and correcting the EDX spectra with commercial software (SQ, Tracor Northern). Analyses were carried out 3 or more times on different portions of the sample. The Pt-Ru (1:1) ratio of a commercial catalyst was used as a standard in this work. The measured Pt:Ru ratio of 1.9 for the 20% (Pt-Ru)/C commercial catalyst (E-TEK) was found to be higher than the reported value of 1.0. The error is probably produced by the systematic error of SEM machine. Thus, ratios measured for Q1-supported catalysts were all corrected arbitrarily by this factor.

Reduced CO_2 oxidation experiments were performed using GDEs in a half-cell. The potential was held at -0.236 V for required times (20 min or one hour) to adsorb reduced CO_2 before starting the stripping scan. Cyclic voltammograms were recorded under two conditions, with CO_2 or N_2 flushing the gas chamber respectively.

Methanol oxidation was studied in a somewhat unusual configuration with a GDE in a half-cell by adding 1 M methanol to the 1 M H_2SO_4 solution in the cell and passing N_2 over the back of the GDE. The methanol therefore had to diffuse through the Nafion membrane to reach the catalyst layer. These experiments were carried out in a temperature –controlled water bath at 60±1°C. With the RDE configuration, methanol oxidation was carried out at both 60±1°C and at room temperature (RT) (22±2°C).

3.3 Results and discussion

3.3.1 Catalyst preparation and composition analysis by EDX

Although Q1 has good electronic conductivity when first prepared, it loses conductivity with time, particularly at high temperature (see **Table 2.2**). Thus, obtaining catalyzed Q1 in a shorter time should provide better activity. However, in our experiments, we found that Ru^{3+} ($RuCl_3 \cdot xH_2O$) was more difficult to reduce than Pt^{4+} ($H_2PtCl_6 \cdot H_2O$), and that the yield of Ru was very low if the deposition time was only 40 min (**Table 3.1**). Therefore, before depositing binary metals (Pt-Ru), Pt and Ru were deposited individually on carbon black to determine the optimal time for obtaining the catalyzed polymer. **Table 3.1** lists the results.

Table 3.1 Tests of deposition of Pt and Ru particles on carbon black.

Catalysts	Targeted metal loading (mass %)	Reaction time (min)	Metal loading obtained (mass %)	Yield *(%)
Pt/C	35	40	25	71
Pt/C	34	120	30	88
Ru/C	21	40	3.3	16
Ru/C	21	120	15	74

* Assuming no loss of carbon.

Yield = (metal loading obtained/Target metal loading) × 100%

Table 3.1 shows that Pt was easily deposited on carbon in high yield for both short (40 min) and long (120 min) deposition times, but that a full deposition of Ru particles would need longer times. Thus, under our experimental conditions, a long time (120 min) is necessary to prepare binary catalysts.

When depositing the two metals together at long time (120 min), however, the yield of Ru was not as high as when depositing it alone. **Table 3.2** lists the deposition results for selected carbon-supported and Q1-supported binary catalysts. Our aim was to obtain 1:1 Pt/Ru catalysts and so initially a ratio of 1:1 Pt^{4+} and Ru^{3+} was used. However, EDAX analysis showed that the ratio of Ru was very low and sometime it could not be detected. Thus, a greater proportion of Ru^{3+} must be used to obtain a Pt to Ru ratio close to 1. From **Table 3.2**, it can be seen that a molar ratio of $H_2PtCl_6 \cdot H_2O$ to $RuCl_3 \cdot xH_2O$ of 0.2-0.3 is required to obtain binary catalysts with an atomic ratio of 1:1. The data on catalysts 1, 2 and 3 demonstrate the reproducibility of the chemical deposition method. From the table, we can find that a long time is needed for the reaction. If the reaction time is too short, the deposition of Pt still dominates (catalyst 5). Thus, by adjusting reaction times, different Pt:Ru ratios can be obtained (catalyst 8 and 9). **Fig. 3.1** and **Fig. 3.2** show EDX spectroscopic results for the commercial catalysts and one Q1-supported Pt-Ru catalyst (catalyst 10 in **Table 3.2**), respectively. The measured ratio for the Pt-Ru/Q1 was 1.7:1, and after being corrected by 1.9, the resulting ratio was 0.89.

The amount of HCHO used was between 30 – 50 molar excess relative to metal salts (based on 1:1 of HCHO/(Pt^{4+} + Ru^{3+})). No significant influence of the HCHO amount was found between this range. The electronic conductivities of the dry polymer-supported catalysts were quite good (around 0.14 – 0.60 S cm^{-1}), showing the acceptability of the

Catalyst	1	2	3	4	5	6	7	8	9	10
	Pt-Ru/C	Pt-Ru/C	Pt-Ru/C	Pt-Ru/C	Pt-Ru/C	Pt-Ru/Q1	Pt-Ru/Q1	Pt-Ru/Q1	Pt-Ru/Q1	Pt-Ru/Q1
Pt/Ru atomic ratio in reaction mixture	0.45 : 1	0.4 : 1	0.41 : 1	0.21 : 1	0.25 : 1	0.33 : 1	0.23 : 1	0.25:1	0.25:1	0.28:1
Pt/Ru ratio obtained	2.6 : 1	2.2 : 1	2.7 : 1	1.1 : 1	4 : 1	1.2 : 1	0.89 : 1	2.5:1	1.3:1	0.89:1
Target metal loading (mass %)	24	24	25	36	36	31	29	42	57	41
Metal loading obtained (mass %)	11	10	14	16	22	15	17	27	36	29
Yield* (mass%)	46	42	56	44	61	48	58	64	64	71
σ (S cm^{-1})	2.3	-	-	-	2.6	0.27	0.60	0.14	0.22	0.25
Reaction time	2 hr	2 hr	2 hr	2 hr	40 min	2 hr	2 hr	1 hr	1.5 hr	2 hr

1. "-" not measured
2. Measured atomic ratios were corrected by dividing by 1.9.
3. "*" See table 3.1

Table 3.2 Compositions, yields and conductivities (σ) of some binary catalysts.

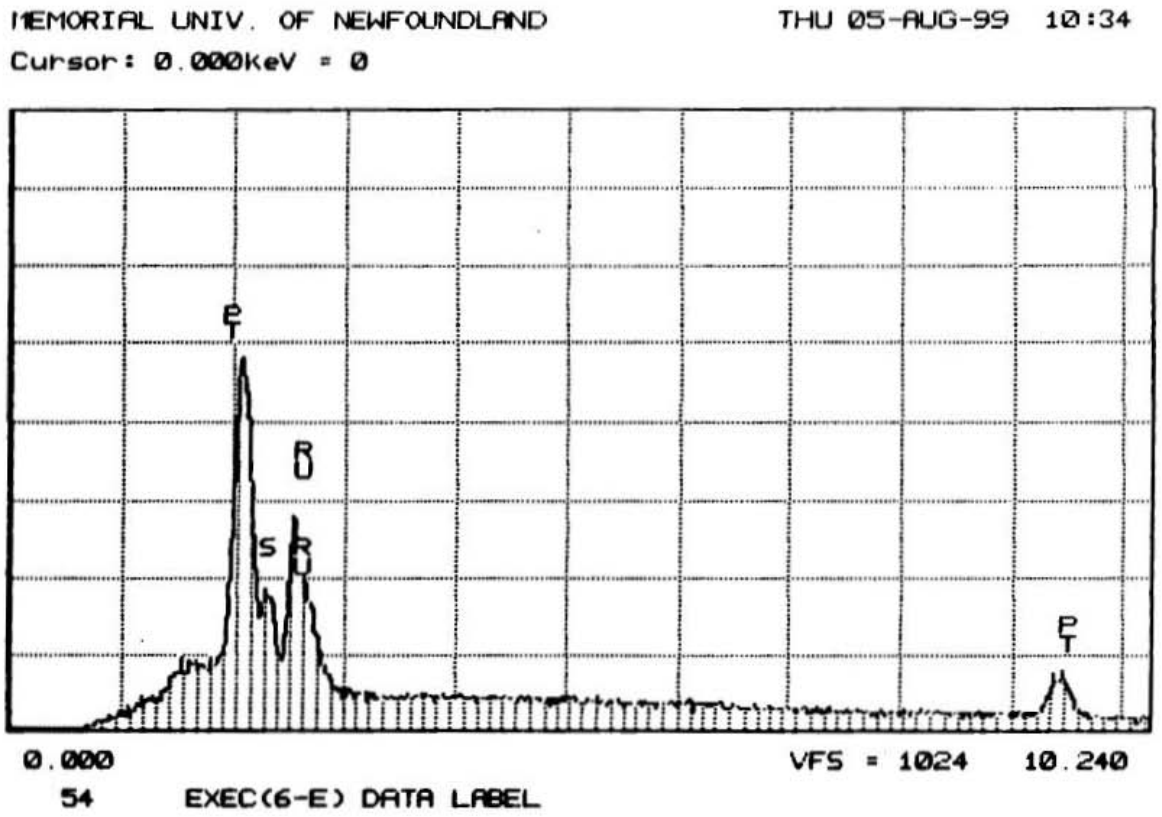

Fig. 3.1 EDX spectrum for a commercial 20% Pt-Ru (1:1)/C catalyst. Measured composition (average): Pt:Ru / 1.9:1.

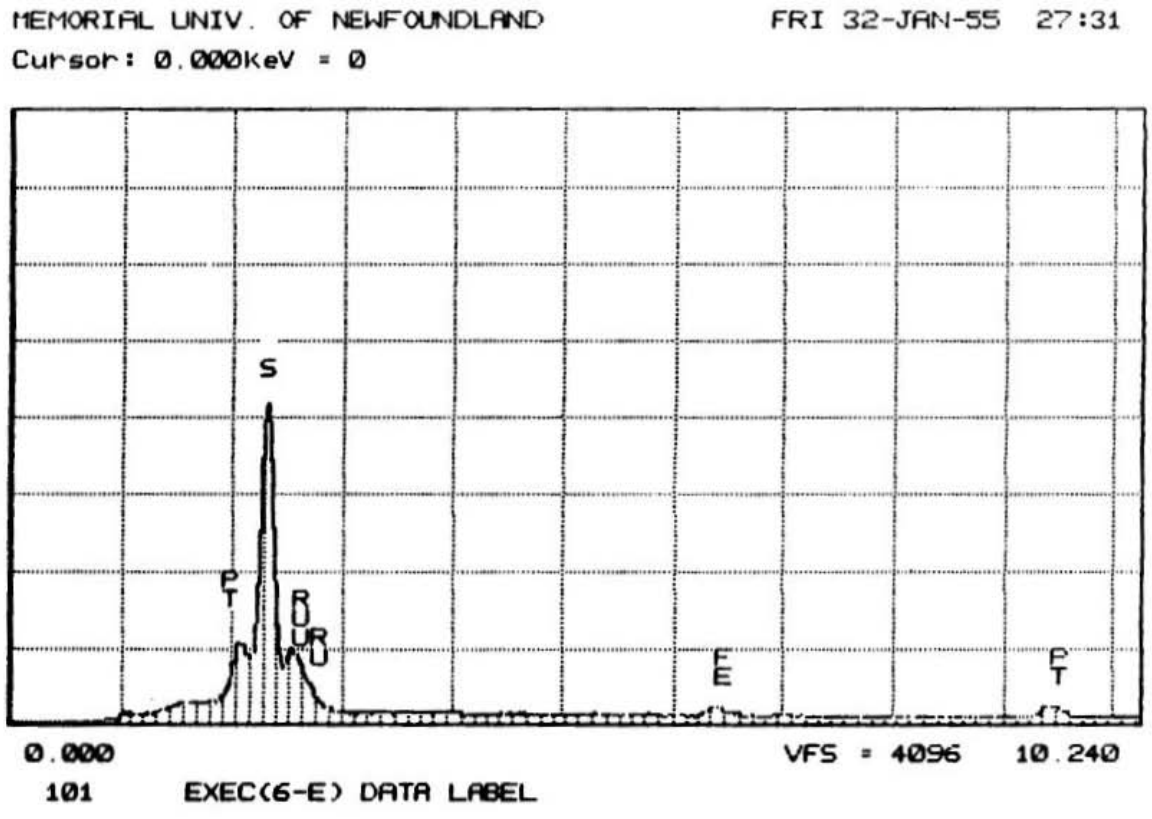

Fig. 3.2 EDX spectrum for a 17% Pt-Ru /Q1 catalyst.
Measured composition: Pt: Ru / 1.7:1.

chemical deposition method for preparing Q1-supported binary catalysts.

3.3.2 X-ray diffraction (XRD) analysis.

Fig. 3.3 shows XRD patterns for commercial 20% Pt/C, 20% Pt-Ru (1:1) /C and 39% (Pt-Ru) (1:1) /C catalysts over a wide range of 2θ scans. Pt diffraction (1,1,1) peaks are seen for all three catalysts, with the peaks for binary catalysts slightly shifted to higher 2θ values with respect to the Pt/C catalyst. For Pt/C, there is a second peak (2,0,0) at a 2θ value of ca. 48^0. From an analysis of the (1,1,1) peaks, (Section 2.2.4), the particle sizes for the three catalysts are 3.8 nm, 3.3 nm and 2.8 nm.

XRD spectra for Q1-supported catalysts with different Ru loading are shown in **Fig. 3.4**. In the case of 36% Pt/Q1, the peaks are similar to those for the commercial 20%Pt/C catalyst. With increasing Ru ratio, the heights and areas of the peaks due to the three Pt indexes, especially those at higher 2θ values, are decreased. For 34% (Pt-Ru)(0.84:1)/Q1, the peaks at (2,0,0) and (2,2,0) have disappeared as for the commercial binary catalysts, indicating that the Ru atoms have changed the structure of the Pt crystallite lattice. This change may be one of the factors influencing the catalytic properties of the alloy.

The particle sizes for the four polymer-supported catalysts measured from the (1,1,1) peak were 9, 9.4, 9.2 and 7.3 nm. The measured particle sizes for all single and binary catalyst were between 6 – 10 nm and without regular change with Pt loading, which means that the depositions of Ru and Pt do not affect the particle sizes with each other. Comparing with data for the commercial catalysts (3.8 nm for a single catalyst and 3.3 nm for a binary catalyst), it was also noted that Ru deposition has no effect on the

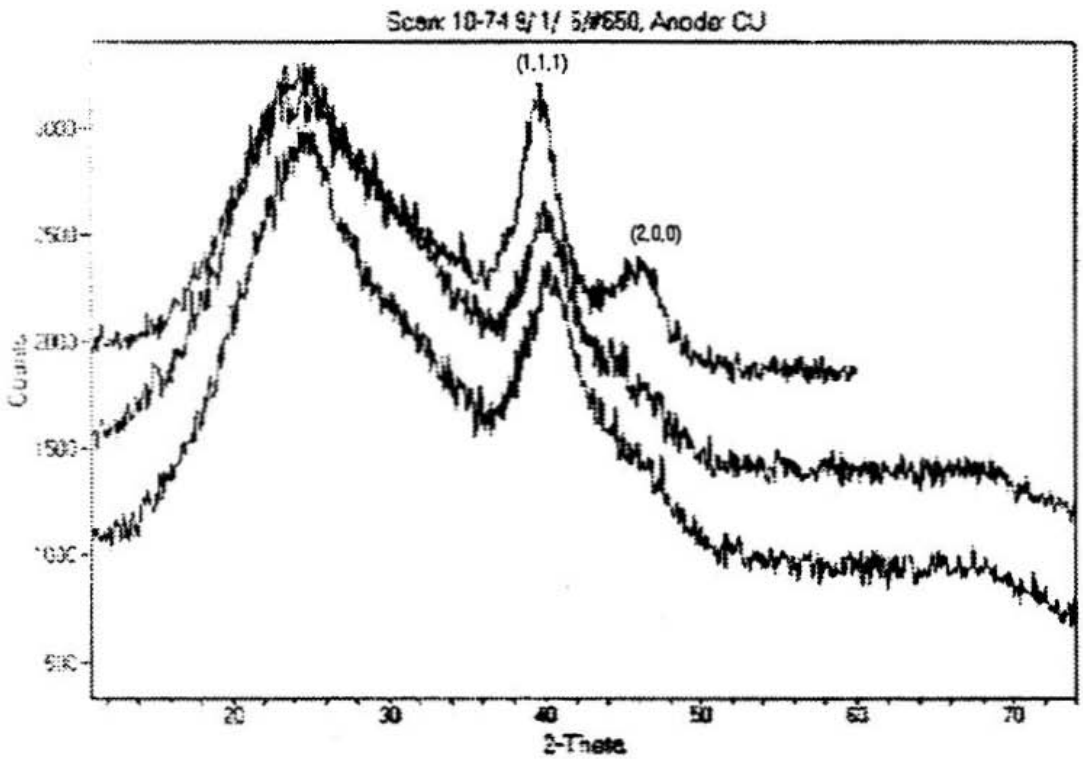

Fig 3.3 XRD spectra for commercial catalysts, 20% Pt/C (top), 20% Pt-Ru (1:1)/C (middle), 39% Pt-Ru (1:1)/C (bottom).

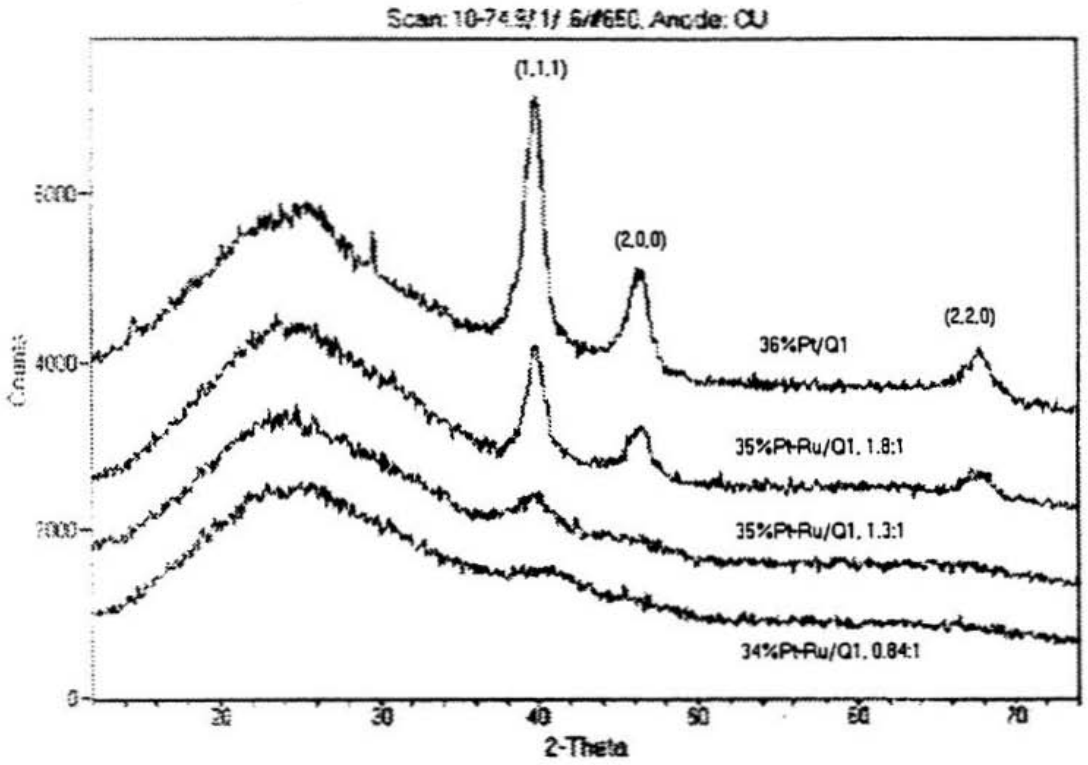

Fig 3.4 XRD spectra for Q1-supported catalysts.

sizes of Pt particles.

3.3.3 Catalytic properties of Q1-supported Pt-Ru binary catalysts, commercial binary catalysts and Pt black anodes in half-cells

3.3.3.1 Methanol oxidation polarization

For methanol oxidation polarization, normal pulse polarography (NP) was applied following the procedure described in Section 2.2.3 and 2.3.2.1, except that N_2 was passed through the chamber at the back of the GDE and different step times up to 40 s were applied. Polarization curves for methanol oxidation at 60 ± 1°C were recorded for some Q1-supported catalysts and a commercial carbon-supported catalyst, and results are shown in **Fig. 3.5.** The commercial catalyst gave the best results with lower overpotentials at most current densities. Of the Q1-supported catalysts, one with a Pt: Ru ratio of 2.2 gave the best catalytic performance. A catalyst with an even higher Pt: Ru ratio (20%Pt-Ru (16:1) /Q1) gave much larger currents than the others at high overpotentials, but inferior results at lower overpotentials. This is more characteristic of a pure Pt catalyst, with the high currents at high overpotential reflecting the high active Pt area. If a catalyst has a high Ru ratio (15%Pt-Ru (0.5:1)/Q1), then the catalytic activity is correspondingly lower.

Unlike the arc-melting method, the Pt: Ru ratio can not be controlled exactly with our chemical deposition method, and our composition measurement has inevitable error, so we can not conclude that a Pt: Ru ratio of 1:1 is the best catalyst for the Q1-support. However, according to our experimental results, ratios of Pt: Ru between 1and 2 give the

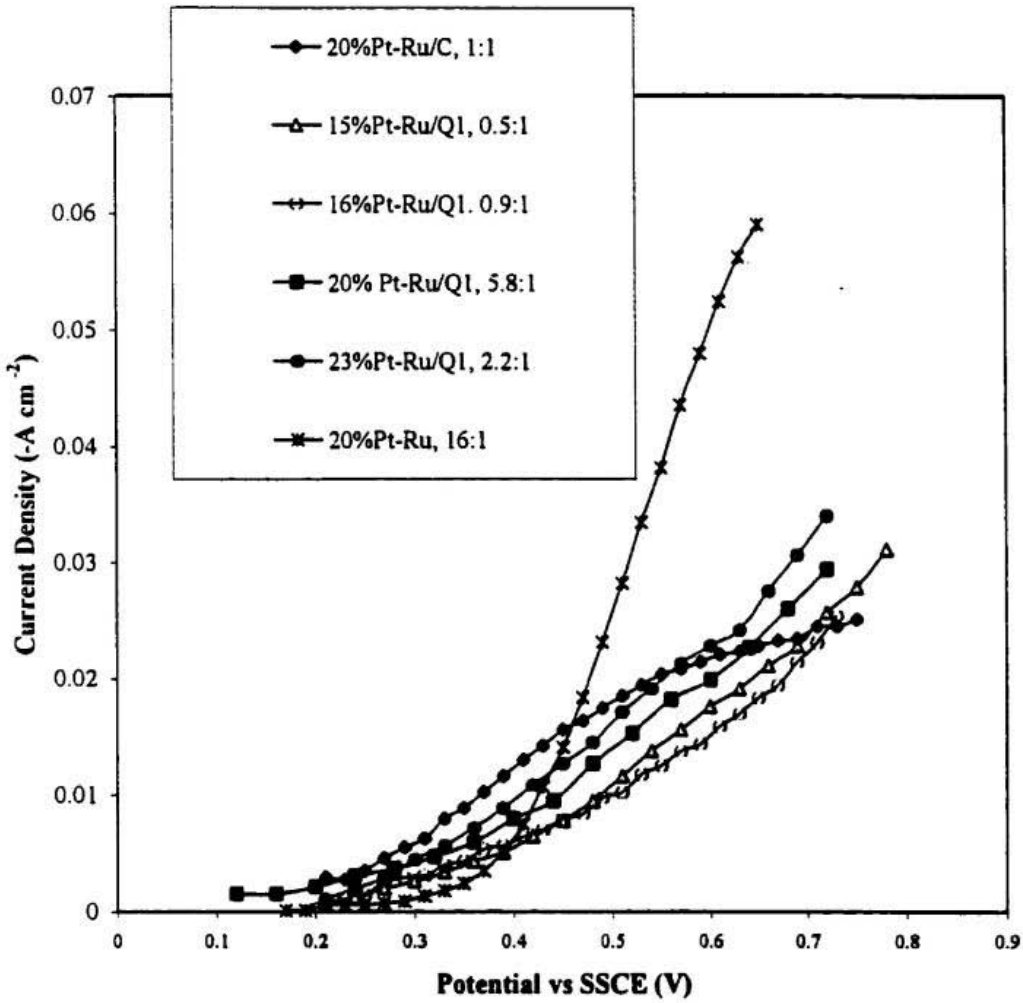

Fig. 3.5 Methanol oxidation polarization curves for Q1-supported binary catalysts and a commercial catalyst at 60 ^{0}C with step time of 2 s in a half cell. Pt-Ru for all were 0.5 mg cm^{-2} except for 20% Pt-Ru/Q1(5.8:1) for which was 0.75 mg cm^{-2}.

best performance, and so catalysts prepared in this ratio range were the focus on of our later studies.

The step time of 2 s used for collecting the data shown in **Fig. 3.5** does not provide a steady state result. In order to find the time to reach a steady state in these experiments, Pt black anodes with very high Pt loadings, a commercial catalyst (39% Pt-Ru (1:1) /C) and one Q1-supported binary catalyst running were tested with longer step times (**Figs. 3.6 – 3.9**). These experiments were done in order of increasing step time, but similar results were obtained when the order was reversed. For all electrodes, 30 s is long enough to approach steady state, although a true steady state for the electro-oxidation of methanol may not be established even after many hours [35]. Further work involved adding PTFE or Nafion solution to a high loading commercial 60% Pt-Ru (1:1)/C catalyst to improve its ionic conductivity. At a step time of 40s, these changes improved the performance as expected, but the current continued to decline when longer step times were used (see **Fig. 3.10**).

In **Fig. 3.9**, the superior performance of the Pt black anode is clearly shown. This indicates that a higher loading of Pt is still necessary for methanol oxidation at high current densities. Both **Fig. 3.9** and **Fig. 3.5** demonstrate that the Pt-Ru binary catalyst decreases the overpotential for methanol oxidation, although higher total loadings are clearly needed for real applications.

3.3.3.2 Reduced CO_2 oxidation and CO stripping voltammetry

Using a GDE in a half-cell configuration, a technique using CO_2 electro-reduction

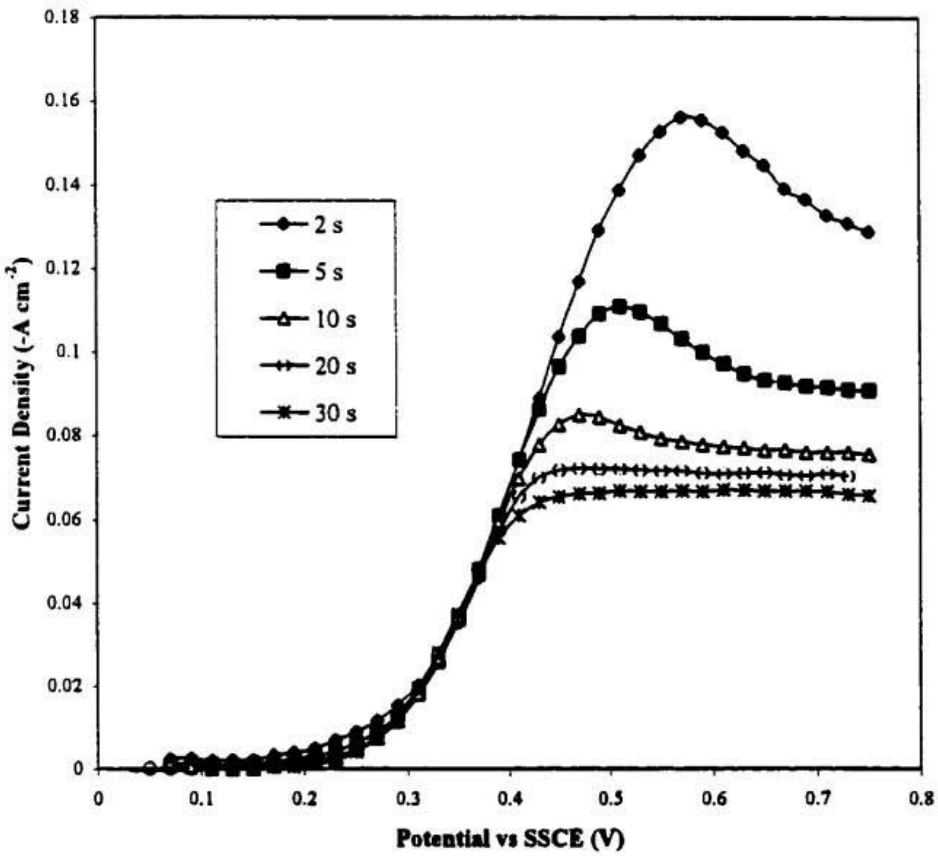

Fig. 3.6 Methanol oxidation polarization curves for 4 mg Pt black cm^{-2} at different step times at 60 ^{0}C.

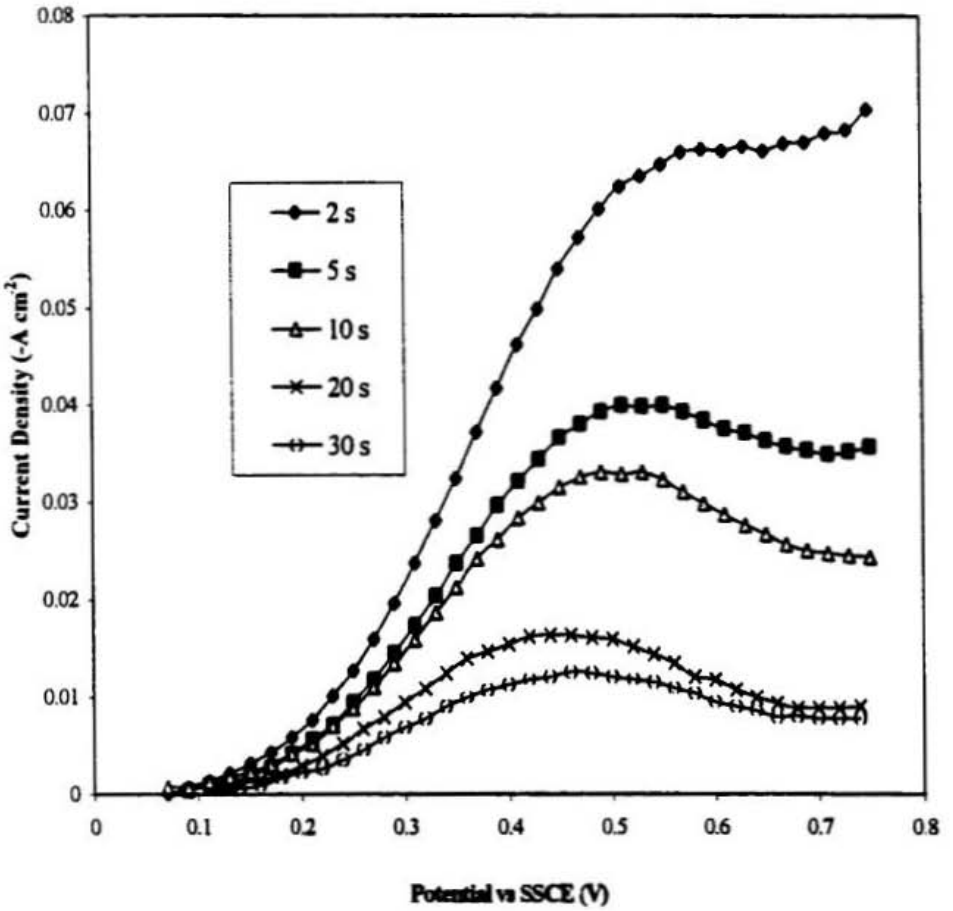

Fig. 3.7 Methanol oxidation polarization curves for a commercial 39% Pt-Ru(1:1)/C catalyst with 0.89 mg Pt-Ru cm^{-2} at different step times at 60 ^{0}C.

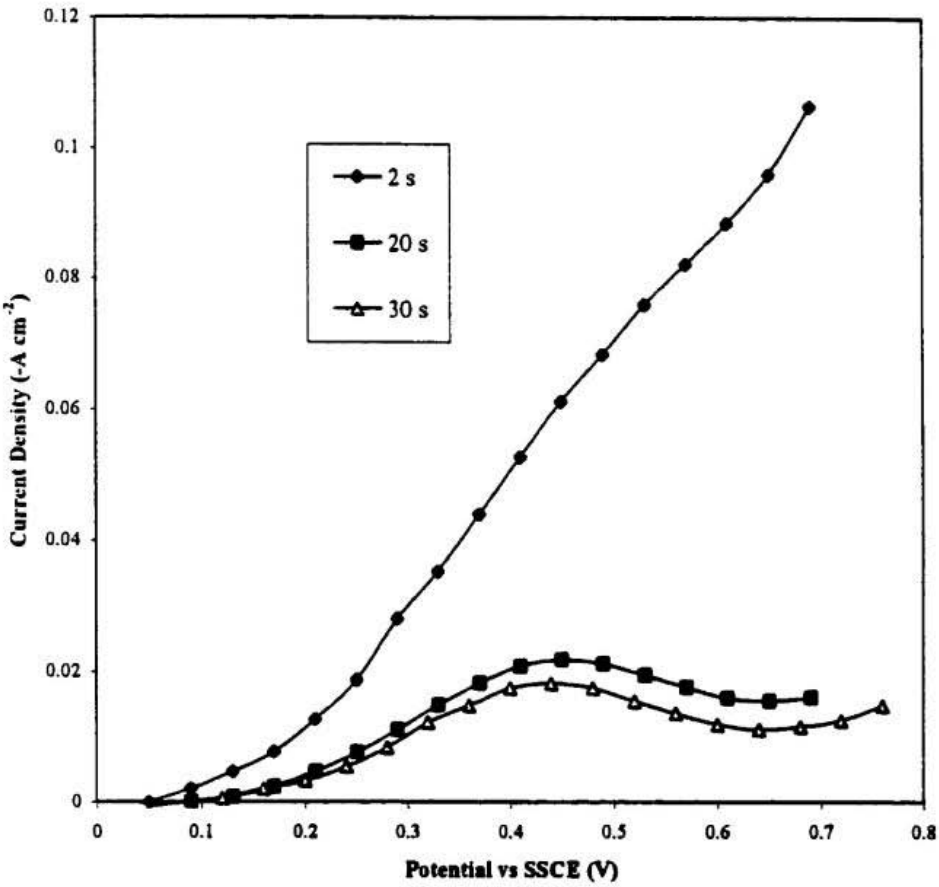

Fig. 3.8 Methanol oxidation polarization curves for a 20% Pt-Ru/Q1 (1.2:1) catalyst with 0.5 mg Pt-Ru cm^{-2} at different step times at 70 ^{0}C.

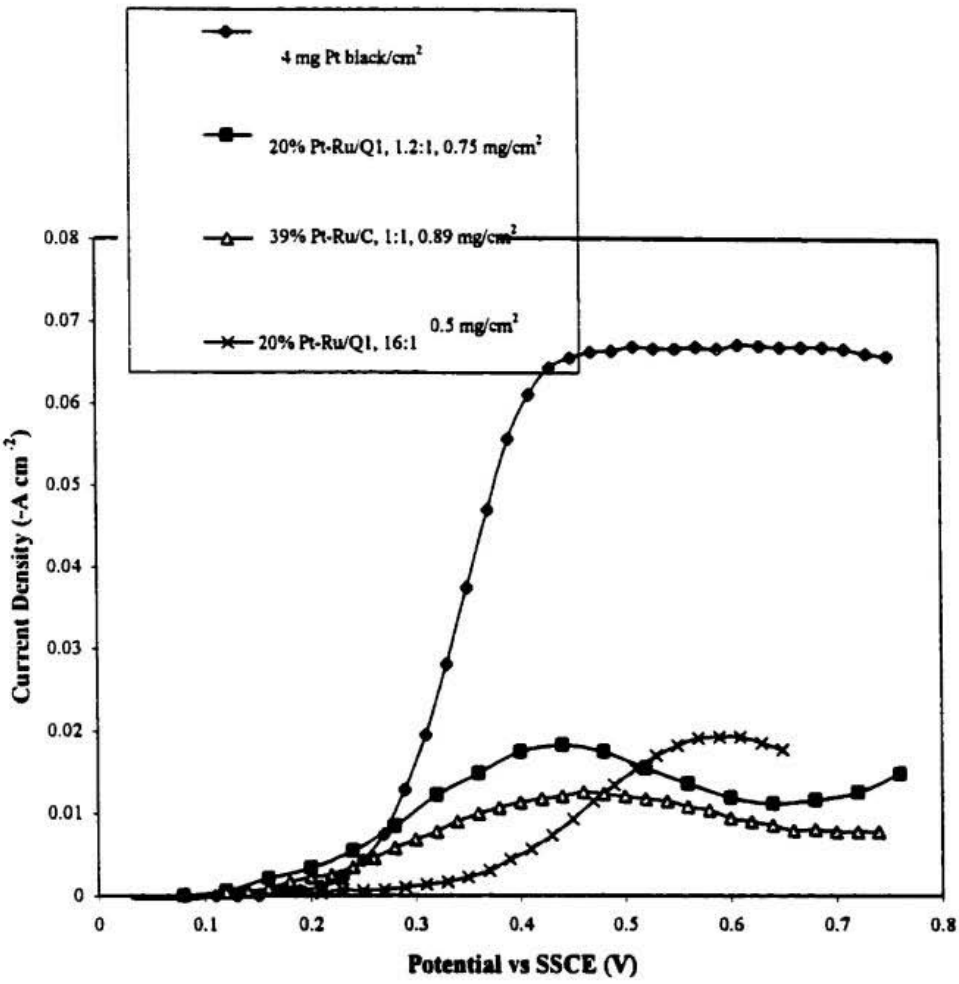

Fig. 3.9 Methanol oxidation polarization curves for catalysts at step time of 30 s. 20 % Pt-Ru(1.2:1)/Q1 was tested at 70 ^{0}C, others were at 60 ^{0}C.

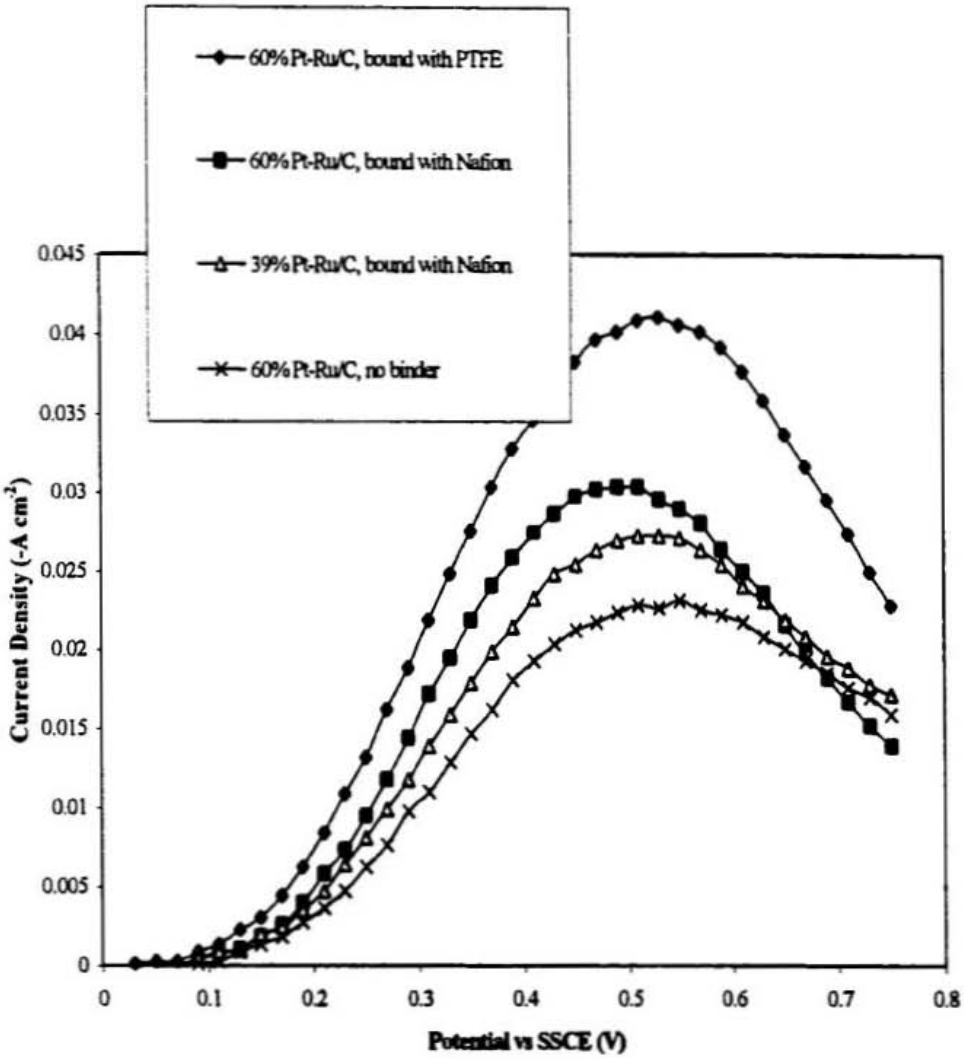

Fig. 3.10 Methanol oxidation polarization curves for commercial catalysts with different binders at step time of 40 s. Loadings for all catalysts were 1.5 mg cm^{-2}.

/reoxidation to measure the active surface area of carbon-supported catalysts has been studied in our group [36]. **Fig. 3.11** shows a CV of a 20% Pt/C commercial catalyst following CO_2 reduction at -0.236 V vs. SSCE, for 20 minutes. The oxidation wave at ca. +0.6 V is due to oxidation of adsorbed products from CO_2 reduction. The active area of the catalyst can be estimated from the area of this peak (the second scan in CO_2 was used as a background). The initial purpose of our work was to apply this technique to characterize the active surface area of binary catalysts. However, the peaks of CVs for commercial and Q1-supported binary catalysts by this method were not as sharp (or obvious) as expected (see **Figs. 3. 12 - 3.14**). The reduced CO_2 area is obviously not suitable here for estimating active areas of binary catalysts. However, we noticed that the onset potentials (E_{onset}) for reduced CO_2 oxidation estimated as the intercepts of the first and second scans as indicated in **Figs. 3.12 - 3.14** were different for different Pt: Ru ratios. For the commercial 20% Pt-Ru (1:1) /C catalyst, E_{onset} was 145 mV (**Fig. 3.12**), for a 25% Pt-Ru (3.3:1) /Q1 catalyst, E_{onset} was at 220 mV (**Fig. 2.13**) and for 19% Pt-Ru (1:1) /Q1, E_{onset} was at 180 mV (**Fig. 3.14**). The commercial 20% Pt/C catalyst has E_{onset} at 360 mV (**Fig. 3.11**). So, this technique may be applied to test relative catalytic activity and poisoning tolerance of the binary catalysts. The smaller the value of E_{onset}, the higher the catalytic activity of the catalyst. This work needs further demonstration.

CO stripping voltammetry was also tried for estimating active areas of binary catalysts in this work. **Fig. 3.15** shows a CV of a commercial 20% Pt/C catalyst following CO adsorption at –0.236 V vs. SSCE for 30 minutes, and the second scan in N_2 is used as background. When this method was applied to binary catalysts, the same problem was encountered as with CO_2 stripping scan. No CO desorption peaks were obtained even

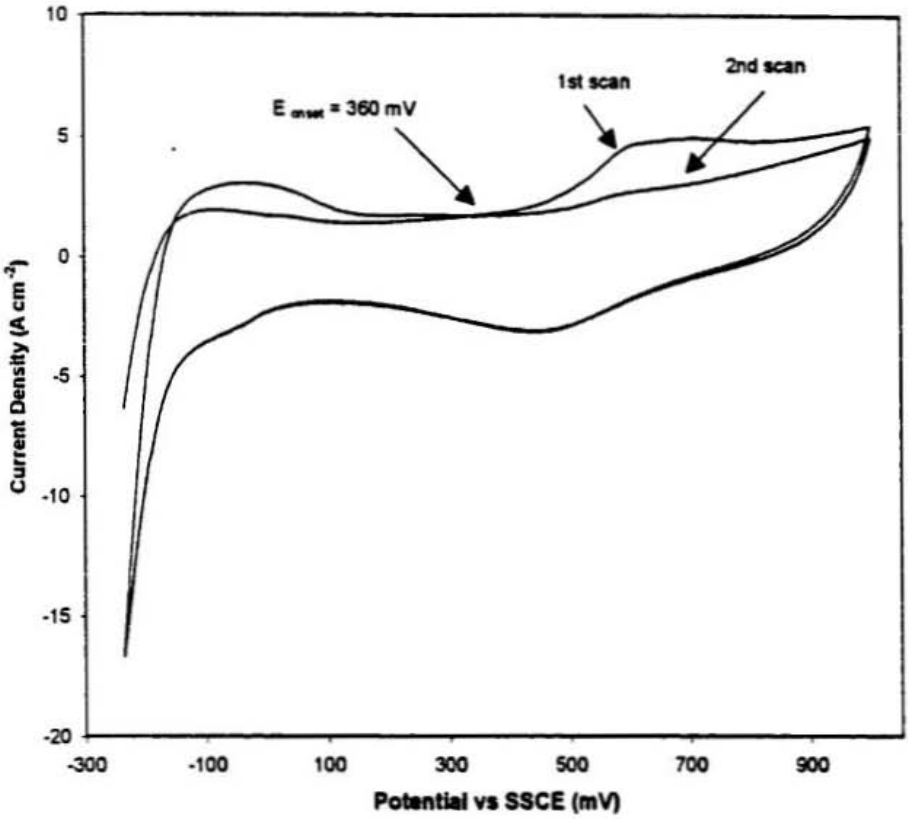

Fig. 3.11 CV at 20 mV/s of reduced CO_2 oxidation following 20 min CO_2 reduction at -0.236 V for a 20% Pt/C catalyst with 0.75 mg Pt cm^{-2} in a half-cell.

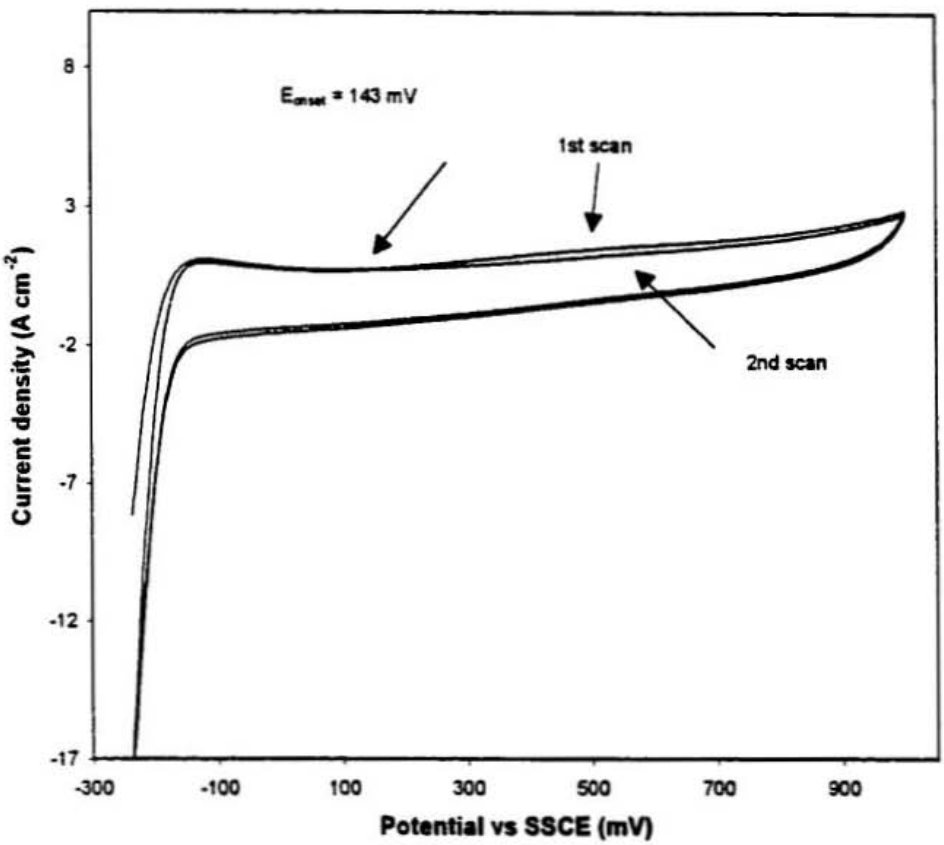

Fig. 3.12 CV at 20 mV/s of reduced CO_2 oxidation following 30 min CO_2 reduction at -0.236 V for 20% Pt-Ru/C catalyst with 0.75 mg Pt-Ru cm^{-2} in a half-cell.

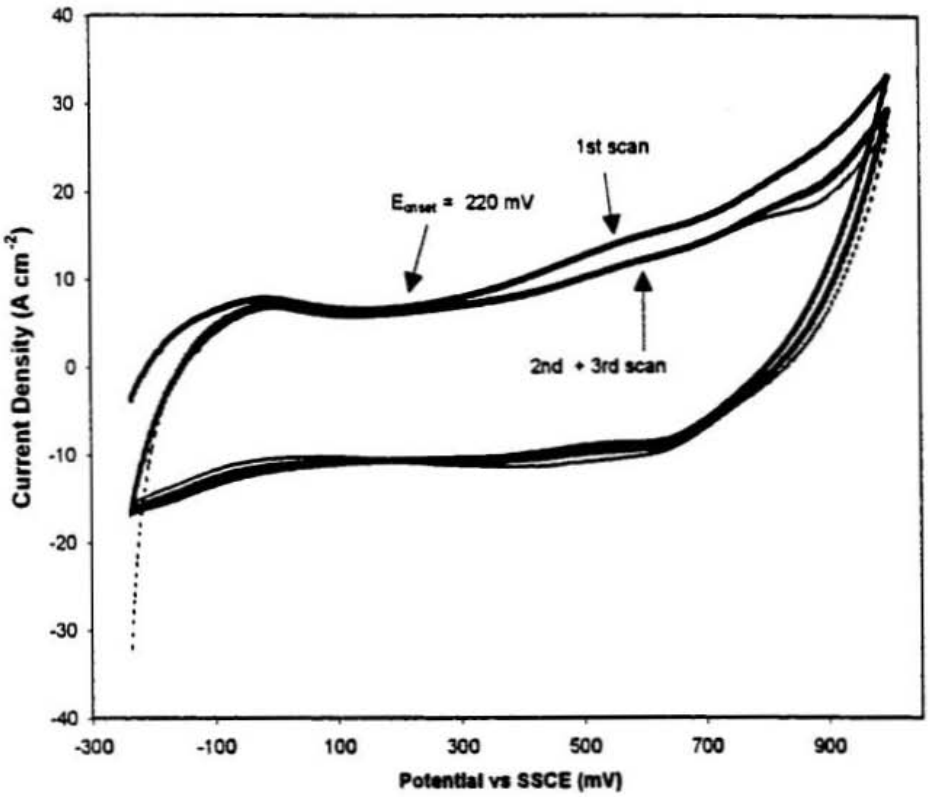

Fig.3.13 CV at 20 mV/s of reduced CO_2 oxidation following 60 min CO_2 reduction at -0.236 V for 25% Pt-Ru (3.3:1)/Q1 with 0.75 mg Pt-Ru cm^{-2} in a half-cell.

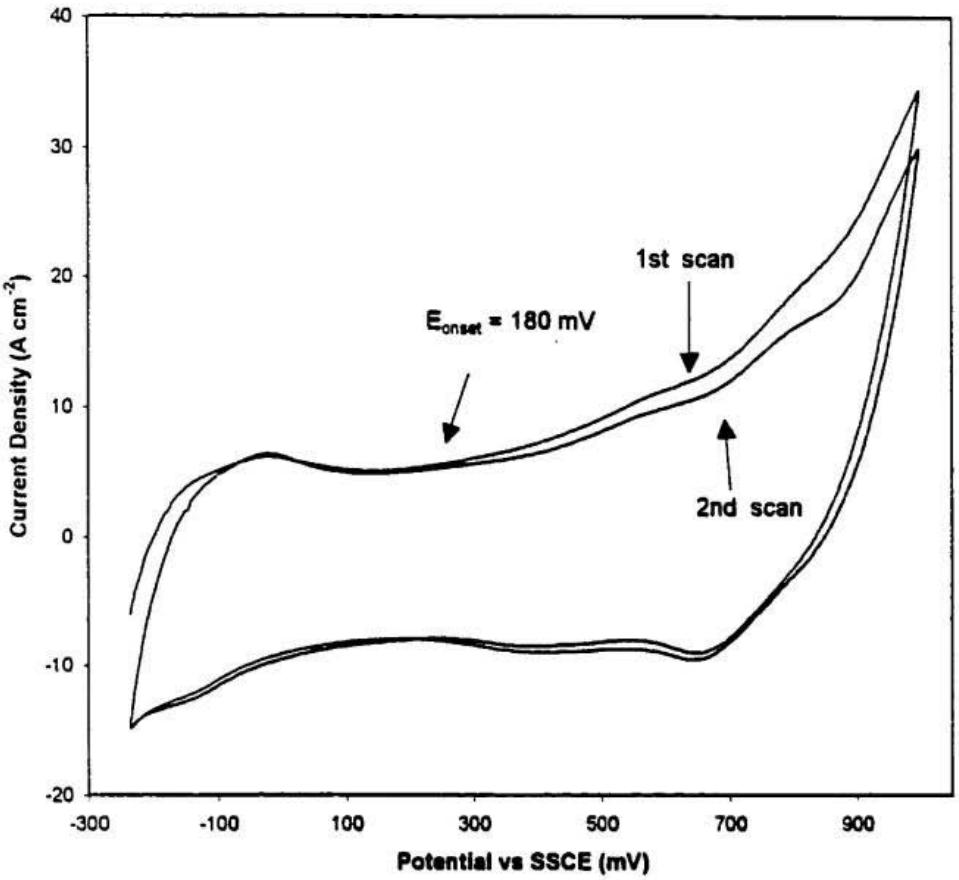

Fig. 3.14 CV at 20 mV/s of reduced CO_2 oxidation following 60 min CO_2 reduction at -0.236 V for 19% Pt-Ru (1:1)/Q1 with 0.75 mg Pt-Ru cm^{-2} in a half-cell.

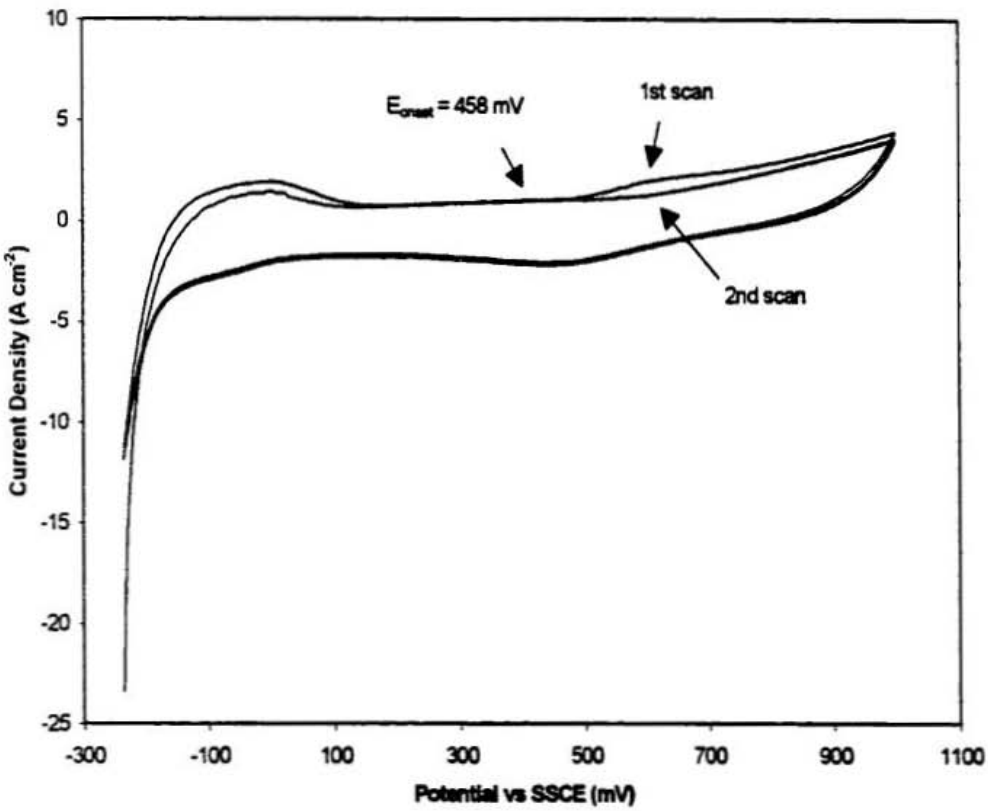

Fig. 3.15 CO stripping voltammetry at 20 mV/s for a commercial 20% Pt/C catalyst with 0.75 mg Pt cm^{-2} in a half-cell.

at adsorption times up to 180 minutes. The reason could be due to the low concentration of CO in N_2 used in our experiments. The reported papers [23, 37-39] always used a high CO concentration ($\exists$1%) gas mixture to prepare adsorbed electrode. However, in these experiments, CO in N_2 was only 55.9 ppm, which is not high enough to run CO stripping voltammetry on our catalysts. Therefore, no further investigations of the use of CO stripping techniques was done in this work.

3.3.4 Characterization of binary catalysts using RDE voltammetry.

3.3.4.1 Cyclic voltammetry

Cyclic voltammograms (CVs) (3^{rd} and 7^{th} cycles) of a commercial 20% (Pt-Ru)/C and a 35%(Pt-Ru)(1.3:1)/Q1 catalyst obtained at room temperature (RT, 22 ^{0}C) and 60 ^{0}C in deaerated 1M (H_2SO_4 + CH_3OH) solution are shown in **Fig. 3.16** and **Fig. 3.17,** respectively. As comparisons, CVs of the two catalysts obtained in 0.5 M H_2SO_4 are also shown in the figures. It can be seen that there is an approximately four-fold increase in current between the CVs obtained at RT and 60 ^{0}C above 0.5 V for both catalysts. The increased currents are related to the negative potential shift for the onset of the nucleation of oxygen-containing species [19]. In addition, at elevated temperature, currents keep increasing with repeated scanning, while at RT a current change is not obvious between two sweep cycles. The reason is probably that the methanol oxidation at high scan speed (100 mV/s used in our experiments) is controlled by kinetics at elevated temperature and

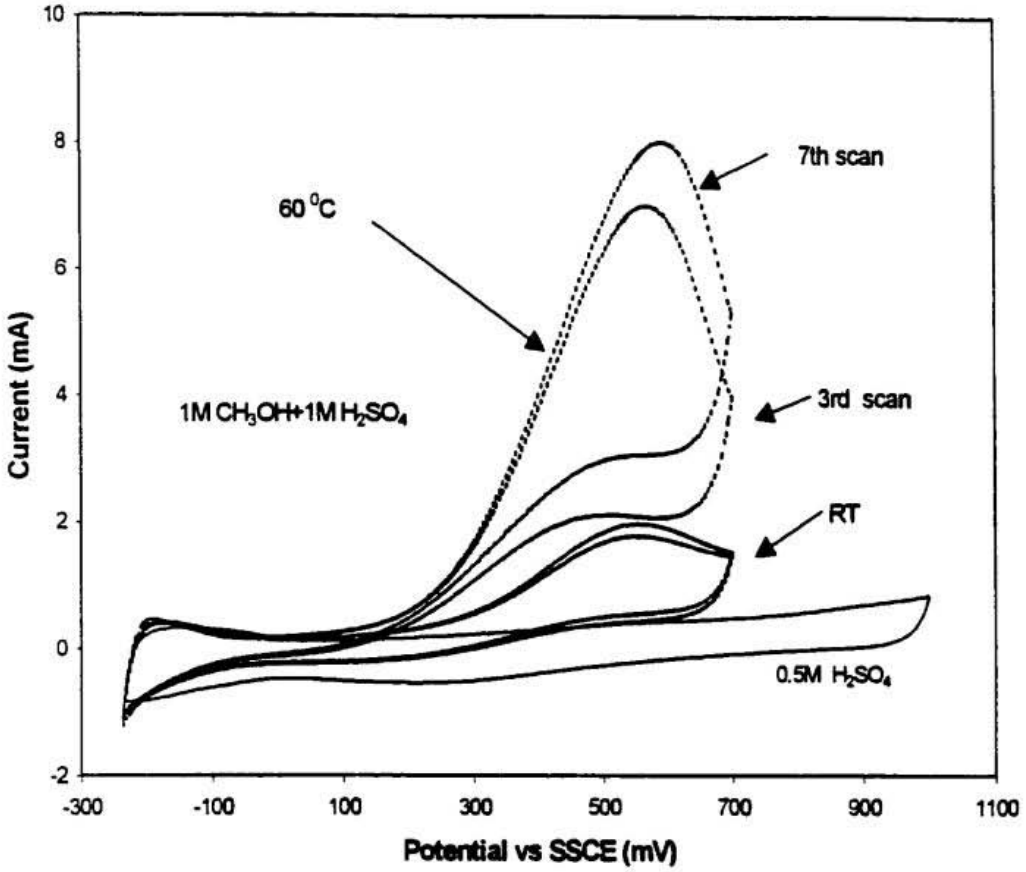

Fig. 3.16 CVs at 100 mV/s for a commercial 20% PtRu/C coated electrode in N_2 saturated 0.5 M H_2SO_4,1 M CH_3OH+ 1 M H_2SO_4 (RT and 60 °C) with 100 μg Pt-Ru cm^{-2}.

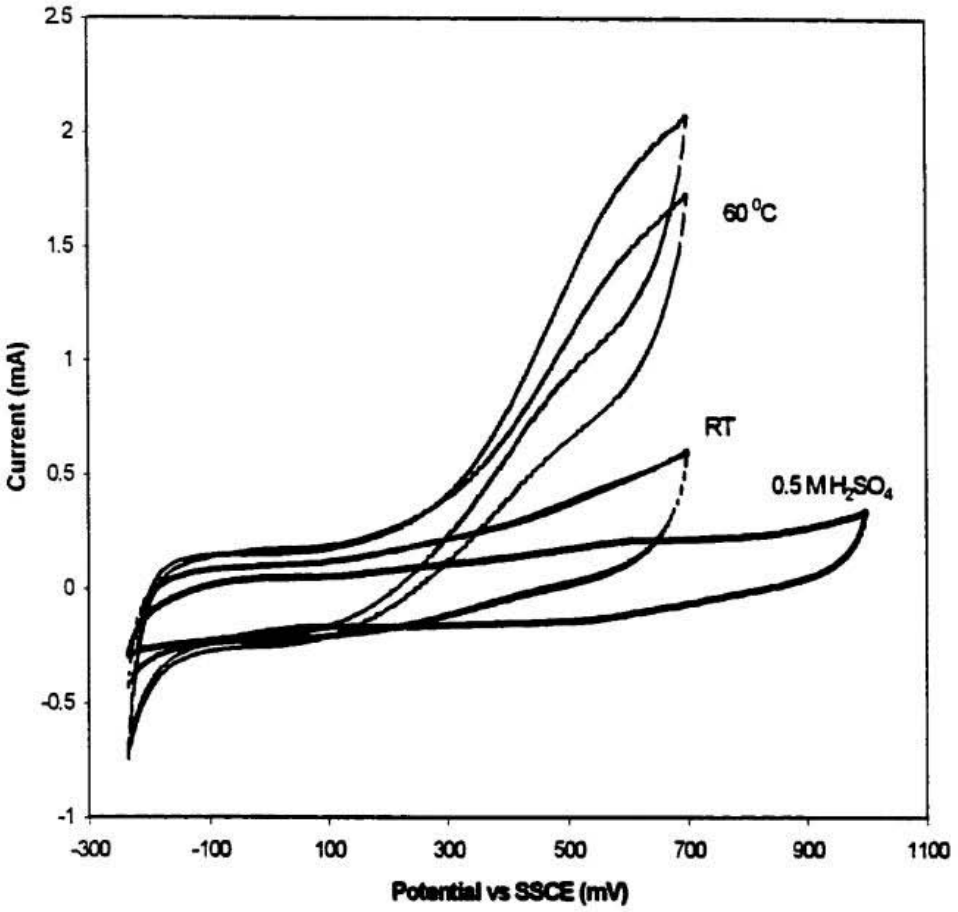

Fig. 3. 17 CVs at 100 mV/s for a 35% PtRu/Q1 (1.3:1) coated electrode in N_2 saturated 0.5 M H_2SO_4, and 1M H_2SO_4 + 1 M CH3OH (at RT and 60 °C) with 100 μg Pt-Ru cm^{-2}.

by diffusion at RT. At elevated temperature, the local temperature at the catalyst surface may increase significantly due to the high current, while at RT, the local temperature change may be insignificant. For commercial binary catalysts, the current also decreases quickly past the maximum due to the reduction of the site accessibility for methanol through lateral sulfate-water interactions [40]. This can be seen on Q1-supported binary and commercial Pt/C catalysts over a wider applied potential range.

Fig. 3.18 and **Fig. 3 .19** compare CVs (third sweep) of the above two catalysts and a commercial 20% Pt/C catalyst obtained at RT and 60 ^{0}C respectively. Compared with the commercial binary catalysts, the Q1-supported binary has no oxidation peak during the oxidation scan (0.05 V - 0.7 V). Compared with the commercial single catalyst, the reversed sweep curve from 0.7 V to 0.05 V of the Q1-supported binary does not overlap with its oxidation curve. The results indicate that there are different accessibilities among Pt-Ru alloys, supports and solutions for Q1-supported catalysts and carbon-supported catalysts. In order to compare the catalytic properties of the three catalysts, just the anodic scans (0.05 V – 0.5 V) of the CVs in **Fig. 3.19** are presented in **Fig. 3.20**. The negative potential shift for both the Q1-supported binary and the commercial binary catalyst with respect to the commercial single catalyst indicates a better catalytic activity for the binary systems. However, the Q1-supported binary catalyst exhibits inferior performance to the commercial binary catalyst by having a higher overpotential, and lower currents at high potentials (above 0.5 V). The reason is probably due to electronic isolation of the Pt-Ru particles as discussed in Chapter 2 (Section 2.3.3.2) for single catalysts. This can be demonstrated by adding a small amount of carbon black to the Q1-supported binary catalyst and running CV again. From **Fig. 3.21,** an enhanced current

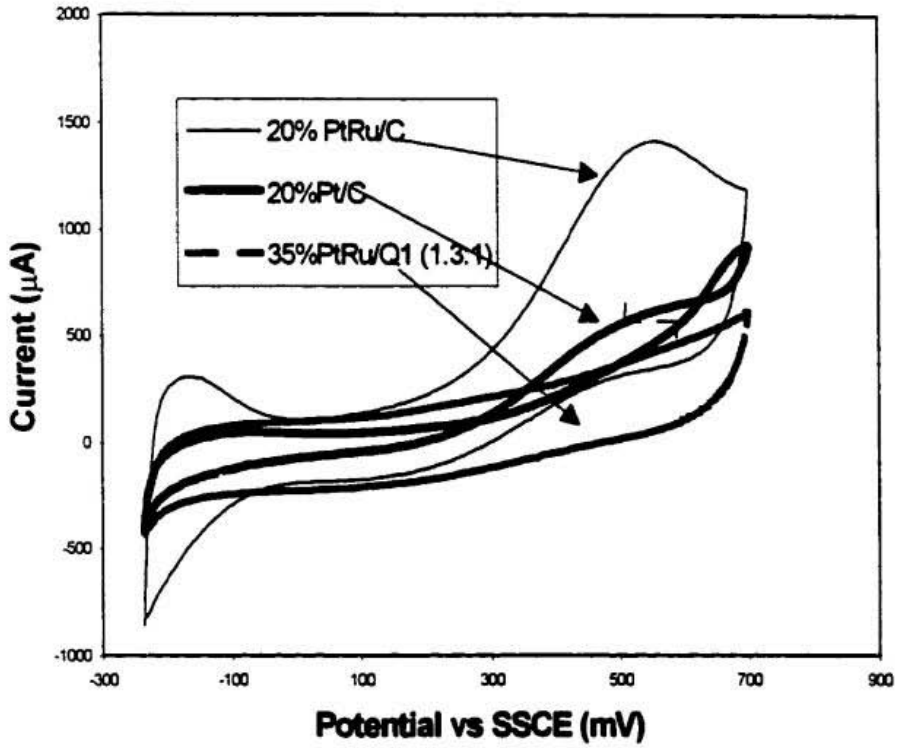

Fig. 3.18 CVs at 100 mV/s for commercial PtRu/C and Pt/C, and 35% PtRu/Q1 (1.3:1) coated electrodes in N_2 saturated 1M H_2SO_4+1M CH_3OH at RT with 100 μg Pt-Ru cm^{-2}.

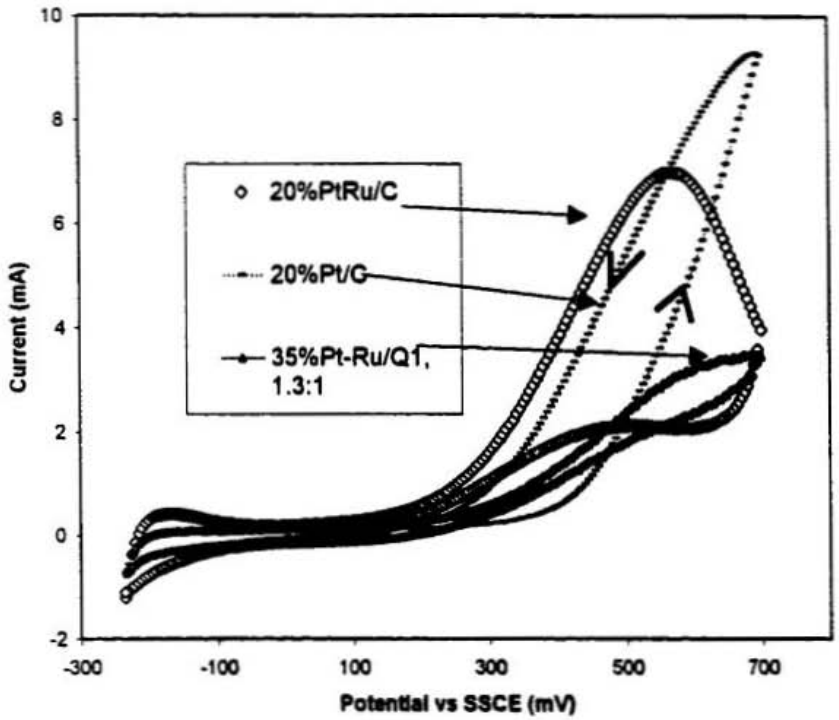

Fig. 3.19 CVs at 100 mV/s for commercial PtRu/C, Pt/C and Pt-Ru/Q1 coated electrodes in N_2 saturated 1M H_2SO_4+1M CH_3OH at 60^0C with 100 μg Pt-Ru cm^{-2}.

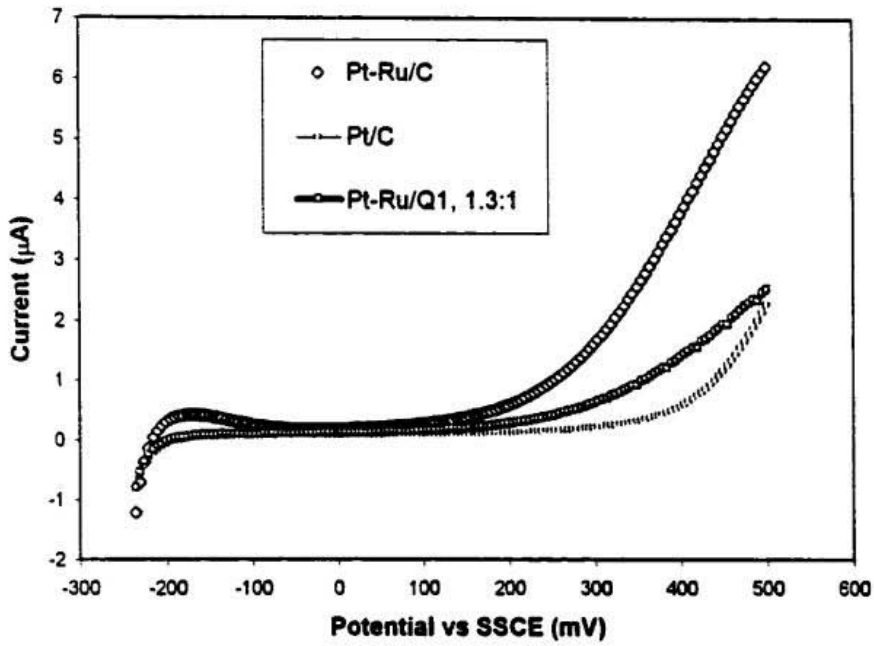

Fig. 3.20 CVs at 100 mV/s in N_2 saturated 1M H_2SO_4+1MCH_3OH at 60 ^{0}C of anodic scans for PtRu/C, Pt/C and PtRu/Q1(35%, 1.3:1) catalyst coated electrodes with 100 μg Pt-Ru cm^{-2}.

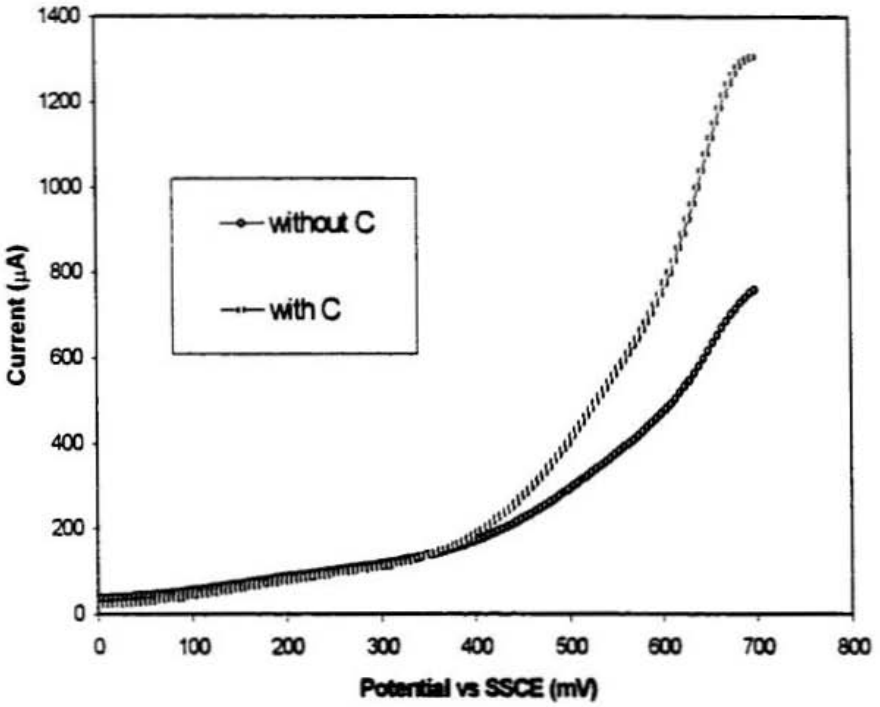

Fig. 3.21 CVs at 100 mV/s in N_2 saturated 1M H_2SO_4 + 1 M CH_3OH at RT of anodic scans for 35% (Pt-Ru) (1.3:1)/Q1 catalyst coated electrodes with (80 μg C cm^{-2}) and without added carbon black.

after adding carbon can be observed, which can be attributed to improved electronic conductivity between the Pt-Ru and support (Q1 and C) after adding carbon.

3.3.4.2 Methanol Oxidation Polarization

Fig. 3.22 shows methanol polarization curves for a pulse width (PW) of 10 s for a 35% (Pt-Ru) (1.3:1)/Q1) catalyst at 60^{B}C in a RDE configuration recorded until a reproducible curve was obtained. **Fig 3.23** compares the methanol oxidation polarization curves for a Q1-supported binary and a commercial binary catalyst at RT and 60 ^{0}C. From the figure, the currents obtained at 60^{0}C for both binary catalysts have increased approximately ten-fold at ca. 0.5 V with respect to those obtained at RT. The onset potential for the Q1-supported binary catalyst is higher than that of the commercial binary catalyst and the currents are still significantly lower at ca. 0.5 V. The results are similar to those obtained from CVs.

Fig. 3.24 shows some polarization curves for a PW of 10 s at RT for commercial and some Q1-supported binary catalysts. Overall, performances of Q1-supported binary catalysts are inferior to that of the commercial binary catalyst. In some cases, the results are difficult to explain. For example, in the case of 21% (Pt-Ru) (1.2:1) /Q1 with carbon added to improve the electronic conductivity, its E_{onset} is moved negatively to become comparable to that of the commercial binary catalyst, but its currents at high potential are still low. In another case, when the performances of 28% Pt-Ru (7:1)/Q1 and 35% Pt-Ru (1.3:1)/Q1 were compared, the former catalyst would be expected to have a higher E_{onset} because of the high Pt:Ru ratio, but this is not seen (**Fig. 3.24**).

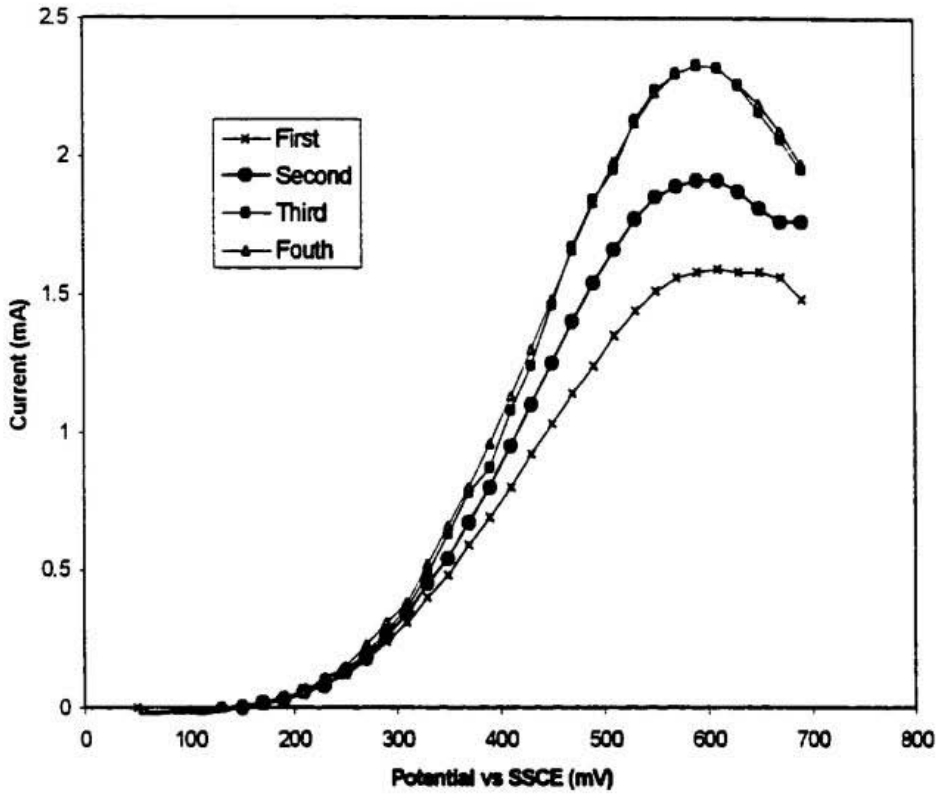

Fig. 3.22 Methanol oxidation polarization curves for a 35% Pt-Ru (1.3:1)/Q1 catalyst coated electrode in 1 M H_2SO_4 + 1 M CH_3OH at 60 ^{0}C for a pulse width(PW) of 10 s.

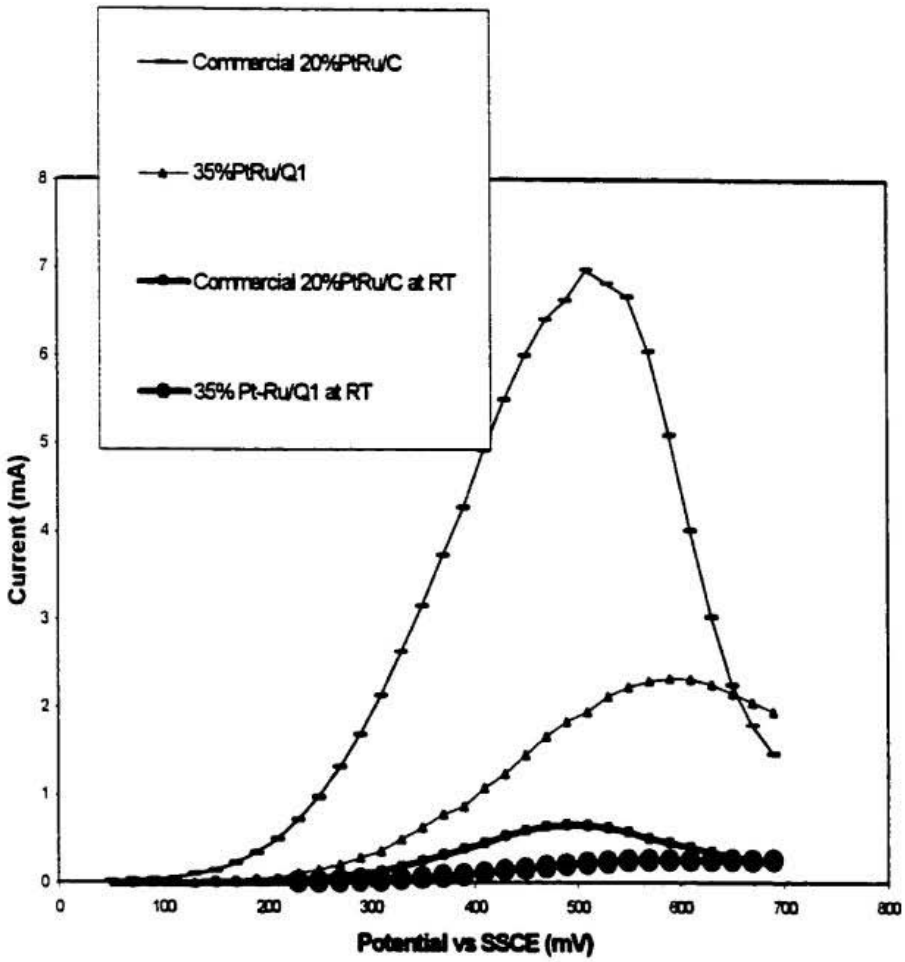

Fig. 3.23 Methanol oxidation polarization curves for commercial and Q1-supported binary catalyst coated electrodes at 60 ^{0}C and RT with 100 μg Pt-Ru cm^{-2} in 1 M H_2SO_4 + 1 M CH_3OH at PW of 10 s and rotation rate 1000 rpm.

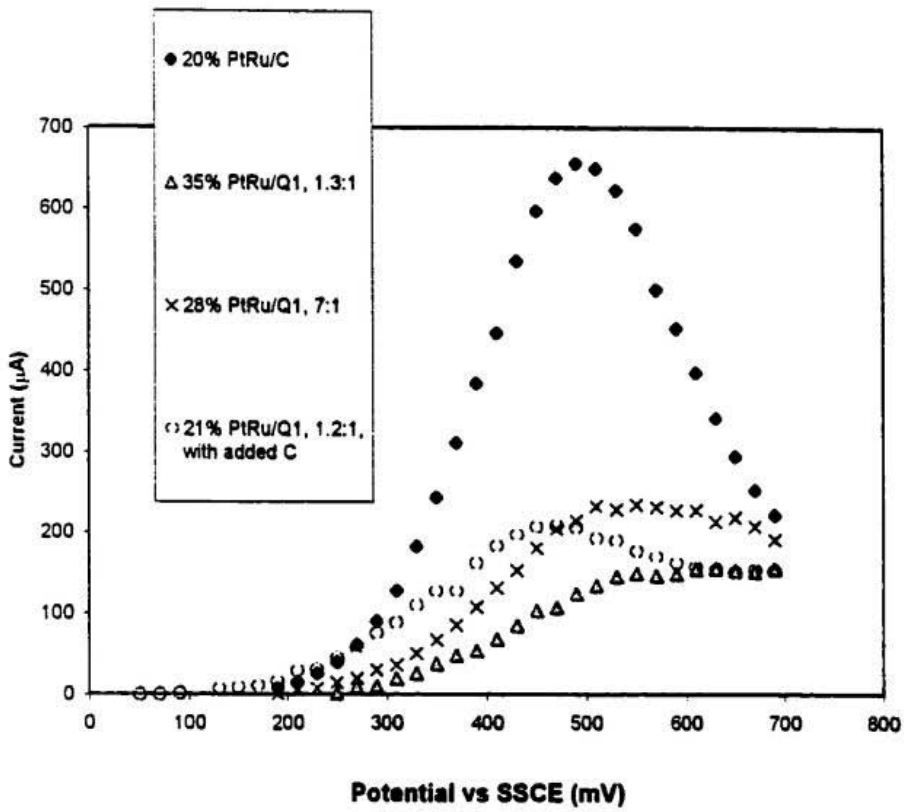

Fig. 3.24 Methanol oxidation polarization curves for electrodes coated by some Q1-supported binary catalysts and a commercial binary catalyst with 100 μg Pt-Ru cm^{-2} at RT. PW 10s.

Thus, whether a PW of 10 s is long enough to compare the performances of these catalysts on a common basis needs reconsideration. Thus, chronoamperometry (CA) in which currents are recorded as the function of time at a fixed potential was used.

3.3.4.3 Chronoamperometry of binary catalysts

Fig. 3.25 and **Fig. 3.26** show CAs of a commercial binary catalyst and a Q1-supported binary catalyst run multiple times until reproducible curves were obtained. The background run for un-catalyzed Q1 demonstrates that polymer charging current does not contribute greatly to the current seen for the Q1 supported catalyst. Background corrected CA curves for a commercial catalyst and some Q1-supported binary catalysts are shown in **Fig. 3.27.** The current declines with time because of sulfate-water interactions discussed in Section 3.3.4.1 [40]. It can be seen that the currents for the commercial binary catalyst are higher than for Q1-supported binary catalysts at long times ($\exists$ 100 s). At short time (< 100s), 35% Pt-Ru (1.3:1)/Q1 has comparable (or a little higher) currents to the commercial binary catalyst. These results indicate that the current declines more quickly for Q1-supported binary catalysts than that for the commercial binary catalyst during the methanol oxidation. Comparisons made at short times may therefore produce different conclusions than those obtained at long times. Therefore, when comparing the performance of the catalysts, the PW time must be taken into consideration.

At different applied potential steps (0.05 – 0.3 V, 0.05 – 0.5 V and 0.05 – 0.7 V), CAs of two kinds of catalysts are shown in **Figs. 3.28 – 3.29** respectively and compared

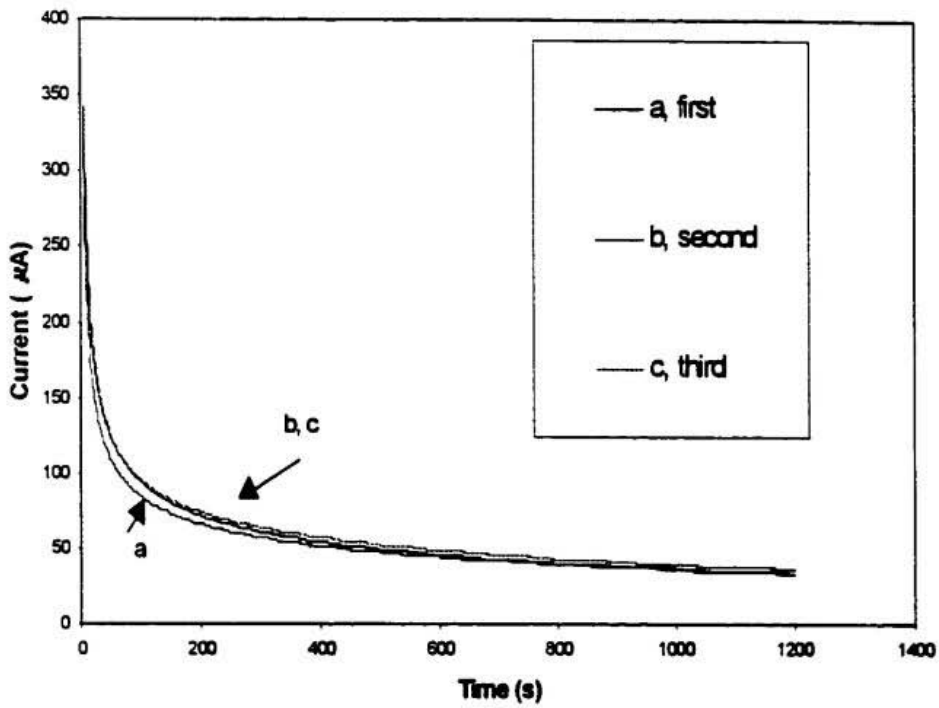

Fig. 3.25 Chronoamperometry (CA) for a commercial 20% Pt-Ru/C catalyst coated electrode with 100 mg Pt-Ru cm^{-2} in 1 M ($CH_3OH + H_2SO_4$) for potential steps of 0.05 - 0.7 V. Rotation rate 1000 rmp.

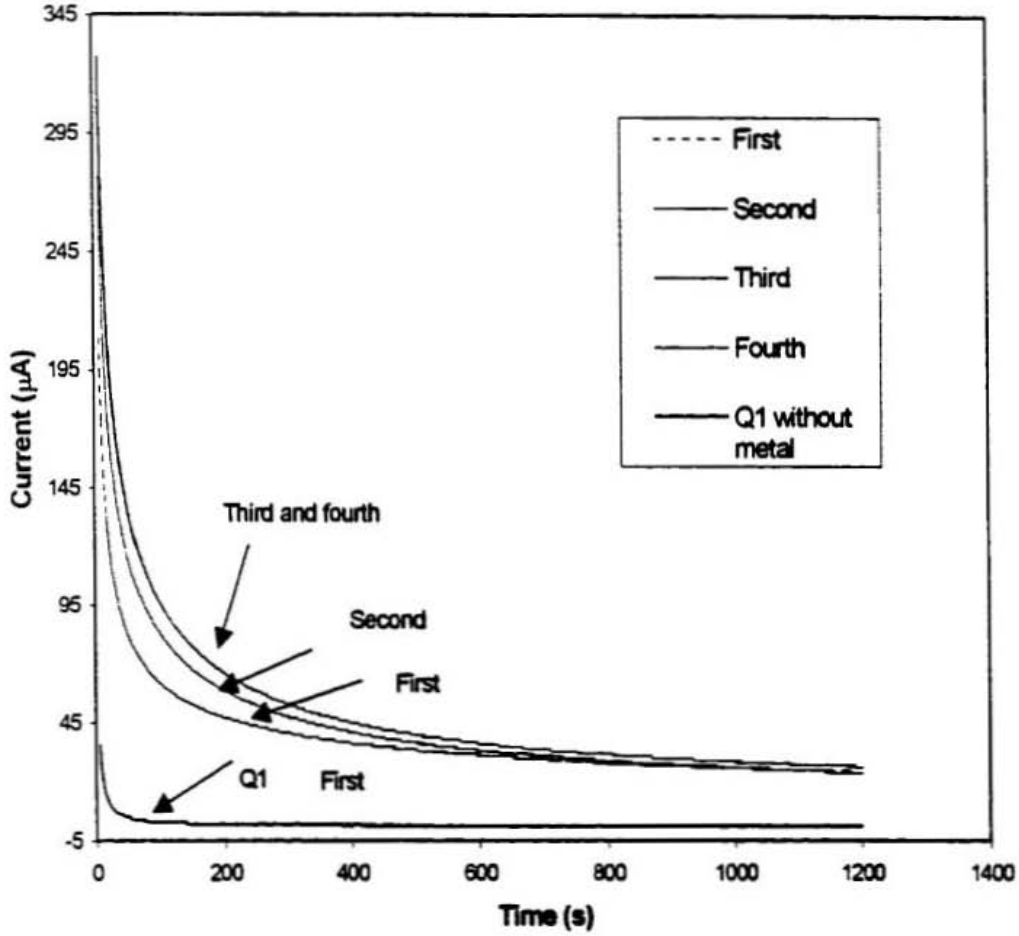

Fig. 3.26 CAs for a 35% Pt-Ru (1.3:1)/Q1 catalyst coated electrode with 100 μg Pt-Ru cm^{-2} and a Q1 alone coated electrode in 1 M (CH_3OH + H_2SO_4) for potential steps of 0.05 - 0.7 V. Rotation rate 1000 rpm.

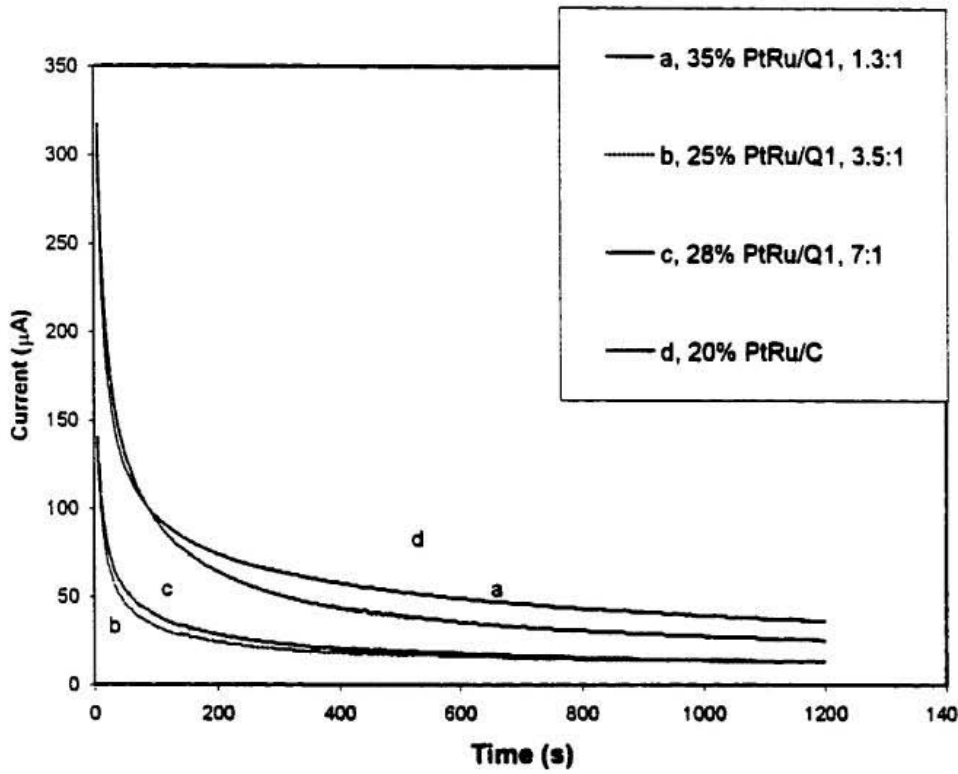

Fig. 3.27 Background corrected CAs for Pt-Ru/Q1 and commercial catalyst coated electrodes with 100 μg Pt-Ru cm^{-2} for potential steps of 0.05 - 0.7 V. Rotation rate 1000 rpm.

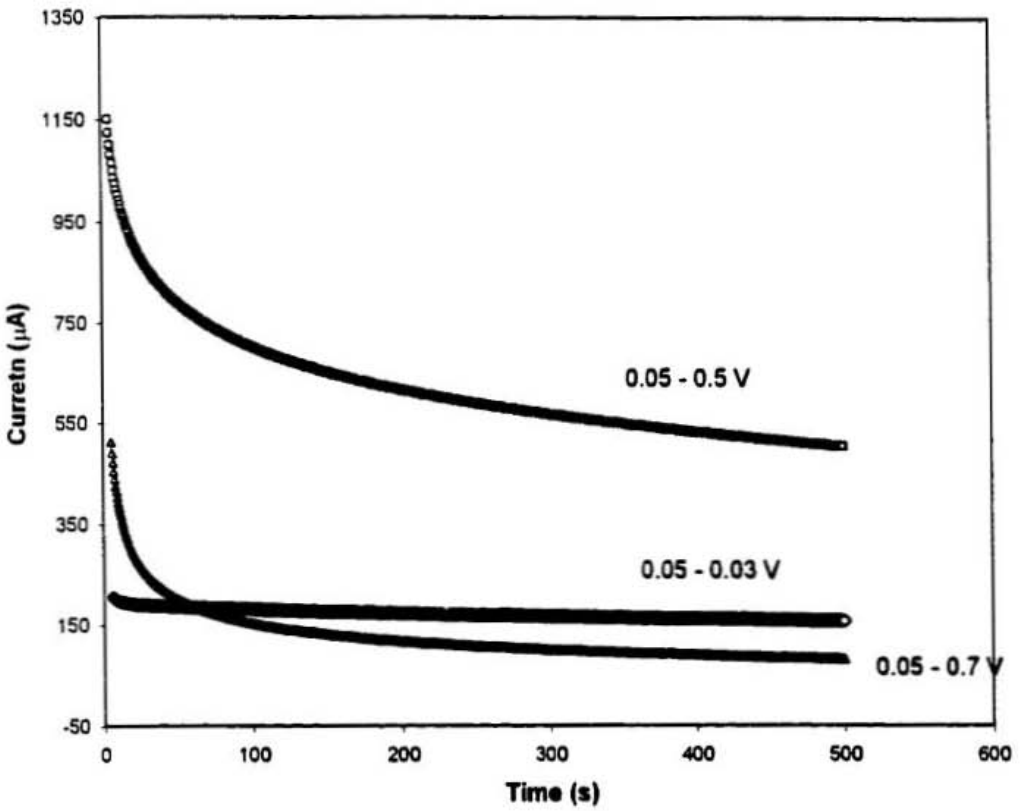

Fig. 3.28 CAs for a commercial 20% Pt-Ru/C coated electrode for different potential steps in 1 M (CH_3OH+H_2SO_4). Rotation rate 1500 rpm.

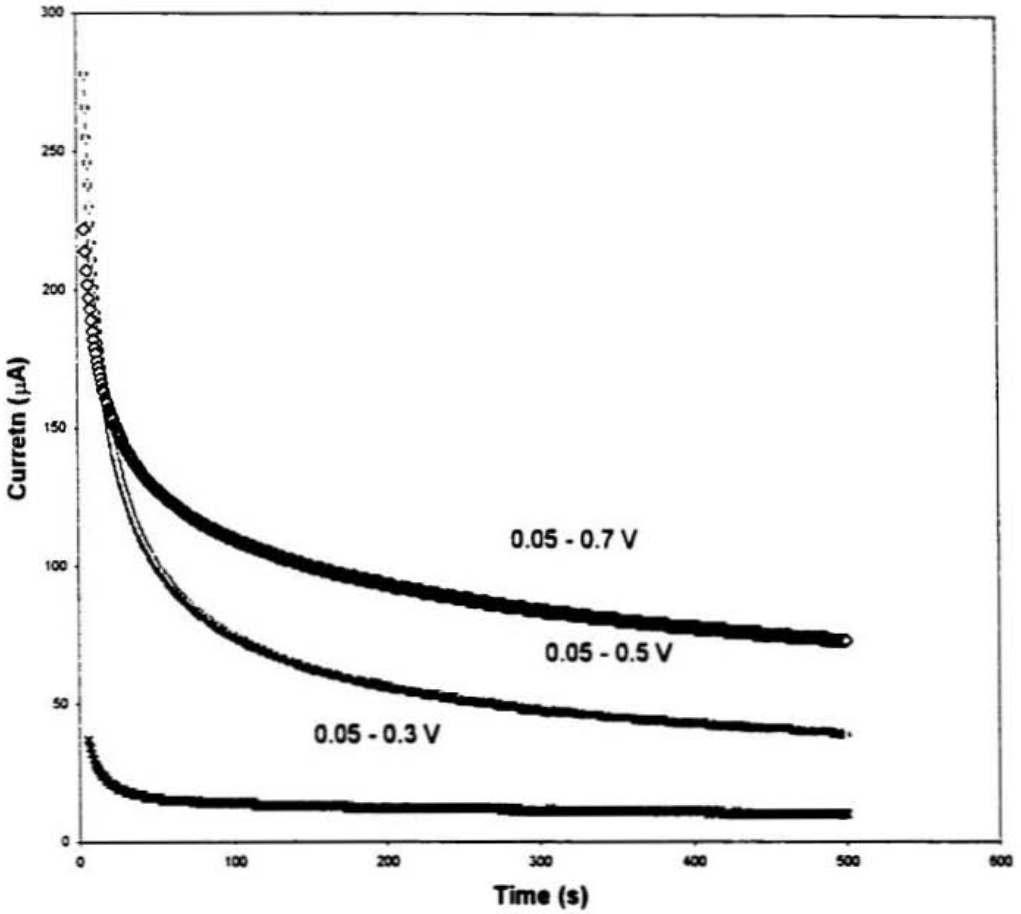

Fig. 3.29 CAs for a 35% Pt-Ru (1.3:1)/Q1 coated electrode for different potential steps in 1 M (CH_3OH+H_2SO_4). Rotation rate 1500 rpm.

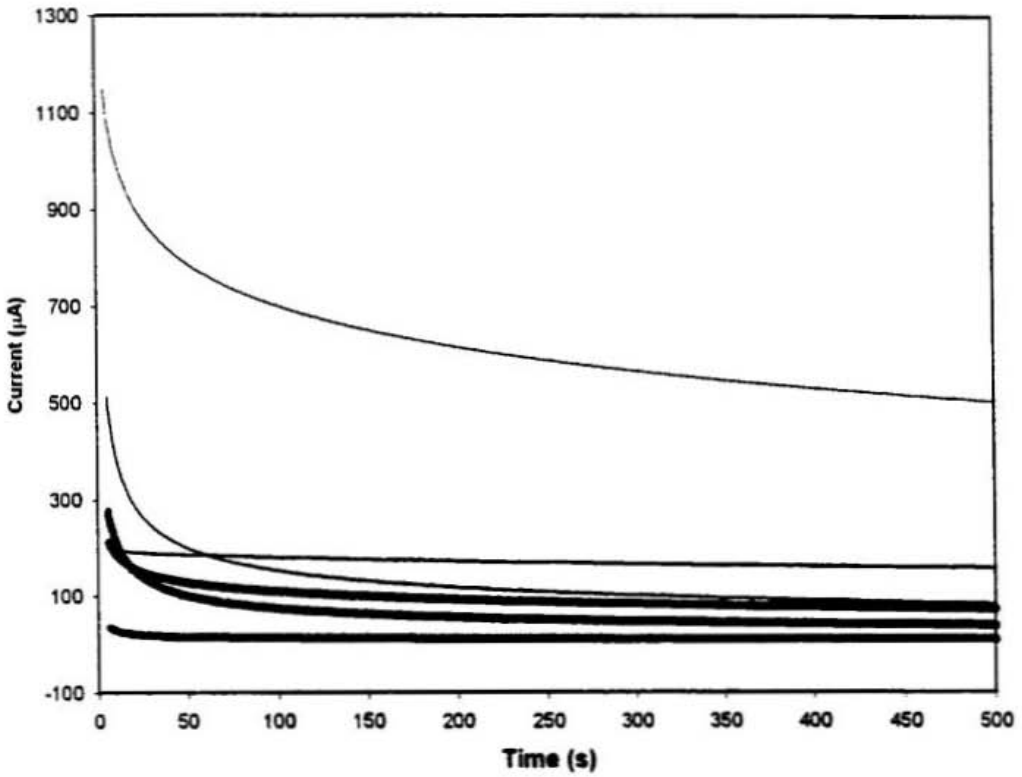

Fig. 3. 30 CAs for 35% Pt-Ru/Q1 (heavy lines) and commercial 20% Pt-Ru/C catalyst (light lines) coated electrodes for different potential steps as in Fig. 3.28 and Fig. 3.29.

in **Fig. 30**. The commercial Pt-Ru/C catalyst gives higher currents at 0.5 V, and for the 35% Pt-Ru/Q1 catalyst is at 0.7 V. The current at 0.7 V for the commercial catalyst declines below that at 0.3 V after ca. 70 s, while the current at 0.5 V for the 35% Pt-Ru/Q1 catalyst is higher than that at 0.3 V. These current changes for the Q1-supported and carbon-supported catalysts are similar to their current changes in CVs. (**Figs 3.16 – 3.18**). When all these CA curves are compared in **Fig. 3.30**, the performances of the two kinds of catalysts can be compared by the current values at a specifc reaction time for different potential steps.

3.4 Conclusions

The optimal reaction conditions for obtaining the required polymer-supported binary catalysts have been found and these catalysts have been studied with gas diffusion electrodes (GDE) in half-cells and on carbon disc electrodes in a rotating disc (RDE) configuration. The characteristics and performances of these catalysts were tested by applying various methods, such as EDX, XRD, CV, reduced CO_2 oxidation, methanol polarization and chronoamperometry.

It was found that in a chemically co-deposited alloy Ru breaks up the Pt lattice structure. Better performances were obtained for polymer-supported binary catalysts having Pt: Ru ratio around 1- 2, but their performances were usually inferior to those of commercial binary catalysts from the results obtained in GDE and RDE configurations. Reduced CO_2 oxidation was not suited here to calculate active areas of binary catalysts,

however, the method was suggested to be used to compare catalytic activity using the onset potentials for CO_2 oxidation.

Chronoamperometry was found to be a good method to follow the current change during methanol oxidation. The result shows that a long step time is needed to compare the performances of catalysts for methanol oxidation.

Reference

1. M. R. Andrew, R. W. Glazebrook, in: K. R. Williams (Ed), *An Introduction to Fuel cells*, Elsevier, p. 127, 1966.
2. K. J. Cathro, *J. Electrochem. Soc.* **116**, 1608 (1969).
3. M. M. Janssen and J. Moolhuysen, *Electrochim. Acta.*, **21**, 861 (1976).
4. S. R. Wang and P. S. Fedkiw, *J. Electrochem. Soc.*, **139**, 3151 (1992).
5. B. Bittins-Cattaueo and T. Iwasita, *J. Electroanal. Chem.*, **238**,151 (1997).
6. P. N. Ross, K. Kinoshita, A. J. Scarpellino and P. Stonehart, *J. Electroanal. Chem.*, **59**, 177 (1975).
7. J. O' M. Bockris, H. J. Wroblowa, *J. Electroanal. Chem.*, **7**, 428 (1964).
8. H. Pahms, J. O' M. Bockris, *J. Electrochem. Soc.*, **11**, 267 (1964).
9. M. Watanabe and S. Matoo, *J. Electroanal. Chem.*, **60**, 267 (1975).
10. N. Ross, K. Kikoshita, A. J. Scarpellino and P. Stonehart, *J. Electroanal. Chem.*, **63**, 97 (1975).
11. K. Franaszczuk and J. Sobkowski, *J. Electroanal. Chem.*, **327**, 235 (1992).

12. B. R. Rache, Jr., F. R. Mclarnon and E. J. Cairns, *J. Electrochem. Soc.*, **142**, 1073 (1995).

13. T. Freelink, W. Visscher and J. A. R.Van Veen, *Electrochim. Acta.*, **39**, 1871 (1994).

14. T. Freelink, W. Visscher, A. P. Cox and J. A. R. Van Veen, *Electrochim. Acta.*, **40**, 1537 (1995).

15. J. B. Goodenough, A. Hamnett. B. J. Kennedy, R. Manoherna and S. A. Week, *J. Electroanal. Chem.*, **240**, 133 (1988).

16. S. Swathirajan and Y. M. Mikhail, *J. Electrochem. Soc.*, **138**, 5 (1991).

17. R. Ianniello, V. M. Schmidt, U. Stimming, J. Stumper and A. Wallau, *Electrochim. Acta.*, **39**, 1863 (1994).

18. H. A. Gasteiger, N. Markovic, P. N. Ross, Jr. and E. J. Cairus, *Electrochim. Acta.*, **39**, 1825 (1994)

19. H. A. Gasteiger, N. Markovic, Jr. and E. J. Cairns, *J. Electrochem. Soc.*, **141**, 1795 (1994).

20. H. A. Gasteiger, N. Markoric, P. N. Ross, Jr. and E. J. Cairns, *J. Phys. Chem.*, **98**, 617 (1994).

21. T. Freelink, W. Visscher, J. A. R.Van Veen, *Surface science*, **335**, 353 (1995).

22. A. S. Arico, P. Creti, H. Kim, R. M Antegna, N. Gioradno and V. Actonucci, *J. Electrochem. Soc.*, **143**, 3950 (1996).

23. T. J. Schmidt, M. Noseke, H. A. Gasteiger and R. J. Behm P. Britz and H. Bonne Mann, *J. Electrochem. Soc.*, **145**, 925 (1998).

24. W. Chrzanowski and A. Wieckowski, *Langmuir*, **14**, 1967 (1998).

25. Li liu, C. Pu, R. Viswanathan, Q. Fan, R. Liu and E. S. Smotkin, *Electrochim. Acta.*, **43,** 3657 (1998).

26. H. M. Staffarian, R. Srinivasan, P. Chu and S. Gilman, *Electrochim. Acta.*, **44,** 1447 (1998).

27. A. S Akicò, A. K. Shukla, K. M. El-khatib, P. Creti and V. Antonucci, *J. App. Electrochem.*, **29,** 671 (1999).

28. G. T. Burstein, C. J. Barnett, A. R. Kueernak, K. R Willams, *Catalysis Today*, **38,** 425 (1997).

29. S. Wasmus, A. Küver, *J. Electroanal. Chem.*, **461,** 14 (1999).

30. V. S. Bagozsky, Yu. B. Vassiliev, Q. A. Khazova, *J. Electroanal. Chem.*, **81,** 229-238 (1977).

31. M. Watanabe, M. Vchida and S. Matoo, *J. Electroanal. Chem.*, **229**, 395 (1987).

32. H. Laborde, J-M.L3ger, C. Lamy, *J. App. Electrochem.*, **24(10)**, 1019 (1994).

33. M. C. Lefebvre, Z. Qi, D. Rana and P. G. Pickup, *Chem. Mater.*, **11**, 262 (1999).

34. M. C. Lefebvre, Z. Qi and P. G. Pickup, *J. Electrochem. Soc.*, **146**, 2054 (1999).

35. B. D. McNicol, D. A. J. Rand, K. R. Williams, *J. Power Sources*, **83,** 15-31 (1999).

36. Nenyou Jia, M.S. thesis. Memorial University, 1999.

37. K. F. Blurtion, P. Greenbery, H. G. Osein and D. R. Rutt, *J. Electrochem. Soc.*, **119**, 559 (1972).

38. T. R. Ralph, G. A. Hards, J. E. Keating, S. A. Gampell, D. P. Wilkinson, M. Davis, J. St-Pierre and M. C. Johnson, *J. Electrochem. Soc.*, **144**, 3845 (1997).

39. K. Kunimatsu, K. Shimazu and H. Kita, *J. Electroanal. Chem.*, **256**, 371 (1988).

40. E. Herrero, K. Franaszczuk and A. Wieckowski, *J. Phy. Chem.*, **98**, 5074 (1994).

Chapter 4

Polymer-Supported Ternary and Quaternary catalysts for Methanol Oxidation, and Transition Metal Sulfides for Oxygen Reduction

4.1 Introduction and Objectives

4.1.1 Ternary and quaternary catalysts for methanol oxidation

To date, most work on catalyst development for methanol oxidation has been concentrated on carbon-supported, platinum-based catalysts. Bimetallic Pt-Ru catalysts were found to be the best catalysts for methanol electro-oxidation until recently [1,2] when a new, promising, ternary Pt-Ru-Os catalyst was developed and found to be a more active anode catalyst than Pt-Ru (1:1) [3,4]. Not very long afterwards, the application of "combinatorial catalysis", a technique used extensively in bio-organic systems, to the identification of electrochemical catalysts showed that a quaternary Pt(44)/Ru(41)/Os(10)/Ir(5) (atomic percent) catalyst exhibited higher activity than the binary Pt-Ru alloy [5].

Thus, in this chapter, Preliminary results are reported on the development of polymer-supported ternary and quaternary catalysts.

4.1.2 Transition metal sulfides for oxygen reduction

In addition to the poor activity of methanol electro-oxidation catalysts, another obstacle inhibiting the application of PEMDMFCs is the phenomenon of methanol crossover through the polymer electrolyte membrane from the anode to the cathode [6,7]. This causes poisoning of the Pt cathode catalyst reducing its activity. To avoid this problem, four possibilities have been considered: the use of cathode catalysts insensitive to methanol, the development of membranes not permeable to methanol, the modification of current membranes, and optimization of operating conditions. In order to find catalysts insensitive to methanol, one approach has tried to find non-Pt based cathode catalysts that are active for oxygen reduction. Mixed-metal catalysts based on transition metal sulfides such as ReRuS and MoRuS were found to give acceptable performances for oxygen reduction [8].

Based on these considerations and the advantages of conducting polymers, Q1-supported transition metal sulfides were prepared and tested for the oxygen reduction reaction at GDEs in a half-cell. Preliminary results are reported.

4.2. Experimental

4.2.1 Preparation of ternary and quaternary catalysts

The preparation procedure was the same as that described in Section 3.2 for binary catalysts except that additional metal salts ($OsCl_3$ and K_2IrCl_6) were used. The resulting catalysts were stored in 5% CH_3OH and tested in GDEs in a half-cell and as thin films

immobilized on carbon disc electrodes, following the procedures described in Section 2.2.

4.2.2 Preparation of transition metal sulfide catalysts

Carbon black or Q1 was refluxed in *p*-xylene (99.8%, bp 138 °C) with $Re(CO)_5Cl$, $Ru(CO)_{12}$ and sulfur for 20 hr under nitrogen. The products were then filtered, washed with acetone and dried. The carbon-supported catalysts were heat-treated at 350 °C for 2h under nitrogen while Q1 supported-catalysts were simply dried under vacuum at room temperature overnight.

4.3 Results and discussion

4.3.1 Catalyst composition

Table 4.1 lists all of transition metal sulfides, and ternary and quaternary catalysts that were prepared. For the transition metal sulfides, yields were satisfactory for both types of support, but the electronic conductivity decreased; even for the carbon support, the electronic conductivity fell below 1 S cm^{-1}.

For Q1-supported ternary and quaternary catalysts, yields were not high. However, the electronic conductivities of these catalysts were still reasonably good (>0.03 S cm^{-1}).

As with chemically deposited binary catalysts, the compositions of the ternary and quaternary catalysts were more difficult to control than those of arc-melted Pt-Ru-Os [4]

Catalyst	1	2	3	4	5	6	7	8	9
	ReRuS /C	ReRuS /Q1	PtRuOs /Q1	PtRuOs /Q1	PtRuOs /Q1	PtRuOs /Q1	PtRuOs /Q1	PtRuOsIr /Q1	PtRuOsIr /Q1
Pt/Ru/OsIr or Re/Ru/S atomic ratio in reaction mixture	2:5:5	2:5:5	0.23:1: 1.6	0.31:1: 1.7	0.17:1: 0.72	0.16:1: 0.31	0.16:1: 3.8	0.16:1: 0.85:0.04	0.18:1: 0.37:0.18
Ratio obtained	3.0:2.9: 4.0	2:2.4: 5.6	3.8:0.29: 1	9.4:2.0:1	2.3:0.8:1	4.6:3.8:1	7.6:1.3:1	10:2.1: 3.3:1	12:1.7: 2.2:1
Yield (mass%)	34	38	43	42	72	66	59	59	60
Result	31	26	23	19	25	26	30	22	34
Yield* (%)	91	68	53	45	35	39	51	37	57
σ ($S\ cm^{-1}$)	0.61	0.0055-0.012	0.39	0.23	0.25	-	-	0.028	-

1. - not measured.
2. "*" See Table 3.1.

Table 4.1 Compositions of Q1-supported ternary catalysts, quaternary catalysts and transition metal sulfide catalysts.

and Pt-Ru-Os-Ir prepared by an "inkjet printer" method [5]. Therefore, it was difficult to systematically investigate the effects of composition. Thus the main objective of this work was to test the performance of the catalysts obtained with varying experimental conditions without considering too much of the compositions among these metals.

4.3.2 Ternary catalysts at GDEs in a half-cell: Methanol oxidation polarizations

Methanol oxidation polarization curves at 30 s step times for a commercial Pt-Ru binary catalyst and a Q1-supported ternary catalyst are shown in **Fig. 4.1**. From the figure, the Q1-supported ternary catalyst can be seen to exhibit a good electrocatalytic activity, but is still inferior to the commercial catalyst.

4.3.3 Ternary and quaternary catalysts tested on carbon disc electrodes

4.3.3.1 Cyclic voltammetry

Fig. 4.2 shows CVs in 1 M CH_3OH + 1 M H_2SO_4 at room temperature at electrodes coated with binary, ternary and quaternary catalysts, while **Fig. 4.3** shows only the anodic scans of the CVs. The methanol oxidation peak position moves slightly negative and becomes somewhat larger for ternary and quaternary catalysts, showing that both are superior to the binary catalyst. The ternary and quaternary catalysts are also

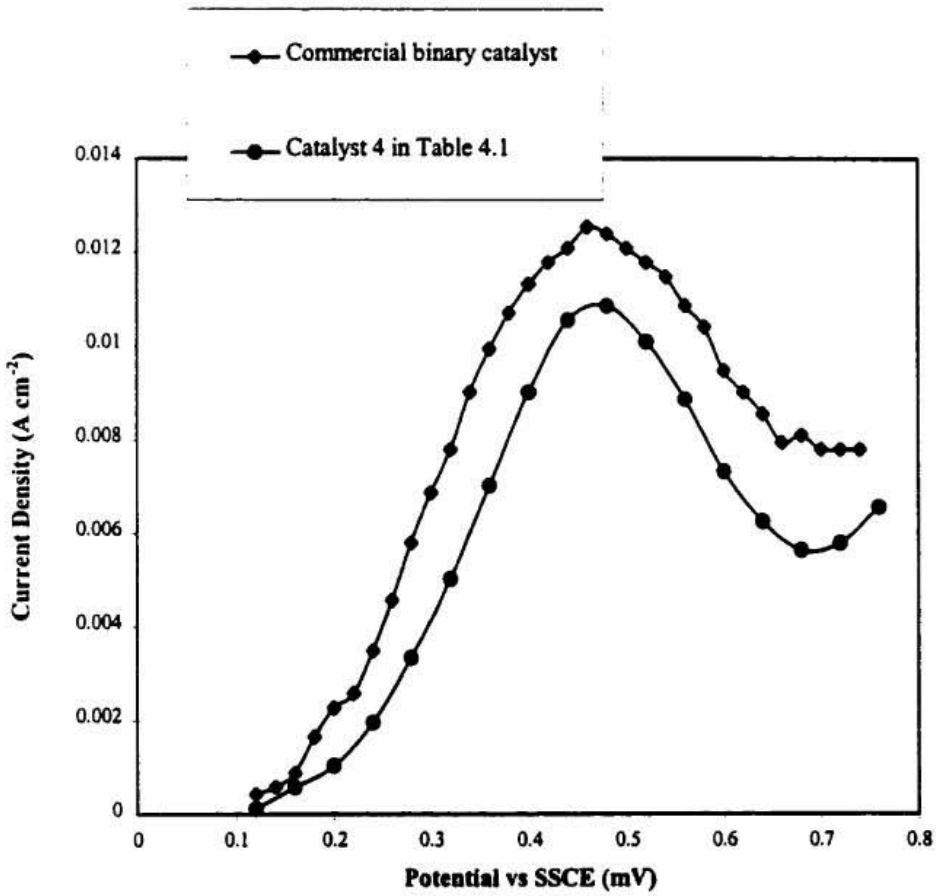

Fig. 4.1 Methanol oxidation polarization curves for a 19% PtRuOs (0.75 mg cm^{-2}) ternary catalyst and a commercial 39% Pt-Ru/C catalyst (0.89 mg cm^{-2}) at step times of 30 s in 1 M (CH_3OH + H_2SO_4) in a half-cell.

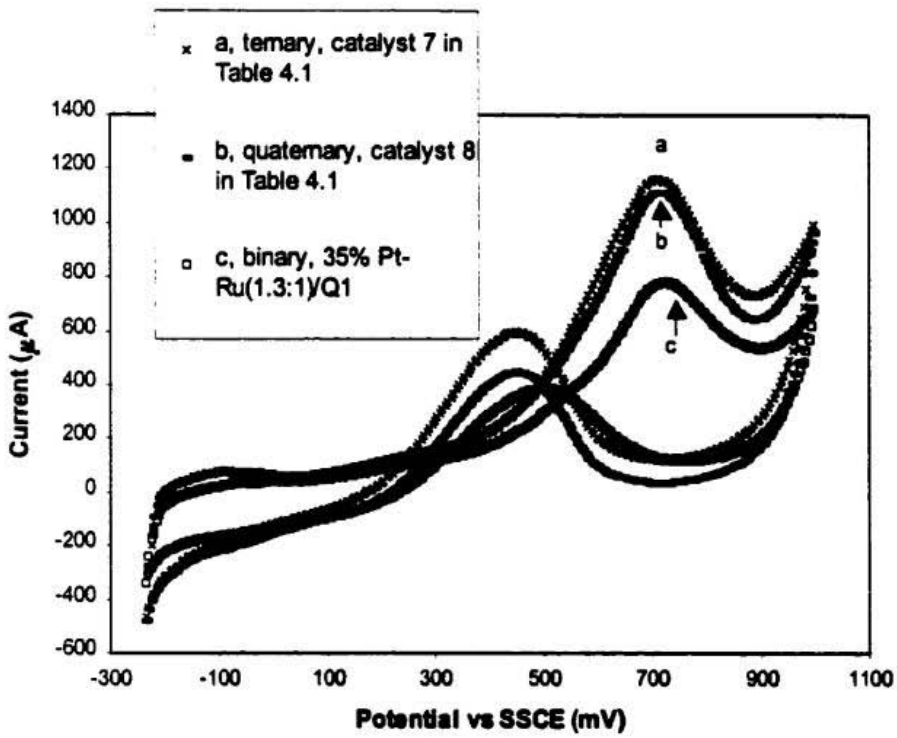

Fig. 4.2 CVs at 100 mV/s for Q1-supported binary, ternary and quaternary catalyst coated electrodes with 100 mg metals cm^{-2} in N_2 saturated 1M CH_3OH + 1M H_2SO_4 at RT.

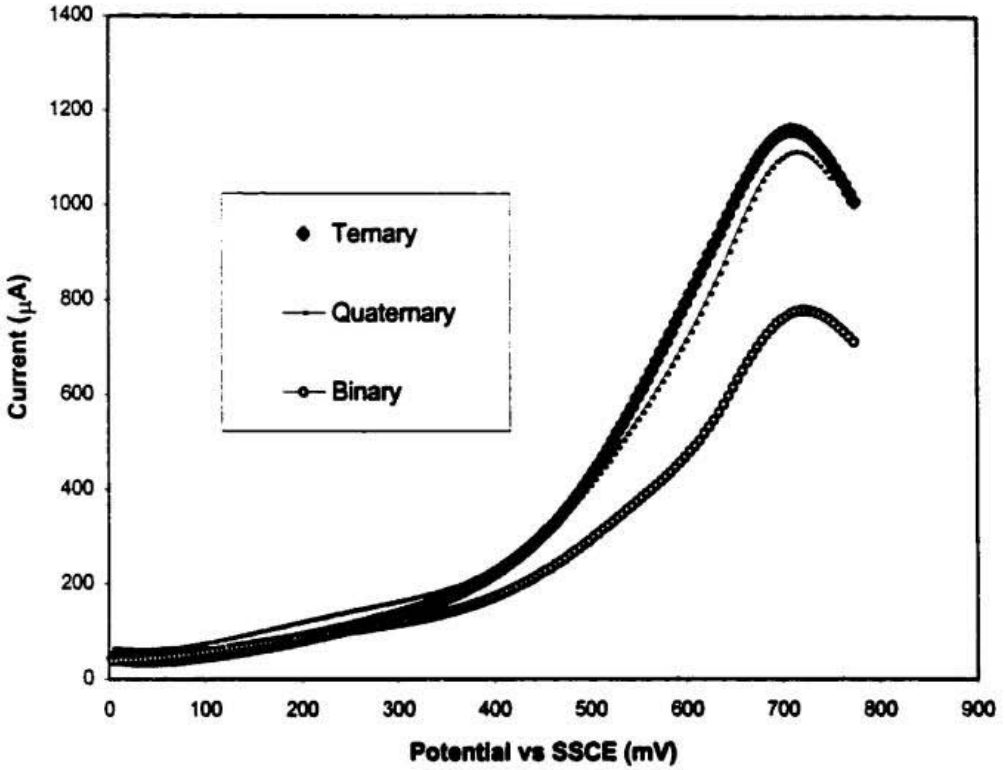

Fig. 4.3 Anodic scans of CVs as in Fig. 4.2 at 100 mV/s for binary, ternary and quaternary catalyst coated electrodes at RT in N_2 saturated 1 M H_2SO_4 + 1 M CH_3OH with 100 mg metals cm^{-2}.

superior at 60 ^{0}C (see **Fig. 4.4**). For the catalysts obtained, ternary catalysts are superior to quaternary catalysts in these experiments.

4.3.3.2 Methanol oxidation polarization

An example of a Q1-supported ternary catalyst tested for methanol oxidation polarization with a step time of 10 s at 60 ^{0}C is shown in **Fig. 4.5.** Polarization curves for Q1-supported binary and ternary catalysts, and a commercial binary catalyst are compared in **Fig. 4.6**. From this figure, the commercial binary catalyst still shows the best performance.

4.3.4 Transition metal sulfides at GDEs in a half-cell: Oxygen reduction

Fig. 4.7 shows oxygen reduction curves for carbon and Q1-supported catalysts at room temperature in sulfuric acid (1M) and 1M CH_3OH + 1M H_2SO_4. The performance of the carbon-supported catalyst is good and comparable with reported results [8]. When running in 1M CH_3OH + 1M H_2SO_4, the performance was degraded a little for both catalysts. The performance of the Q1-supported catalyst is much poorer than for the carbon-supported catalyst, which could be ascribed to the low electronic conductivity of the sample.

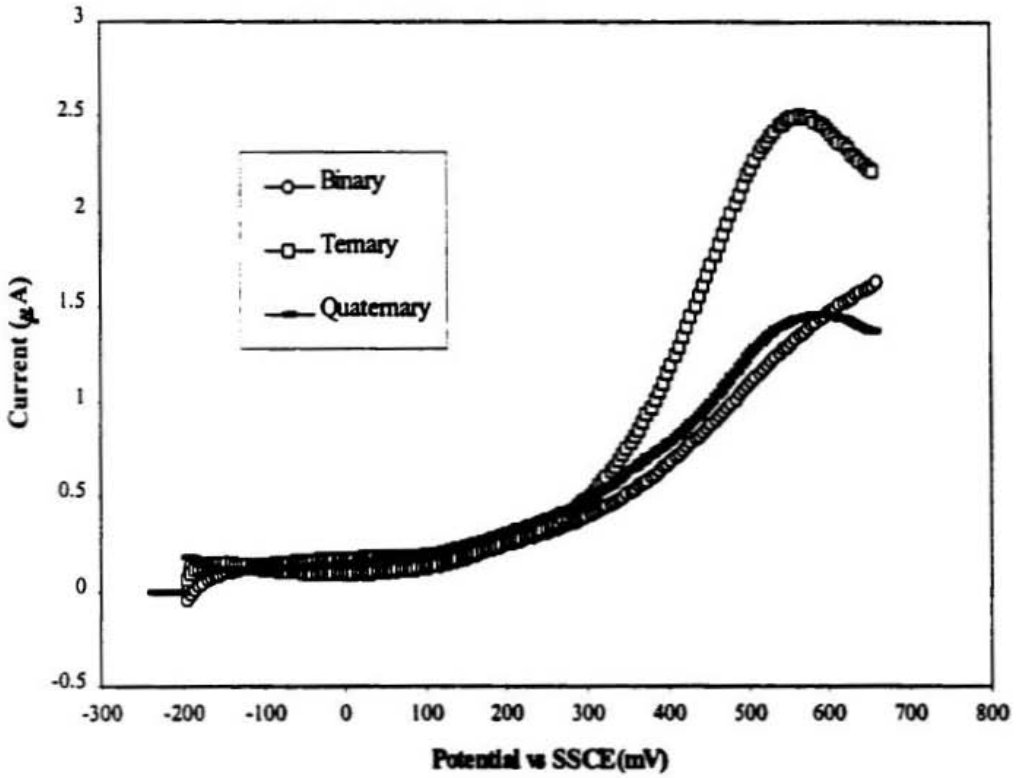

Fig. 4.4 Anodic scans of CVs at 100 mV/s for binary, ternary and quaternary catalyst as in Fig. 4.2 coated electrodes at 60 ^{0}C in N_2 saturated 1 M CH_3OH + 1 M H_2SO_4 with 100 μg metals cm^{-2}.

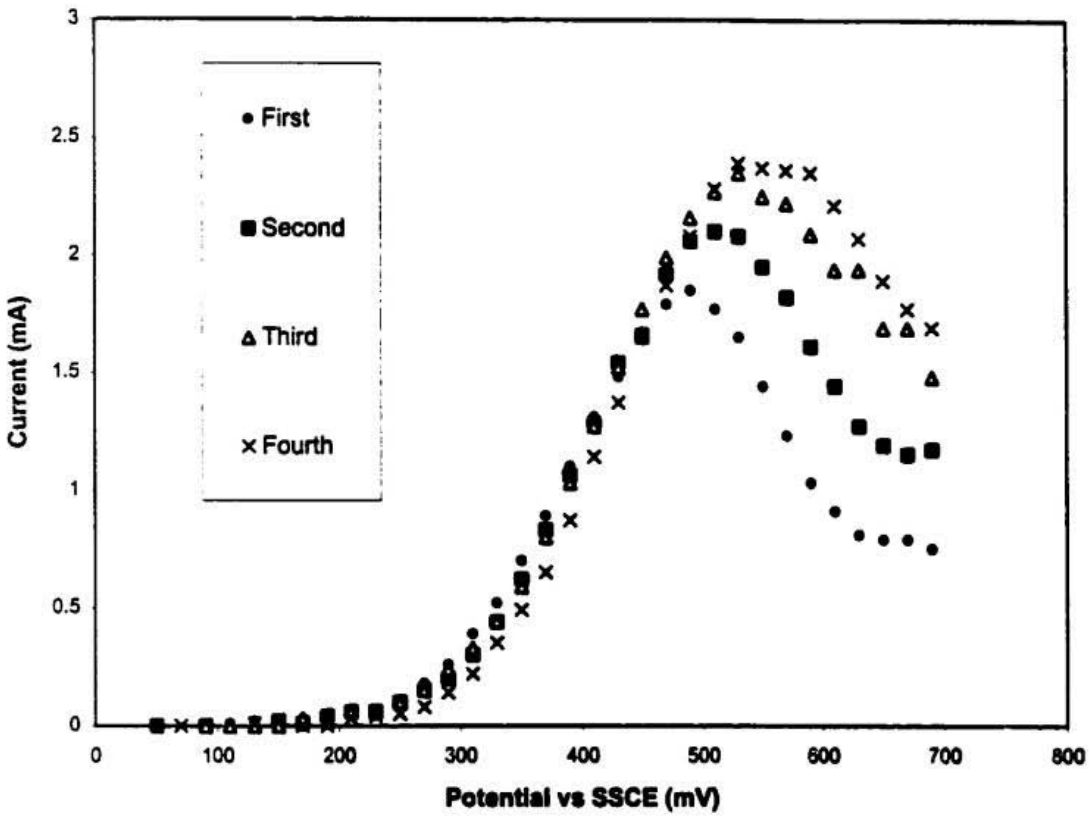

Fig. 4.5 Consecutive methanol polarization curves at 60 °C for a 29% ternary Pt-Ru-Os/Q1 coated electrode with PW of 10 s and 100 mg metals cm^{-2}.

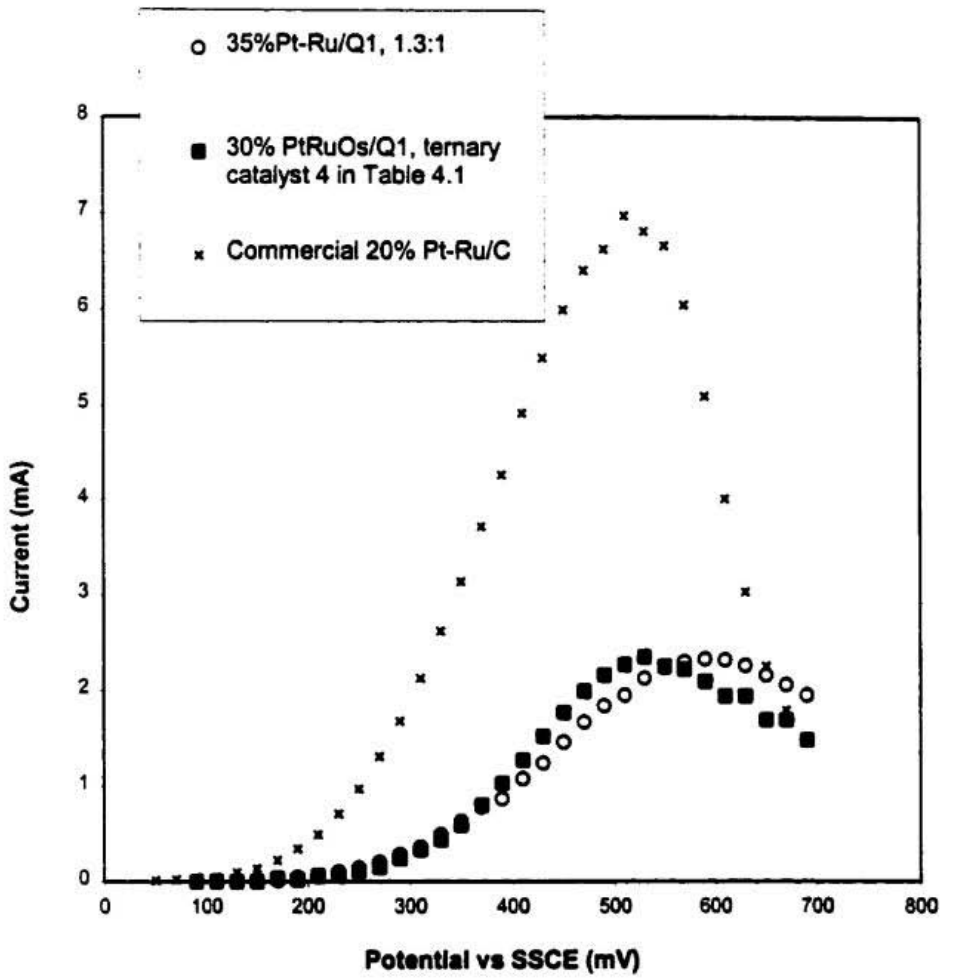

Fig. 4.6 Methanol oxidation polarization curves for 35% Pt-Ru/Q1 binary, 30% PtRuOs/Q1 ternary and commercial 20% Pt-Ru/C binary catalyst coated electrodes at 60 ^{0}C with PW of 10 s and 100 mg metals cm^{-2}.

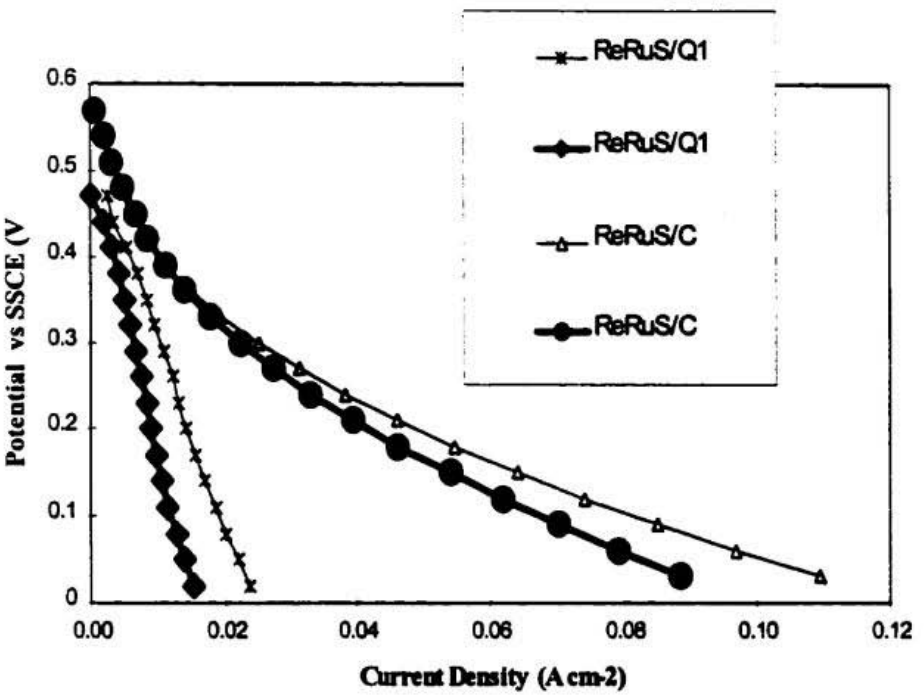

Fig. 4.7 Oxygen reduction curves for transition metal sulfides on Q1 and C in 1M H_2SO_4 (light lines) and 1 M (H_2SO_4 + CH_3OH) (bold lines) at GDEs in a half-cell. Catalyst loadings were 2.0 mg cm^{-2}.

4. 4 Conclusion

In summary, the performances of Q1-supported ternary and quaternary catalysts are superior to those of Q1-supported binary catalysts but are still inferior to those of commercial binary catalysts. Although further work is needed, promising applications for these mixed polymer-supported catalysts are envisaged.

The results of polymer-based transition metal sulfides for oxygen reduction were significantly inferior to carbon-supported catalyst, which suggests that the stability of the polymer is one of the important issues for future research activities.

References

1. S. Wasmus, A. Küver, *J. Electroanal. Chem.*, **461**, 14-31 (1999).
2. B. D. McNicol, D. A. J. Rand and K. R. Williams, *J. Power Sources*, **83,** 15 - 31 (1999).
3. R. Liu, K. Triantafillou, L Liu, C. Pu, C. Smith, and E. S. Smotkin, *J. Electrochem. Soc.*, **144,** L148 (1997).
4. K. L. Ley, R. Liu, C. Pu, Q. Fan, N. Leyarovska, C. Segre and E. S. Smotkin, *J. Electrochem. Soc.*, **144,** 1543 (1997).
5. E. Reddington, A. Sapienza, B. Gurau, R. Viswanathan, S. Sarangapani, E. S. Smotkin and T. E. Mallouk, *Science*, **280,** 1735 (1998).
6. M. R. Verbrugge, *J. Electrochem. Soc.*, **136,** 417 (1989).

7. D. L. Maricle, B. L. Murach, and L. L. Van Dine, Abstract 35, p. 58, *The Electrochemical Society Extended Abstracts*, Vol. **94-1**, San Francisco, CA, May 22-27, 1994.

8. R. W. Reeve, P. A. Christensen, A. Hamnett, S. A. Haydock and S. C. Roy, *J. Electrochem. Soc.*, **145**, 3463 (1998).